

Newsletter n°5

27 March 2024

ACC RD

A Consortium for COnvection-scale modelling
Research and Development

7th ACCORD hybrid-Assembly

ECMWF, Reading, UK and on-line



Credit: Patricia Pottier

ACC RD

A Consortium for COnvection-scale modelling
Research and Development

CONTACT US

Claude Fischer, ACCORD Programme Manager

@ pm@accord-nwp.org

Anne-Lise Dhoms, Consortium Scientific Secretariat

@ css@accord-nwp.org

<http://www.accord-nwp.org/>

Contents

Edito	3
<i>Claude Fischer, PM</i>	
ACCORD events	4
<i>Anne-Lise Dhomps, CSS</i>	
High-resolution and Dynamics Experiments at Met Éireann	6
<i>Colm Clancy, James Fannon, Eoghan Harney, Tatjana Kokina, Eoin Whelan</i>	
Creation of high-resolution Austrian regional reanalysis ensemble with AROME	16
<i>Nauman K. AWAN, C. Wittmann, C. Wastl, F. Meier, F. Weidle</i>	
Evaluation of Surfex/TEB offline over the city of Algiers: a first step toward high-resolution operational forecast	21
<i>Nour El Isslam Kerroumi, Rafiq Hamdi</i>	
Evaluation of the ALARO temperature forecast for Romania	32
<i>Mirela Pietriși, Alina Dumitru, Alexandra Crăciun, Simona Tașcu, Raluca Pomaga, Mihaela Neacșu</i>	
Evaluation of HARMONIE-AROME cycle 46h1 at AEMET	41
<i>Gema Morales, Javier Calvo, Joan Campins, María Díez, Pau Escribà, Daniel Martín, Jana Sánchez-Arriola, Samuel Viana y Teresa García</i>	
New version of harpSpatial	49
<i>Alex Deckmyn, Ahto Mets, Daniel Yazgi</i>	
Optimisation of Regional Weather Forecasts for Northern Algeria Using a Convolutional Neural Network and AROME Model Analysis	56
<i>Islam Bousri</i>	
ALARO and AROME analysis of derecho case in Poland.	60
<i>Bogdan Bochenek, Małgorzata Szczęch-Gajewska, Piotr Sekuła, Gabriel Stachura, Natalia Szopa, Marcin Kolonko</i>	
ALADIN activities in Poland	70
<i>Marcin Kolonko, Jadwiga Róg, Piotr Sekuła, Gabriel Stachura, Małgorzata Szczęch-Gajewska, Natalia Szopa, Bogdan Bochenek</i>	
Adaptation of C-LAEF for Türkiye	76
<i>Mustafa BAŞARAN</i>	
Patricia around ACCORD 26 beautiful countries	78
<i>Patricia Pottier</i>	
Previous editions	80
<i>Anne-Lise Dhomps, CSS</i>	

Edito

Claude Fischer, ACCORD Programme Manager

The previous ACCORD newsletter (NL4) was published in June 2023 and incidentally was the last one under the lead of Patricia. Our former CSS however still is present with us as is illustrated in this newsletter. From June last year until March this year, quite some activity has taken place and a number of events have been organized. They are not specifically described in the newsletter however it might be worth mentioning a few highlights here. In the autumn 2023, the preparations for the ACCORD scientific (and technical) strategy for the next five year period (2026-2030) have entered their concrete steps, with the Assembly on 4 December providing a few first orientations. The Assembly also has approved the appointment of a Documentation Officer who will soon be officially announced. At the level of governance, efforts are continuing in order to define a strategic vision for the expansion of international collaboration (and membership) in ACCORD, triggered by the very concrete example of the request by the Indonesian NHMS to join our consortium. Back to managerial considerations and to this newsletter (NL5), it is the first one produced under the lead of our new CSS Anne-Lise, whose involvement in ACCORD has already been welcomed by a number of key actors of the consortium.

In the first set of papers of NL5, the reader will find a large variety of contributions relating to validation and verification in a broad scope. The papers comprise use cases for a 750m model configuration with an emphasis on the impact of the LBC strategy (by our Irish colleagues), statistical verification (Alaro-Romania), the evaluation of a new model version based on CY46 (AEMET), the evaluation of an offline version of SURFEX with TEB over Algiers. The ACCORD team of Geosphere Austria is presenting the work on computing and using a high resolution reanalysis ensemble, the kind of dataset that recently has gained an increased interest ranging from verification and calibration purposes to training AI/ML tools. Last in order but not least in importance, an update on the progress and plans regarding the common verification tool “harpSpatial” is provided by a few of our key developers of the tool.

The second set of contributions include the use of a CNN for statistical post-processing and its evaluation on surface parameters (by our Algerian colleagues), a specific case study of the forecast of a Derecho case (IMGW-Poland) and two national team contributions (an overview of activity by the Polish team and the design of an EPS under construction by our Turkish ACCORD team).

I wish all readers, whether close or somewhat further away from ACCORD NWP activities, a good time consulting this NL5.

ACCORD Events

Anne-Lise Dhomps, ACCORD Consortium Scientific Secretary

1 Introduction

The outcomes of the [ACCORD events](#) such as governance body meetings (Assembly, PAC, STAC, LTM), Management Group (MG) meetings, Working Days, Working Weeks, thematic WG meetings can be found on the [ACCORD “Events” webpages](#): slides, minutes, summary, photos, videos, ... (when available). The material and conclusions of the thematic meetings (WW/WD) organised by the MG with the team or WG in their area are available on the relevant part of the [ACCORD wiki](#).

2 ACCORD meetings in 2023

Committees ([PAC](#), [STAC](#)), [Assembly](#) and Bureau

2023 has been a rich year with numerous meetings.

- Selection committee meetings for DA and Physics ALs, 27 February
- 1 PAC online meeting
- 2 STAC meetings (1 online and 1 hybrid)
- 2 Assembly meetings (1 online and 1 hybrid)
- 7 Bureau online meetings (1 for DA and Physics ALs, 2 meetings to prepare for the Assembly, and 4 monthly meetings from autumn onwards.)

[Management Group](#)

The Management Group resumed their every other Friday morning meetings from the beginning of January 2023. With a summer break it represents, in 2023, no less than 24 online meetings to work on the DAP, the RWP and other tasks such as actively preparing and fuelling the discussions for the next phase Strategy.

There were also 3 in-person meetings:

- Visit to INM and in-person meeting: 4-5 May 2023, Tunis (hybrid)
- Visit to Icelandic team and in-person meeting: 28 or 29 September 2023, Reykjavík, after EWGLAM/SRNWP meetings (hybrid).
- A STAC and MG joint in-person meeting: 25-26 October 2023 in Brussels (hybrid).

[LTM meetings](#)

6th LTM meeting, Tallinn, Estonia, 27 March 2023 (besides the All Staff Workshop)

7th LTM meeting, Reykjavik, Iceland, 26 September 2023 (besides EWGLAM)

8th LTM meeting, online, 5 October 2023

Scientific and technical meetings

2023 has been a very active year with:

- 57 weeks of scientific visits (27 visitors for 1 to 4 weeks),
- 13 working weeks or working days, plus lots of thematic meetings.

Find more information on the [ACCORD wiki](#)

All Staff Workshop

A few figures of the ASW2023:

- 198 registered participants of which 90 on site,
- in addition 32 remote participants just popped up without registering,
- 65 to 95 remote participants during the sessions,
- 8 sessions plus the opening & closing sessions, and 3 side-meetings,
- 78 speakers including 19 poster presenters,
- video-recording: 30 hours.

EWGLAM

Although not an ACCORD event, but with the participation of many ACCORD colleagues, the meeting offered the opportunity to the LTMs and to staff to meet in-person during the week. The MG intends to meet the Icelandic team on 29 September.

3 ACCORD meetings in 2024

The year has started with many of visits and working weeks and in only a few days time now, the 4th ACCORD All Staff Workshop will be held at the premises of SMHI in Norrköping. All informations are available on <http://www.accord-nwp.org/?4th-All-Staff-Workshop-15-19-April-2024-Noorkoping-hybrid>

Follow all our meetings, visits, working weeks and workshops on the [ACCORD website](#):

[PAC](#)

[STAC](#)

[Assembly](#)

[Bureau meeting](#)

[Management Group](#)

[LTM meetings](#)

[Working weeks / working day / Strategy workshop](#)

[All Staff Workshop](#)

High-resolution and Dynamics Experiments at Met Éireann

Colm Clancy, James Fannon, Eoghan Harney, Tatjana Kokina, Eoin Whelan

1 Introduction

The current operational IREPS suite at Met Éireann uses a horizontal grid-spacing of 2.5 km with 65 levels, similar to other centres running HARMONIE-AROME. Based on previous work (Clancy et al., 2022) investigating the potential benefit of higher resolutions, we are currently running a parallel e-suite called HECTOR, which uses a 750 m grid with the 90 vertical levels used by Météo France (hereafter MF_90). HECTOR uses boundaries directly from IFSHRES; previous experiments found this to be preferable to nesting within an intermediate HARMONIE-AROME host.

Soon Met Éireann operations will be carried out within the UWC-West group, and the common domain will have a 2 km grid with the MF_90 vertical levels. Additionally, a deterministic forecast will run every hour, giving more LBC options for the HECTOR suite. In this article we summarise the key results from a series of experiments to determine the “optimal” LBC configuration (if it exists) for a high-resolution subdomain like HECTOR. A more comprehensive technical note detailing this work is available from Met Éireann.

In addition, a number of dynamics settings were tested, both in these high-resolution and standard configurations during Storm Ophelia in October 2017. The various domains used throughout are shown in Fig. 1.

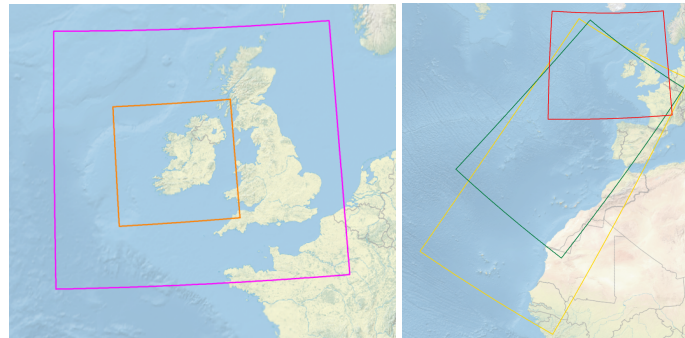


Figure 1: Domains used throughout this article. Left, for sub-kilometre testing: 750 m domain used by HECTOR (orange, 800×800) and 2 km reference for nesting (purple, 720×648). Right, Ophelia testing at 2.5 km: operational IREPS domain (red, 1000×900) along with larger 1080×2160 (yellow) and 1000×1600 (green).

2 Boundary options

The experiments carried out here all used the bugfix version of HARMONIE-AROME Cycle 43h2.2. The reference simulations use the purple domain in Fig. 1 with horizontal resolution of 2 km and the MF_90 vertical levels. In order to mimic the UWC-West configuration, a quadratic grid was used in these simulations, with a time-step of 60 s and an uncentring parameter value of XIDT=0.14. Note that experience with the UWC-West domain suggests that 50 s is a preferable time-step; however, this smaller domain here does not contain the

Table 1: Set of experimental boundary options. The last two columns show what LBC files are used in the chain for the 1200 UTC forecast of a given hectometric experiment; for example, the har3 1200 UTC uses LBC from the HARM ref0 0900 UTC, which in turn uses LBC from the IFSHRES 0000 UTC.

Name	Host	LBC age	HARM used by 12z	IFSHRES used by HARM host
ifs	IFSHRES	6-hour old	-	0600 UTC
har3	HARM	3-hour old	0900 UTC	0000 UTC
har2	HARM	2-hour old	1000 UTC	0000 UTC
har1	HARM	1-hour old	1100 UTC	0000 UTC
har0	HARM	same forecast	1200 UTC	0600 UTC
harS	HARM	same forecast	1200 UTC	1200 UTC

same complex orography, and no problems were encountered. For 3DVAR data assimilation, the UWC-West structure functions were used.

For the hectometric experiments, the 800×800 domain with 750 m horizontal resolution, shown in orange in Fig. 1, was used with the basic HECTOR set-up as follows: cubic grid truncation, MF_90 vertical levels, 30 s time-step with no uncentring, and increased spectral horizontal diffusion through RDAMPX=10 for all parameters X. Structure functions for this HECTOR domain have been generated, allowing the use of 3DVAR (this has in general led to a slight improvement in scores in the first few hours, although more neutral later on). For all of the experiments, three-hour cycling was used with a five-day warm-up period. Four times a day 36-hour forecasts were run, at the “main” hours of 0000/0600/1200/1800 UTC. Conventional observations were assimilated using upper-air 3DVAR, along with the usual surface OI.

Ideally a limited-area forecast will use LBC from the most recently available IFSHRES forecast. In an operational setting, due to the IFS schedule, the LBC will be either 6- or 9-hours old: that is, a 1200 UTC will use the 0600 UTC IFSHRES, as will the 1500 UTC. When using IFSHRES LBC directly in the hectometric experiments (as with HECTOR), this approach is also used.

When nesting a hectometric domain within a HARMONIE-AROME forecast, researchers often use the “same forecast” option, which means that the nested 1200 UTC would use the host LBC from 1200 UTC, i.e. the same forecast cycle. However, this is not practical for operations, as the nested experiment would have to wait until the host first completes. An option under our current operational set-up would be 3 hour-old boundaries; i.e. the 1200 UTC nested uses LBC from the 0900 UTC host.

As mentioned, UWC-West operations will produce an hourly forecast, thus giving more host boundary options. The suite will still use three-hourly cycling, and in order to mimic this for our tests, we define three sets of 2 km references: ref0 cycling at 0000, 0300, 0600, . . . using 6- and 9-hour old IFSHRES LBC; ref1 cycling at 0100, 0400, 0700, . . . using 7- and 10-hour old IFSHRES LBC; and ref2 cycling at 0200, 0500, 0800, . . . using 8- and 11-hour old IFSHRES LBC. Once these are available, we can then define a set of nested hectometric experiments (har3, har2, har1, har0) with reducing boundary ages. As mentioned, the “same forecast” har0 option is impractical in operations. For experimental purposes, we define a further, even less practical harS option. In this, each nesting step uses “same forecast”, so the 1200 UTC harS uses LBC from a 1200 UTC “refS” experiment, which in turn uses LBC from the 1200 UTC IFSHRES. All of these are listed in Table 1.

2.1 February 2022 test period

The main testing period used was the 10-20 February 2022, during which three named storms impacted Ireland: Dudley, Eunice, and Franklin. As we are mainly interested in high-impact extreme weather applications for very high-resolution modelling, this period is ideal. Figure 2 shows results for just the hectometric domains nested within HARMONIE-AROME experiments. Across many of the parameters we see quite a clear separation in the performance: harS is the best followed by har0 (both of which are sadly not feasible). After these, the remaining experiments with 1-, 2-, and 3-hour old LBC are quite clustered, with essentially no difference.

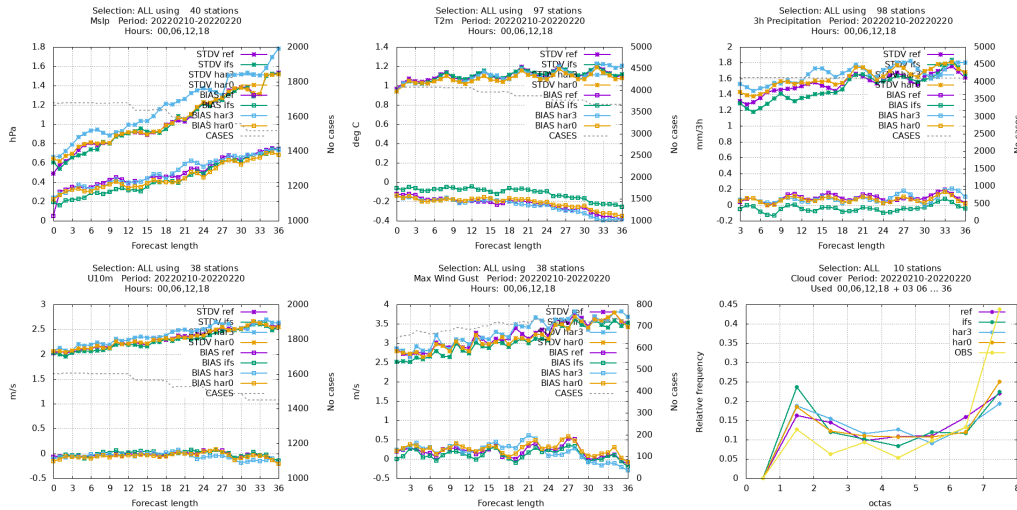


Figure 3: Verification for various parameters for the February 2022 period. Experiment details given in Table 1.

Differences are small closer to the centre of the domain, emphasising the need for as large a domain as possible. We also see that the HARMONIE-AROME driven experiments give higher totals over Ireland.

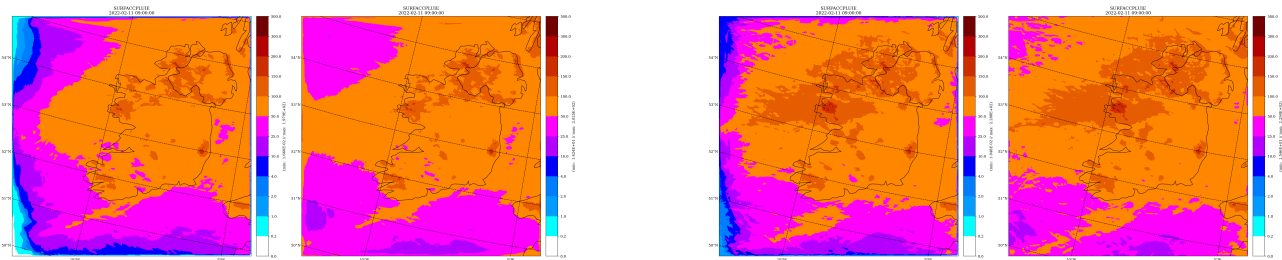


Figure 4: Total 09-09 rainfall accumulations for 10-20 February 2022, for hectometric experiment with IFSHRES LBC (left) and HARMONIE-AROME, har3 option (right). For each is shown coupled with just cloud liquid and water (to the left), plus with all available hydrometeors (right).

We use the Irish rainfall network to evaluate accuracy, which consists of around 400 observations of 24-hour accumulations recorded daily at 0900 UTC. A gridded product at 1 km resolution is produced from this: totals for our 10-20 February 2022 period are shown on the left of Fig. 5. We see a typical Irish pattern with highest amounts in the west, particularly over mountainous regions, and also over the Wicklow mountains in the east.

Figure 6 shows the forecasted accumulations, to be compared with these observed values, from the various experiments. We would hope the higher-resolution simulations to better capture the highest amounts. In the west, this is indeed the case for the hectometric simulations using HARMONIE-AROME boundaries. The IFSHRES-driven experiment (middle panel of top row) is less successful: it is in general too dry in the west. As we saw above, less rainfall seems to be produced at the inflow boundaries with IFSHRES LBC; here the ifs experiment does a better job in the mountains on the east coast. On the other hand, we see that all experiments struggled with the amounts in the south-west.

For a more quantitative measure of accuracy, we now turn to the Fraction Skill Score (FSS), computed using the standard methodology outlined in Roberts and Lean (2008). Percentile thresholds are used in order to mitigate the impact of model biases; e.g. the 90th percentile threshold compares the location of the highest 10% of observed and forecasted 24 h rainfall. Used in this way, the FSS measures the spatial accuracy of the forecasts. Note that the entire spatial extent of the observed gridded product, as illustrated in Fig. 5, is used for the FSS

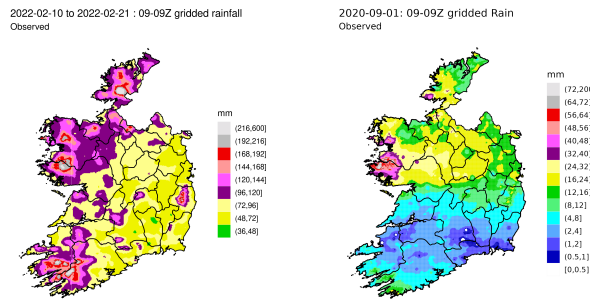


Figure 5: Gridded rainfall observations. Left: for the February 2022 period, from 0900 UTC on the 10th to 0900 UTC on the 21st. Right: for the flooding case overnight of the 1st September 2020.

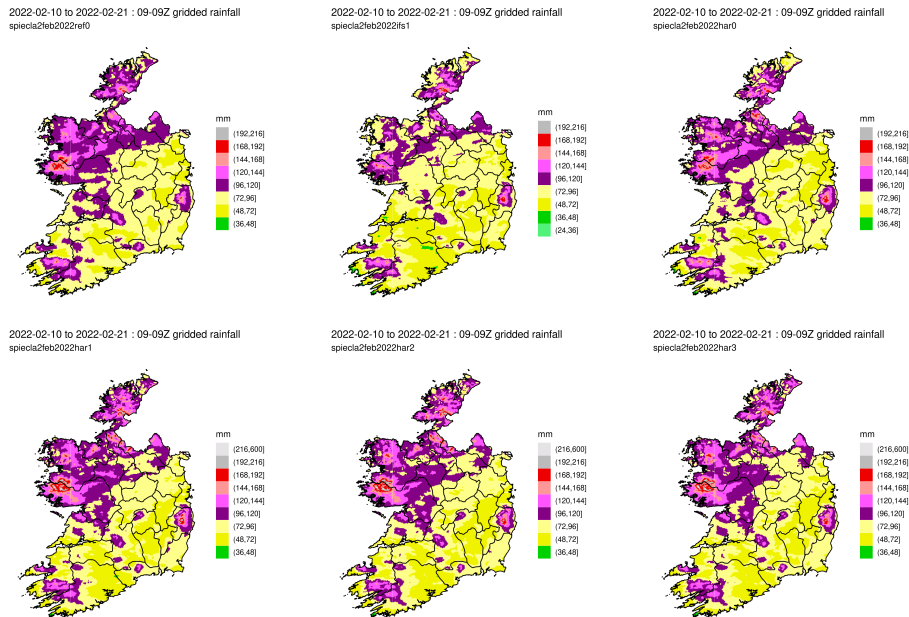


Figure 6: Forecasted rainfall accumulations for the February 2022 test period, using the 0000 UTC cycles from each day. Experiments shown are (top, left to right): ref0, ifs, har0; and (bottom, left to right) har1, har2, har3. Details in Table 1.

analysis (missing data close to the boundaries is simply omitted when upscaling).

For the February test period only forecasts from the 0000 UTC and 0600 UTC cycles at leadtimes of 33 h and 27 h, respectively, could be used for the FSS computation (giving a total of 22 samples). Results averaged over the whole period showed no significant differences. FSS performance for days with lighter (75th percentile of observed rain less than 10 mm in 24 hours) or heavier rainfall was also considered, as illustrated in Fig. 7. For lighter rainfall days (February 10, 13, 14, 16, and 18), ref0 generally outperforms the ifs and har experiments, however har1-3 tends to perform better for the heavier rainfall days (February 11, 12, 15, 17, 19, and 20). It is interesting to note that har0 is outperformed by har1-3 for the heaviest rainfall in the period (i.e. the 95th percentile on the left Fig. 7), which was also evident in standard surface skill scores (not shown). This may reflect spin-up of precipitation in the HARMONIE-AROME forecasts used for LBCs. However, one should also bear in mind the limited sample size available for this analysis.

Finally, we look at a particular event on the 1st-2nd of September 2020, when heavy rainfall overnight led to serious flooding in the Connemara region. The right-hand of Fig. 5 shows the gridded observed 24-hour

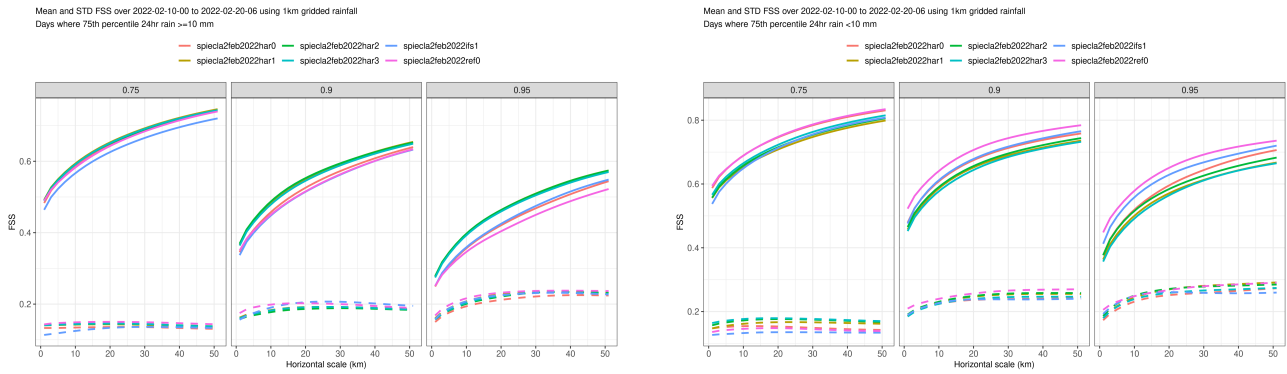


Figure 7: FSS (mean, solid, and standard deviation, dashed) for the February 2022 period, divided into “heavier” (left) and “lighter” (right) rainfall days; see text for days used. The fraction above each panel indicates the rainfall percentile. For experiment names, the last part (ifs, har0 etc) corresponds to Table 1.

accumulations valid at 0900 UTC on the 2nd. A system moved in from the west overnight, bringing highest accumulations to the mountainous areas around Connemara.

For simulations of this event the usual five-day warm-up period was used. Long forecasts from just the 0000 and 0600 UTC cycles on the 1st were used, to compare with the 09-09 observations at lead-times of 33 and 27 hours, respectively. An initial subjective view of the results showed that, once again, the age of the originating global LBC seemed to be of most importance, and so we order the results shown below in Fig. 8 by these. In this case, the “newer” global LBC actually lead to poorer performance: at the time of this event, there was considerable differences noted between runs of IFS.

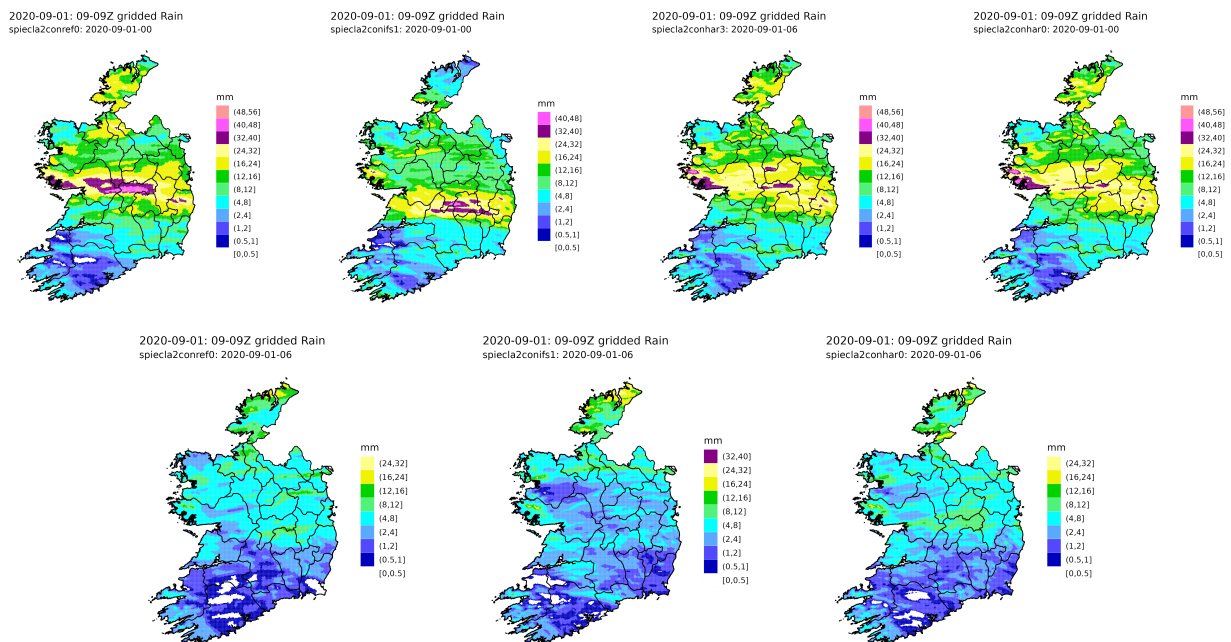


Figure 8: Experiments for the Connemara case, showing forecasted 24-hour rainfall to be compared with the right-hand panel of Fig. 5. Originating with IFSHRES LBC from 18z on the 31st (top) and 00z on the 1st (bottom). For experiment names, the last part (ifs, har0 etc) corresponds to Table 1.

Focussing on the top row of Fig. 8, we see that the HARMONIE-nested experiments (right-hand two panels)

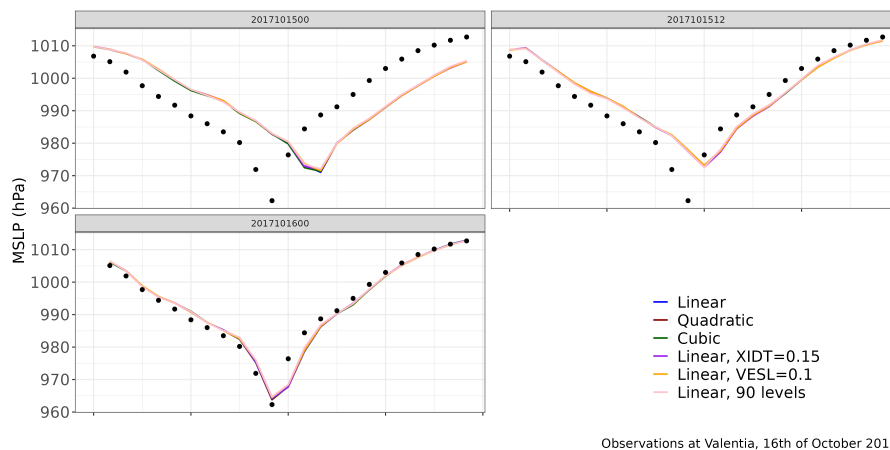
were most successful in the positioning of the heaviest rain. The IFS-driven hectometric simulation (second from left) is much too dry in the west, which is consistent with what we saw in previous sections. Given the spatial extent of this boundary spin-up we see when using IFSHRES LBC, we also extended the domain to the west to see the effect. The results were not perfect, but showed a slight improvement over the smaller domain (not shown). Increasing the number of points in the boundary coupling zone (to match the width at operational resolutions) did not significantly improve simulations either.

3 Storm Ophelia experiments

As well as the LBC tests described above, cycling experiments were carried out with other dynamics options, such as the XIDT parameter. Off-centring such as with XIDT or VESL can be used to improve stability, as does the use of a truncated grid. Averaged verification scores do not often show much effect from these options, and so a series of experiments was run to test their impact on a high-impact storm case, namely Storm Ophelia which had transitioned from a hurricane and reached Ireland on the 16th of October 2017.

The simulations again used the bugfix Cycle 43h2.2, this time on our operational domain (red in Fig. 1). The reference used all defaults: linear grid, 65 levels, 75 s time-step. No upper air assimilation was used. To see the effects at different lead-times with different boundaries, three-hour cycling was used from 2017/10/15/00 to 2017/10/16/00, with longer forecasts run at 0000 and 1200 UTC.

The changes from the default that were tested were quadratic and cubic grids, off-centring with either XIDT=0.15 or VESL=0.1, and the use of MF_90 vertical levels. We look first at point values compared with observations. The centre of Ophelia passed quite close to Valentia station in the south-west, providing a useful comparison of the intensity. Figure 9 shows forecasts from the various tests, from three different starting times. In general, we see that results were very similar, with differences due to lead-time/boundaries dominating.



Observations at Valentia, 16th of October 2017

Figure 9: Forecasted MSLP on the 16th October 2017 at Valentia, along with observations (black dots). The forecast start time is given in each panel heading.

Figure 10 shows similar series for 10 m wind, but at two locations. Roches Point is on the coast and recorded the strongest winds during Storm Ophelia. Moorepark is further inland. Compared to the MSLP results, we see more differences, mainly with the use of MF_90 levels, which has more of an effect over land and reduces our peak winds in particular. This is consistent with previous findings, and has been found to be beneficial.

For a more spatial view, we consider forecasts valid at 1200 UTC on the 16th and plot the differences in fields from the default linear experiment. For MSLP, we show those a lead-time of 24 hours in Fig. 11, which includes the original fields overlaid. Differences are very small in magnitude. The MF_90 simulation shows the largest

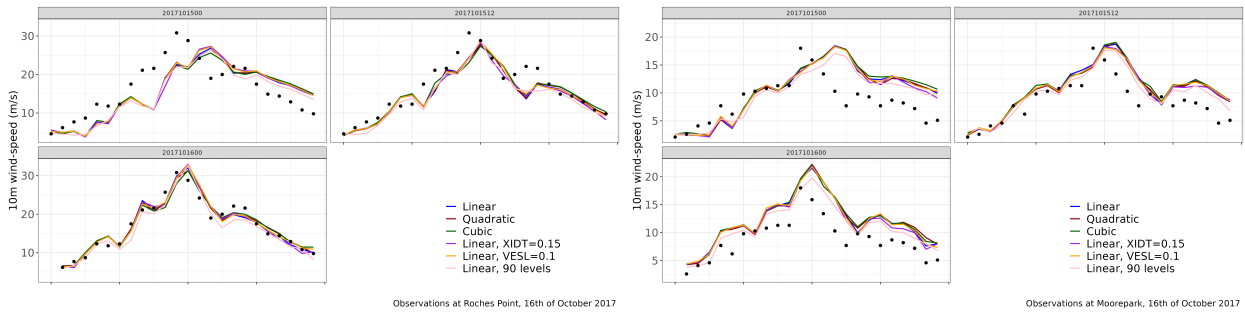


Figure 10: Forecasted 10 m wind-speed on the 16th October 2017 at Roches Point (left) and Moorepark (right), along with observations (black dots). The forecast start time is given in each panel heading.

differences, due to a very slight shift in the position of the storm.

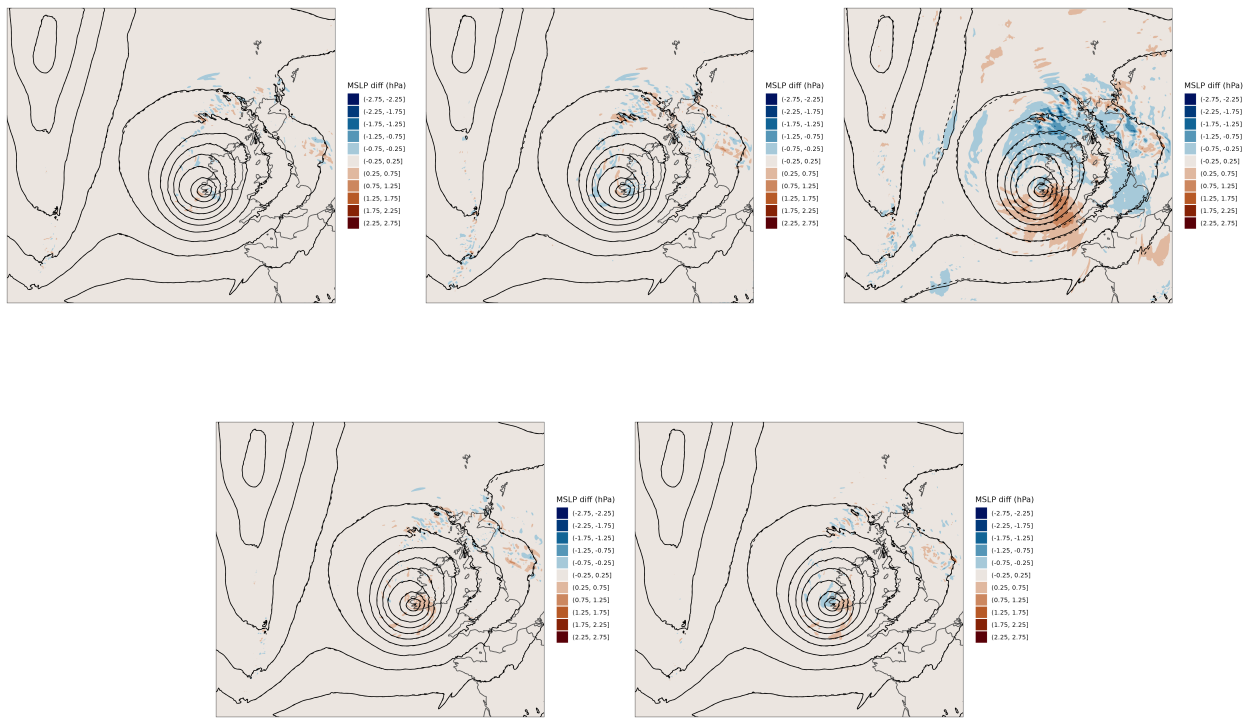


Figure 11: MSLP differences at +24 hours from the default linear experiment valid at 1200 UTC on the 16th of October 2017. For each experiment, the MSLP field is shown (solid isobars) along with the default (dashed). Top, left to right: quadratic grid, cubic grid, MF_90 levels. Bottom, left to right: VESL=0.1, XIDT=0.15

Figure 12 shows differences in 10 m wind-speed, this time for three lead-times. Most of the largest differences are due to slight positional shifts. The most obvious systematic difference is seen with the MF_90 vertical grid (middle row). As discussed above, we see reduced wind-speeds, particularly in areas where we have the strongest winds from the storm. Differences due to the off-centering options (bottom two rows) are smaller, with bigger variations due to lead-times. Longer cycling experiments did not show significant differences in scores when using XIDT, for example.

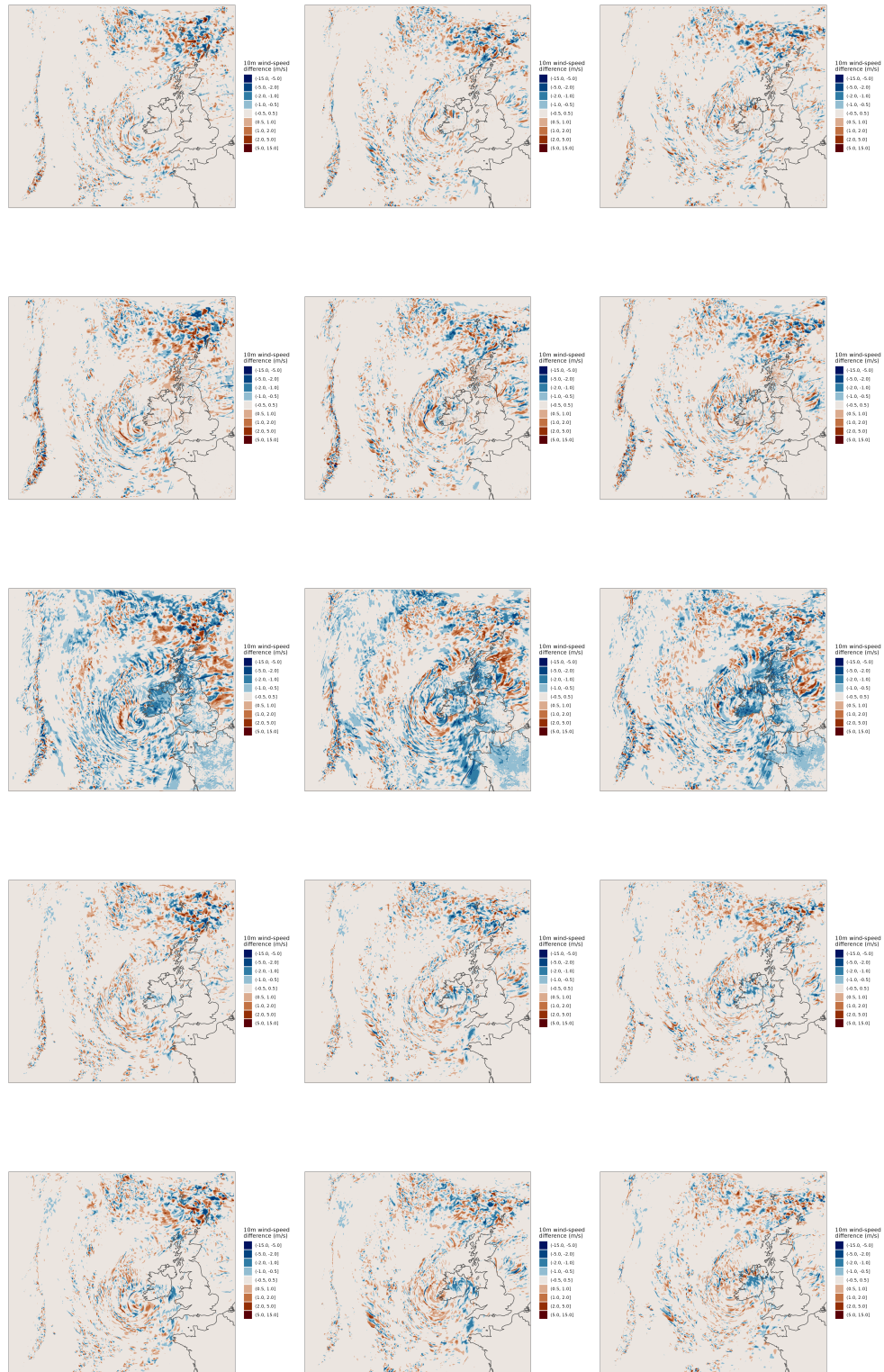


Figure 12: Wind-speed differences from the default linear experiment for forecasts valid at 1200 UTC on the 16th of October 2017. Lead-times are (left to right) 36, 24, and 12 hours. Experiments, top to bottom: quadratic grid, cubic grid, MF_90 levels, VESL=0.1, XIDT=0.15.

4 Summary

The main focus of these hectometric experiments was the choice of boundary conditions and the various related settings. Whether we use IFSHRES LBC directly or nest within an intermediate kilometre-scale HARMONIE-AROME experiment, it was seen that the age of the initiating global boundary files tends to dominate performance. While this is not overly surprising, it is perhaps sometimes overlooked when planning nested experiments. On the other hand, it is worth bearing in mind the practical operational constraints in terms of the delivery times of various LBC files; in general these rule out the “same forecast” nesting option.

When nesting within HARMONIE-AROME, little difference was found between 1-, 2-, and 3-hour old boundaries. In terms of point verification scores, the experiments directly using IFS LBC were found to give slightly better results. This is consistent with previous work, and is the basis for the current configuration of the HECTOR e-suite. However, previously the host HARMONIE-AROME had 65 levels. With a 90-level host, as will be available in UWC-West, the wind scores are much better and closer to those using IFS LBC.

In addition, the spatial rainfall analysis here suggests a possible benefit to nesting within HARMONIE-AROME. The simulations with IFS LBC showed a much drier spin-up region near the inflow boundaries, causing particular trouble in forecasting rainfalls in the west of Ireland. An option to mitigate this is to increase the domain size. This, of course, will come with an increased computational cost. The FSS analysis also suggested that the location of heavy rainfall may be more accurately captured when using HARMONIE-AROME-nesting. Furthermore, this nesting option is possibly wiser in the longer-term, if the resolution of the hectometric suite is to decrease further.

This work also looked at a few other dynamics settings in the case of Storm Ophelia. The use of truncated grids or uncentring did not greatly affect the intensity of the storm, and remain as attractive options for controlling the stability and cost of a forecast, particularly as resolutions increase. It is worth noting of course that these tests involved a synoptic-scale system over a domain with reasonably low-lying orography; more challenging situations would likely show more pronounced impacts from the choices.

Finally, we note some preliminary tests carried out with simulating the earlier track and development of Storm Ophela, including its post-tropical transition. These were carried out on the large domains plotted in yellow and green in Fig. 1. Cycle 46 had to be used, to benefit from the recent work in speeding up PGD preparation and climate generation, although technical problems still require the chosen domain to have “enough” land points. Stable simulations were eventually completed, and will be reported on in the future.

5 Acknowledgements

Computing resources for this work were provided through two Special Projects at ECMWF.

6 References

- Clancy C., J.Fannon and E.Whelan, Hectometric-Scale Experiments at Met Éireann, ACCORD Newsletter 2, 129–138 February 2022
- Pálmason B., G.N.Petersen, S.Thorsteinsson and X.Yang, Hectometric experiments with the HARMONIE-AROME system at IMO. ACCORD Newsletter 2, 139–146 February 2022
- Roberts, N. and H.Lean, Scale-Selective Verification of Rainfall Accumulations from High-Resolution Forecasts of Convective Events. *Mon. Wea. Rev.*, 136, 78–97, 2008

Creation of high-resolution Austrian regional reanalysis ensemble with AROME

Nauman K. AWAN, C. Wittmann, C. Wastl, F. Meier, F. Weidle

1 Introduction

The high-resolution Austrian Regional reanalysis ensemble with AROME (ARA) is a three-year project funded by Bundesministerium für Klimaschutz, Umwelt, Energie, Mobilität, Innovation und Technologie (BMK), via Austrian Space Applications Programme (ASAP). Within the framework of this project, GeoSphere Austria, in collaboration with our partner, the Wegener Center for Climate and Global Change (WEGC) of the University of Graz, is working towards the main goal of creating a first of its kind high-resolution (2.5 km) reanalysis ensemble. This reanalysis ensemble is created by assimilating soundings, satellite and station-based observations with the aid of three-dimensional variational assimilation system (3DVAR), implemented in the AROME (Seity et al. 2011) model, covering Austria and the greater Alpine region. Figure 1 below shows the conceptual outline of our reanalysis ensemble system along with the geographical extent of our model domain. The final dataset will be created with a unified setup to downscale the ECMWF ERA-5 (Hersbach et al. 2020) full 10+1 member ensemble with a 3-hourly assimilation frequency. It will span over a period of ten years, i.e. 2013-2023. The model setup used in this research (see Table 1) is adapted from our operational C-LAEF model setup (Wastl et al. 2021). The observations assimilated are shown in Table 2.

This C-LAEF reanalysis ensemble system includes i) an ensemble 3D variational blending technique including Ensemble Jk to deal with atmospheric initial uncertainties (Kerresturi et al., 2019); ii) an ensemble of land surface data assimilation to account for uncertainties in the initial land surface conditions (Bellus et al., 2016; iii) a pure parameter perturbation scheme (SPP - stochastically perturbed parametrizations; Ollinaho et al., 2017) , iv) perturbations of the key parameters in SURFEX following Bouttier et al. (2016), and v) a coupling with the global ERA-5 ensemble system of the ECMWF to consider uncertainties in the lateral boundary conditions. The final reanalysis product is computed on a 2.5 km regular lat / lon grid and has an hourly resolution for instantaneous parameters and 3-hourly resolution for accumulated variables. We are running the system eight times per day, which is also similar to our operational system.

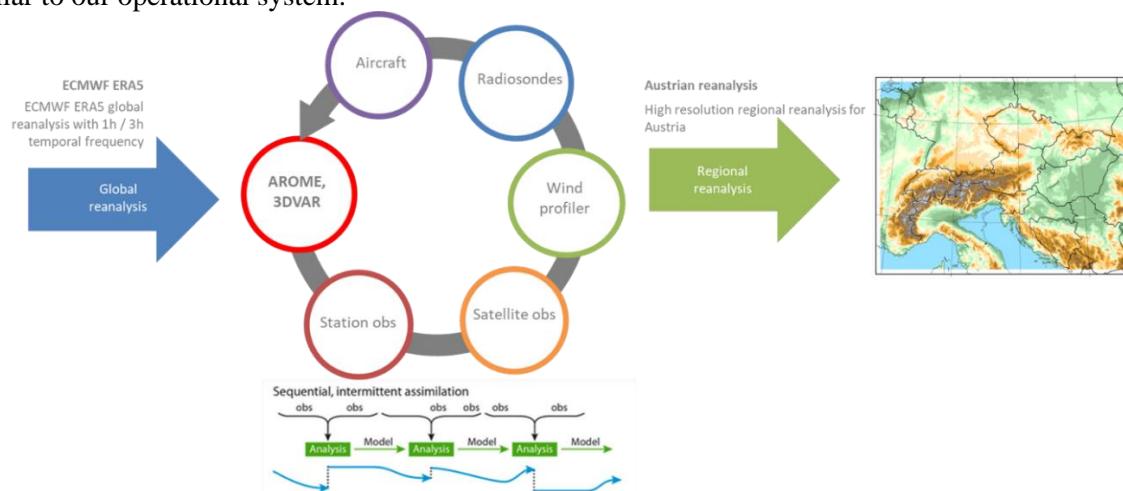


Figure 1 Conceptual outline of Austrian high-resolution (2.5 x 2.5 km) regional reanalysis ensemble (C-LAEF reanalysis ensemble) along with the selected geographical extent.

Table 1: The model setup used for creating C-LAEF reanalysis ensemble

	C-LAEF reanalysis ensemble
Model version	cy43t2bf11
Resolution	2.5km
Members	10 + 1
Vertical levels (lowest / highest)	90 (5m / 35km)
Time step	60s
Area (no of gridpoints)	Alpine area (600 x 432)
Orography / Physiography	GMTED2010 ECOCLIMAP I1
Initial conditions	ENS 3DVAR / ENS OI
Boundaries	ECMWF ERA-5
LBC update frequency (control / ensemble)	1h / 3h
Surface scheme	SURFEX 8.0
Runs per day / Start time	8 / 00, 03, 06, 09, 12, 15, 18, 21 UTC
Cycle interval	3h
Forecast range	5h
Hardware	BullSequana XH2000

The model error representation in the operational C-LAEF EPS has been changed from a hybrid stochastic perturbation scheme, where perturbations of tendencies in shallow convection, radiation and microphysics are combined with parameter perturbations in the turbulence scheme to a pure parameter perturbation scheme (SPP - stochastically perturbed parametrizations; Ollinaho et al., 2017) with a C-LAEF upgrade in September 2023. The idea was to increase the physical consistency in the model error perturbation scheme. In SPP uncertain parameters are directly perturbed in the physics parametrizations with some random noise generated by a pattern generator. The SPP scheme in C-LAEF consists of 13 stochastically perturbed parameters in 5 physics parametrization schemes.

Table 2 Details of the available observations used for data assimilation purposes.

Observations	Observation type	Assimilated variables	Availability from - to	Remarks
Pilot balloons	PILOT (weather balloon)	Upper-air wind	1996-present	The density changes over time
Radiosondes	TEMP	Upper-air wind, temperature, humidity, geopotential height	1964-present	
	TEMP	Surface-level wind, temperature, humidity	1964-present	
Aircraft	AMDAR	Wind, temperature, humidity	2010-present	Humidity only on few LH aircraft
	MODE-S	Wind, temperature	2018-present	Doesn't cover the whole period
Wind profiler		Upper-air wind	2010-present	
Surface level	SYNOP	Station pressure, 10 m wind, 2 m humidity, 2m temperature	1972-present	
	SHIP	Station pressure, 10 m wind, 2 m humidity	1994-present	
Satellite	NOAA/MetOp	AMSU-B radiances	2011-present	
	MSG	SEVIRI Water Vapour	2011-present	
	MSG	AMVs, upper air wind	2011-present	

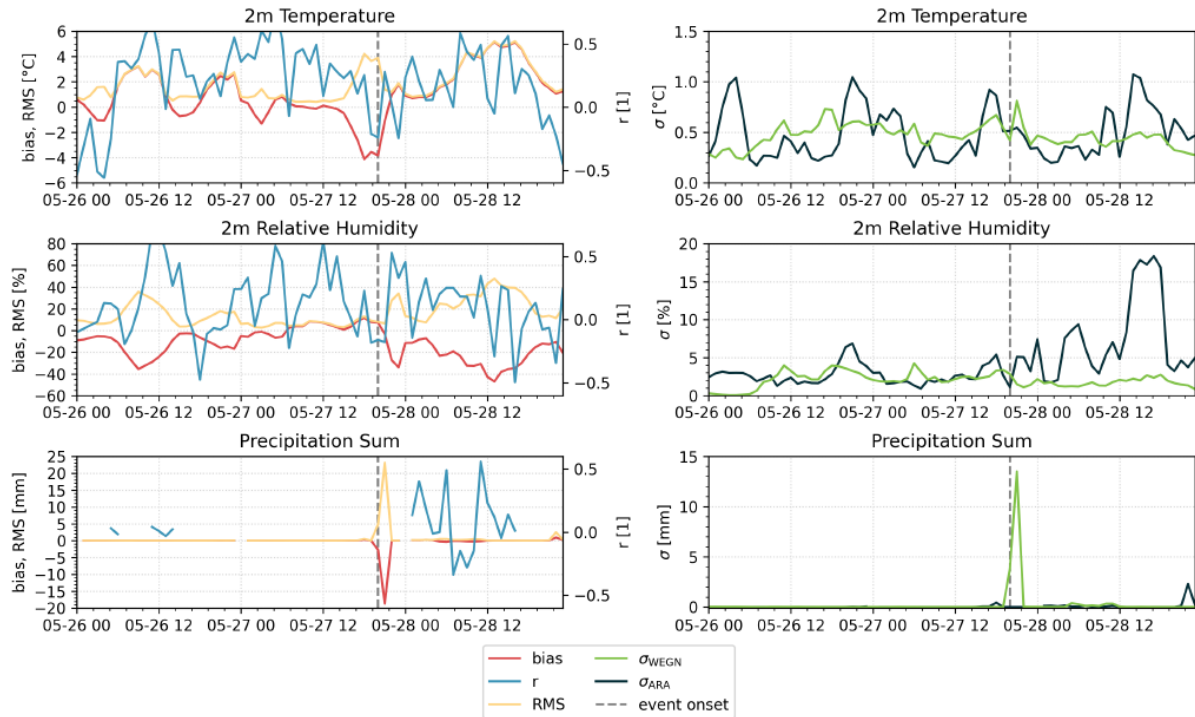


Figure 2 Standard metrics of the 27-05-2022 event (spatial mean over Feldbach region). Each row corresponds to one atmospheric parameter: 2m temperature (1st row), relative humidity (2nd row), and precipitation sum (bottom row). In the left column, the bias (red), correlation coefficient (“r” light blue), and root mean square error (“RMS”, yellow) are shown. The standard deviation of both datasets (WEGN in green and ARA in dark blue) are depicted in the right column. The dashed grey line indicates the time, when the event started.

2 Current status & Preliminary results

We have already completed the initial work, which included, evaluation of C-LAEF reanalysis ensemble performance on high spatial and temporal scales (sub-mesoscale to sub-daily / hourly), as well as its ability to simulate heavy precipitation events on time scales relevant to climate simulations and investigate possible spatial and temporal drifts in the simulation results. The long (10 year) simulation is being computed and the final data is expected to be made available to user’s by March 2025.

Before commencing the long ten-year simulation, we conducted several short experiments (1-3 days) and a long (1 ½ year) simulation covering the same period of the test simulations. We present here results from one of the case studies, i.e. May 27, 2022, taken from the 1 ½ year simulation. On this day, scattered thunderstorm activity was observed in many parts of Austrian Alps. Localized convection was triggered by interaction of a mix of weak large scale and local scale forcing and local moisture recycling played a significant role in enhancing the amount of precipitation. These localized convective events pose a significant challenge as for Numerical Weather Prediction (NWP) models forecasting location and timing of such events is often difficult. They are also notorious for being either poorly represented or entirely missed in climate simulations.

However, for this case, our reanalysis ensemble demonstrated good performance for short experiment as well as for the 1 ½ year-long simulation. The model performance was evaluated by comparing the hourly model output with a high-resolution station observational network (Wegener Net, 100m x 100m) data and high-resolution gridded observational analysis known as INCA (Haiden et. Al. 2011).

Figure 2 illustrates the standard statistical metrics like, bias, root mean square error, spatial correlation co-efficient, and standard deviation, both a day before and after the event. For this comparison, ARA data within the WEGN region are compared to the independent WEGN data (<https://wegcenter.uni-graz.at/en/wegenernet/wegenernet-home/>).

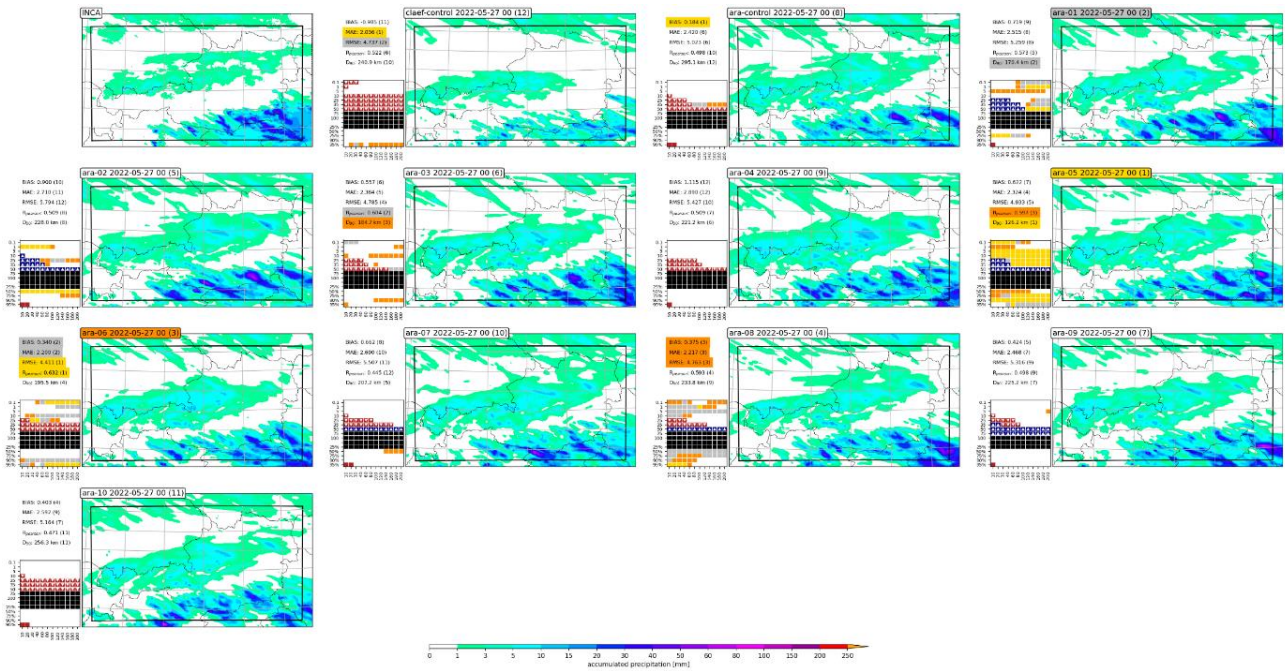


Figure 3 Daily sum of precipitation for 27-05-2022. Panel plot showing comparison of ARA ensemble with gridded INCA observations and GeoSphere Austria operational C-LAEF system. Statistical metrics, like Bias, Mean Absolute Error, Root Mean Square Error, Pearson Number, and displacement of the 90th percentile is displayed on the left-hand side of each panel. The small table depicts the performance of each realization for specific thresholds of precipitation and 25th, 50th, 75th, 90th and 95th percentile. The colours used in the title, Gold, Silver and Bronze and the number in brackets shows the rank 1-3 given to top three ranked realizations.

These statistical metrics show disparities in the basic atmospheric parameters between the two datasets. Given the limitations stemming from the small size of the investigated domain and time span, these disagreements may arise from a shift in the modelled events in space and/or time, or from a more general disagreement of the model errors. Further, investigations are on-going to understand the model performance on very high spatial and temporal scales.

Figure 3 depicts the spatial structure of the daily sum of precipitation as simulated by the whole ensemble alongside our operational C-LAEF model and high-resolution gridded observational analysis known as INCA. In addition to presenting the spatial structure of total precipitation received that day, this figure also includes results from our statistical analysis. The statistical metrics displayed on the left-hand side of each panel include Bias, Mean Absolute Error, Root Mean Square Error, Pearson Number, and displacement of the 90th percentile. These metrics are used to rank these realizations. It's important to note that such ranking based on statistical metrics is highly relative and changes according to your choice of evaluation criteria like, selected region, and selected time slice. However, for the Austrian Alpine region for which these scores are computed, they serve as a fundamental performance metric to determine which ensemble member outperforms the other in the Greater Alpine region. Another benefit of such broad analysis is that the users can themselves decide which simulation is performing better for their region. The small table on left hand side of each sub-figure depicts the performance of each realization for specific thresholds of precipitation, 25th, 50th, 75th, 90th and 95th percentile and displacement of 90th percentile of precipitation. Furthermore, the colours used in each title, Gold, Silver and Bronze and the number next to the title in the brackets shows the rank based on its statistical score. For example, it is difficult to rank these models with eyeball method the statistical scores rank ARA05, ARA02, and ARA06 as top three performing simulations for this event. One can also notice that in this case the ensemble is outperforming the operational C-LAEF control member. This also highlights the importance and benefit of the use of ensemble system for such applications.

3 Summary & Outlook

The statistical analysis shows that the C-LAEF reanalysis ensemble has the ability to simulate extreme precipitation events with good accuracy, however, spatial and temporal shifts are observed. These results also indicate that our reanalysis ensemble is performing at par with our operational models. Further evaluations are on-going e.g. 3D evaluation by using a Radar and comparison with novel WegenerNet data.

We are planning on extending this product beyond 2023 and hope to add it to our list of operational products. Moreover, our intention is to use this data to create extreme forecast index (EFI), evaluate NWP models, calibrate and train statistical and AI based algorithms. There are several other cross cutting ventures in pipeline e.g. using this dataset for forecasting renewable energy generation, in agriculture, hydrology, aviation, tourism etc.

We are also in contact with stake holder groups and potential end user's which include, Meteo France, TeamX, CORDEX-FPS, as well as national Austrian universities. We extend a warm welcome to any potential end users or future collaborators. For queries please contact nauman.awan@geosphere.at.

4 References

- Bellus, M., Wang, Y. and Meier, F. (2016): Perturbing surface initial conditions in a regional ensemble prediction system. *Monthly Weather Review*, 144, 3377–3390. <https://doi.org/10.1175/MWR-D-16-0038.1>.
- Bouttier, F., Raynaud, L., Nuissier, O. and Ménétrier, B. (2016) Sensitivity of the AROME ensemble to initial and surface perturbations during HyMeX. *Quart. J. Roy. Meteor. Soc.* 142, 390-403, <https://doi.org/>
- Haiden, T., Kann, A., Wittmann, C., Pistotnik, G., Bica, B., and Gruber, C. (2011): The Integrated Nowcasting through Comprehensive Analysis (INCA) System and Its Validation over the Eastern Alpine Region, *Weather Forecast.*, 26, 166–183, <https://doi.org/10.1175/2010WAF2222451.1>, 2011
- Hersbach H, Bell B, Berrisford, P, et al. (2020): The ERA5 global reanalysis. *Q J R Meteorol Soc.* 2020; 146: 1999–2049. <https://doi.org/10.1002/qj.3803>
- Keresturi, E., Wang, Y., Meier, F., Weidle, F., Wittmann, C. and Atencia, A. (2019): Improving initial condition perturbations in a convection-permitting ensemble prediction system. *Quarterly Journal of the Royal Meteorological Society*, 145, 993–1012. <https://doi.org/10.1002/qj.3473>.
- Kirchengast, G., Kabas, T., Leuprecht, A., Bichler, C., and Truhetz, H. (2014): WegenerNet: A Pioneering High-Resolution Network for Monitoring Weather and Climate, *B. Am. Meteorol. Soc.*, 95, 227–242, <https://doi.org/10.1175/BAMS-D-11-00161.1>, 2014.
- Seity, Y., P. Brousseau, S. Malardel, G. Hello, P. Bénard, F. Bouttier, C. Lac, and V. Masson, 2011: The AROME-France Convective-Scale Operational Model. *Mon. Wea. Rev.*, 139, 976–991, <https://doi.org/10.1175/2010MWR3425.1>.
- Wastl C., Y. Wang, A. Atencia, F. Weidle, C. Wittmann, C. Zingerle, E. Keresturi, 2021: CLAEF: Convection-permitting Limited-Area Ensemble Forecasting system. *Quarterly Journal of the Royal Meteorological Society*, 147: 1431-1451, <https://doi.org/10.1002/qj.3986>
- Wastl, C., Wang, Y., Atencia, A. and Wittmann, C. (2019a) Independent perturbations for physics parameterization tendencies in a convection permitting ensemble. *Geoscientific Model Development*, 12, 261–273. <https://doi.org/10.5194/gmd-12-261-2019>.
- Wastl, C., Wang, Y., Atencia, A. and Wittmann, C. (2019b) A hybrid stochastically perturbed parametrization scheme in a convection permitting ensemble. *Monthly Weather Review*, 147, 2217–2230. <https://doi.org/10.1175/MWR-D-18-0415.1>

Evaluation of Surfex/TEB offline over the city of Algiers: a first step toward high-resolution operational forecast

Nour El Isslam Kerroumi¹, Rafiq Hamdi²

⁽¹⁾Numerical Weather Prediction Department, Office Nationale de la Météorologie, Algiers,ALGERIA.

⁽²⁾ Climate modeling and impact studies Unit, Royal Meteorological Institute, Brussels,BELGIUM.

1 Introduction

This report documents a research journey in Brussels, Belgium, within the ACCORD consortium. Our focus lay in evaluating Surfex Offline version 8.1 with the Town Energy Balance (TEB) scheme turn on over Algiers city.

Surfex, an externalized surface model, plays a crucial role in numerical weather prediction and environmental studies. The integration of the TEB scheme promises improved representation of urban processes. Our objectives involved using Surfex offline for urban meteorological forecasts over Algiers city and comparing Surfex offline to Surfex coupled inline with the AROME atmospheric model within two setups: “Ideal” where both the online and offline set-up of SURFEX uses the same grid resolution of 500m, and “Operational” where the initialization and forcing of the offline set-up of SURFEX comes from the operational configuration AROME 3km. This report elucidates our methodologies, presents the results and their interpretations, offers conclusions, and references.

2 Methodology

1.Data Observation:

Meteorological observations from five stations situated in Algiers city within the Meteo-Algerie network, namely Kouba, Mehalma, Reghaia, Ain Benian, and Baraki, were collected. These observations encompassed standard variables, including temperature, humidity, wind direction, and wind speed, recorded at hourly intervals for the months of January and July 2023.

In our study, meteorological observations were obtained exclusively from the Kouba automatic meteorological station, selected based on its urban characteristics determined through the calculation of the land cover (Cover 7: Urban and built-up.) from the PGD file using “EcoClimap v1.6” data (Table1).

Table 1: Urban and built-up Cover fraction.

station	Kouba	Ain Benian	Reghia	Mehalma	Baraki
FRAC_Town	1	0	0	0	0

This meticulous selection ensures that the data used for model validation aligns with urban settings, enhancing the relevance and accuracy of our research findings. The other 4 stations were used for the

second part of this study where these observations were used to compute the scores in an operational set-up (see section 3).

The figure 1 shows the geographic location of the five station from google earth to see better the fraction of each station, it looks only the kouba station that has an urban character.



Figure 1: geographic location of the five stations

2. AROME configurations:

In order to realize this work, three AROME configurations were established within two distinct setups. The first setup, considered as the Ideal setup, involves both the online and offline set-up of SURFEX using the same grid resolution of 500m. In the second setup, referred to as the Operational setup, the initialization and forcing for the offline SURFEX setup are derived from the operational configuration of AROME at a resolution of 3km.

- **Ideal Setup :**

We set up an AROME configuration with 0.5 km of resolution and 90 vertical levels. This allowed us to obtain high-resolution data considered as the reference urban simulations over the study area. The table 2 show the characteristics of this AROME configuration:

Table 2: AROME configurations characteristics for Ideal Setup.

Characteristics	AROME 500m
Cycle	CY46T1.bf.07
Initial Conditions	Operational Coupling (ALADIN 6Km) [2]
Coupling frequency	1h
Horizontal resolution	0.5 km x 0.5 km
Vertical resolution	90 Levels
Time-step	10 s
First level from ground	5 meters
Grid	241x 241
Lead Time	24 hours
Domain	Center : 3.2°E – 36.5°N Latitude : 35.9°N – 37.1°N Longitude : 2.6°E – 3.8°E

- Operational Setup:**

We set up two AROME configurations, the first which is the AROME operational configuration with 3km of resolution and 41 vertical levels (Sara Chikhi and al [2]), we use this configuration to initialize Surfex offline with the files as surfex inline with AROME. The second one which is a fullpos AROME configuration with 500m of resolution and 41 vertical levels. This configuration is used to have a Fullpos with the same offline domain resolution and also to improve the forcing files with a better interpolation method. The table 3 show the characteristics of the two AROME configurations:

Table 3: AROME configurations characteristics for Operational Setup.

Characteristics	AROME 3km	AROME fullpos 500m
Cycle	CY43T2.bf.03	CY43T2.bf.03
Initial Conditions	Coupling (ALADIN 6Km)	AROME 3km historical outputs
Coupling frequency	1h	1h
Horizontal resolution	3 km x 3 km	500m x 500m
Vertical resolution	41 Levels	41 Levels
Time-step	180 s	180s
First level from ground	17 meters	17 meters
Grid	400x 400	300 x 300
Lead Time	24 hours	24 hours
Domain	Center : 3°E – 34°N Latitude : 28°N – 40°N Longitude : 3°W – 9°E	Center : 3°12'E – 36°30'N Latitude:35°45'N– 37°14'42''N Longitude:2°26'42''E– 3°57'E

3. Surfex offline simulations inputs :

The figure 2 displays a diagram illustrating the various input files required to perform surfex offline simulations, along with the respective methods used in their creation :

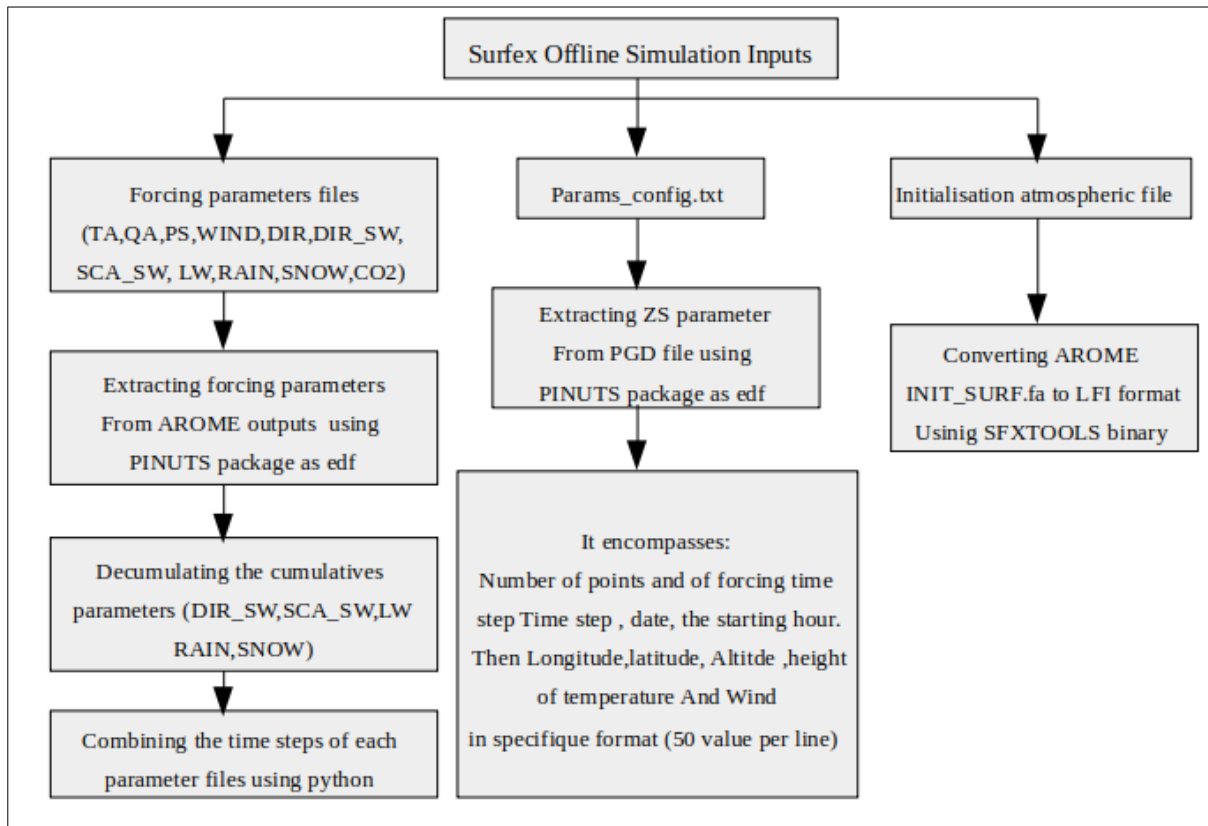


Figure 2: Surfex offline Simulation inputs diagramme.

- **Extracting forcing parameters:**

The parameters we included in the extraction process are atmospheric temperature (TA), atmospheric humidity (QA), atmospheric pressure (PS), rain (RAIN), snow precipitation (SNOW), wind speed (WIND), wind direction (DIR), long-wave radiation (LW), direct short-wave radiation (DIR_SW), diffuse short-wave radiation (SCA_SW), and near surface CO2 concentration (CO2).

We extract the “I” zone of these parameters from the AROME model historical outputs "ICMSH" using PINUTS package with edf tool and We have chosen 50 meters as the height of wind and temperature forcing.

- **Combining parameter files:**

We created a Python script that combines the individual parameter files (for all days each time step) into a single file. This script reads the contents of each parameter file and extracts the data, which is then written to a new file called **Forc_(name of the forcing parameter).txt**.

In order to study the impact of the initialisation on the TEB, we run two different surfex offline simulations (daily and monthly) for january and july 2023, we combined the parameter files of each day separatly for the daily simulation and the parameter files of all the month for

the monthly simulation. These files are specifically designed to force the SURFEX offline simulations.

- **Creation of Params_config File:**

The Params_config.txt file serves as a critical component for the coupling of AROME and SURFEX. This file is generated by consolidating information from various sources and is essential for configuring the model coupling. In our study, the Params_config.txt file encompasses the following crucial details:

- **Number of Points:** This parameter specifies the total number of grid points in our study domain, totaling 90,000 grid points.
- **Forcing Time Steps:** We define the number of forcing time steps during the run, which directly influences the temporal resolution of our simulations.
- **Forcing Time Step (seconds):** The time interval between consecutive forcing time steps is set to 3,600 seconds (1 hour) in our configurations.
- **Date and Time Information:** The Params_config.txt file includes date and time information, including the year, month, day, and the starting hour (in seconds) of the simulation.

In addition to the temporal parameters, the Params_config.txt file contains essential spatial and atmospheric properties for each grid point:

- **Longitude, Latitude, and Altitude:** The file specifies the longitude, latitude, and altitude of each grid point. These values are derived from the extracted parameter "ZS" from the PGD file. We have adjusted the format to adhere to the specific requirements of SURFEX source code by modifying the routine in "src/OFFLIN/ol_read_atm_conf_ascii.F90". Our modification introduced spaces between each value «FMT='(50(F15.8),1X)'», ensuring compatibility with our Python script.
- **Height of Temperature and Wind Forcing:** For temperature and wind forcing, we have defined a height of 50 meters.

By meticulously incorporating these details into the Params_config.txt file, we establish a robust connection between AROME's atmospheric model outputs and the corresponding grid points and atmospheric properties within SURFEX. This alignment ensures the accuracy of land surface simulations in our research.

4. FA to LFI Conversion:

To create a PREP file using an AROME atmospheric output, We faced the challenge of converting AROME outputs from the FA format to the LFI format, which is the required atmospheric file format for Surfex Offline v8.1, as specified in the SURFEX user guide. To accomplish this conversion, we utilized the binary SFXTOOLS tool generated on the Cy43T2 pack, following these steps:

```
./SFXTOOLS sfxfa2lfi -sfx-fa—file INIT_SURF.fa -sfx-file-file INIT_SURF.lfi
```

5. Simulations:

Table 4 provides a summary of the land surface model simulations conducted for the months of January and July 2023, encompassing various configurations to assess the performance of Surfex offline. The simulations are categorized based on simulation type, resolution, and initialization source, shedding light on the diverse scenarios investigated. It is noteworthy that the offline simulations were performed at both daily and monthly temporal scales, offering a comprehensive evaluation of the model's behavior. The table aims to offer a concise overview of the research scope, guiding readers through the key simulation setups explored in this study.

Table 4: Summary of Land Surface Model Simulations for January and July 2023.

Setup	Simulation	Type	Coupling files	Forcing File Source	Resolution	Initialization File
Ideal	Simulation 1	Online (AROME Coupled)	ALADIN 6km	/	500m	AROME 500m
	Simulation 2	Surfex Offline	/	AROME 500m	500m	AROME 500m
Operational	Simulation 3	Surfex Offline	/	AROME fullpos 500m	500m	AROME 3km
	Simulation 4	Surfex Online (AROME Coupled)	ALADIN 6km	/	3km	AROME 3km

3 Results

1. Ideal Setup:

The Ideal Setup serves as a controlled environment for evaluating Surfex Offline's performance when both the initialization and forcing data match the same grid resolution of the Surfex Online coupled with AROME model where grid resolutions is the same (500m). This setup allows for a systematic exploration of how grid consistency impacts model outcomes, with a particular focus on the variable temperature. After running the three simulations online, daily offline “offline” and a continuous offline “offline month” of the two month january and july 2023 in this setup, the figures 2 and 3 show the calculated Bias and the Rmse against to the observation data:

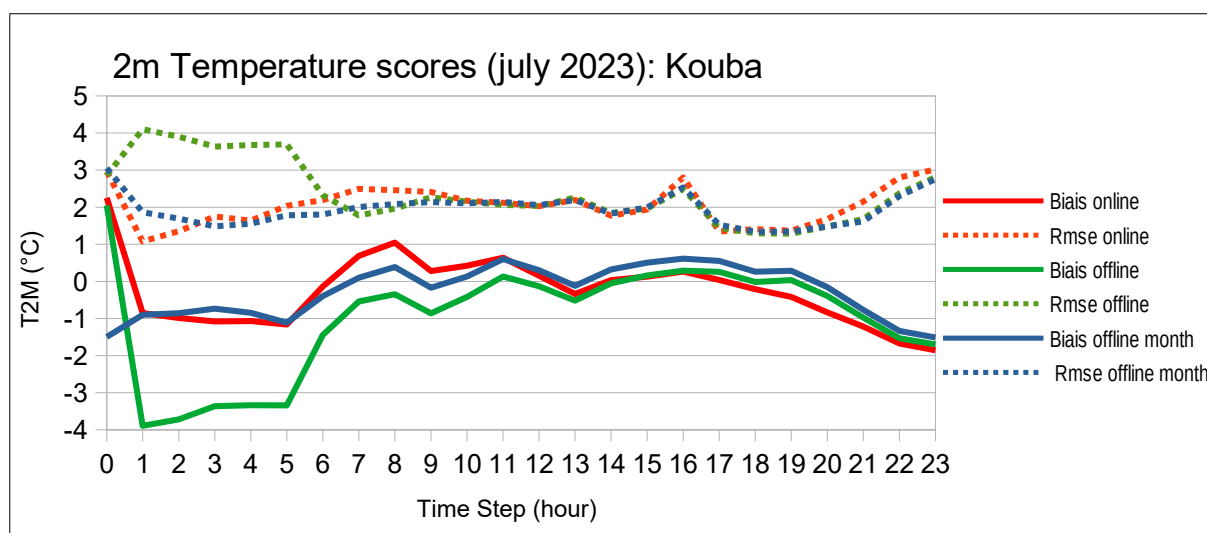


Figure 3: Statistical scores of 2-m temperature against observations at the Kouba station of July for Surfex online, offline and offline month simulations.

Figure 3 presents the scores obtained for the Kouba station which is situated some 10 km East of the center of Algiers in an urban area (36.7166N, 03.1E) for July, In both the online and offline simulations, a significant discrepancy is observed between the 1st and 2nd time steps. This discrepancy is attributed to the suboptimal initialization, as these 'init surf' data are generated by ALADIN 6km historical files, a phase known as 'Spinup'. Over time and with the forcing files, the offline model gradually reduces this disparity. To mitigate the effects of initialization, we conducted an offline continuous simulation called 'offline month' for the entire month of July. It is evident that the scores from the 'offline month' simulation are as favourable as those from both the online and offline simulations and we see also that the “Spinup” phase doesn’t exist.

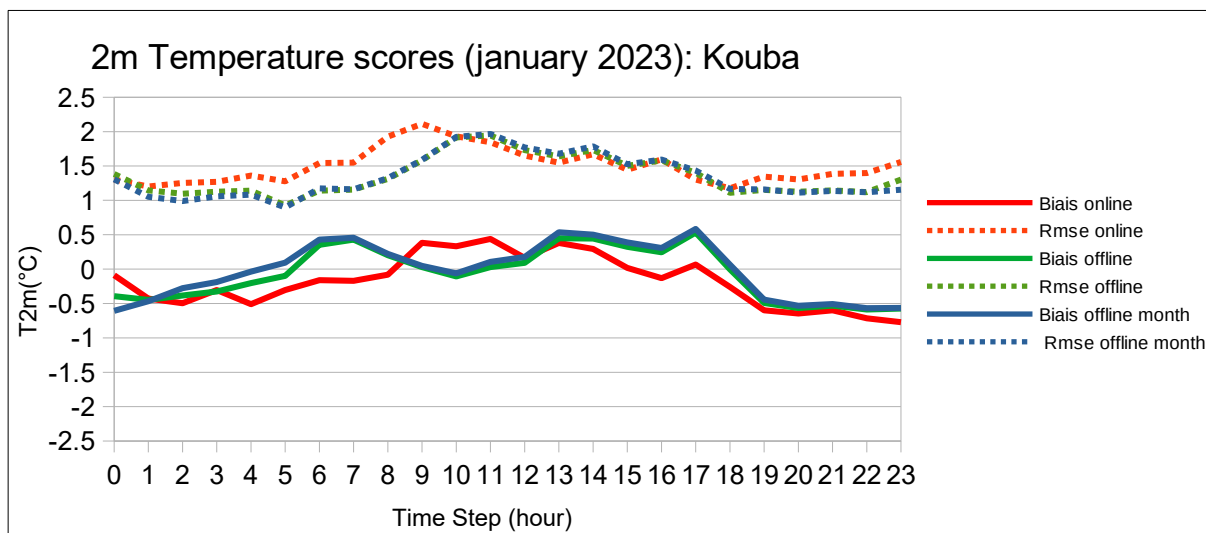


Figure 4: Statistical scores of 2-m temperature against observations at the Kouba station for January for Surfex online, Surfex offline and Surfex offline month simulations.

Figure 4 presents the scores obtained for the Kouba station for January, we see that both offline simulations represent better scores than the online simulation. We notice too that the discrepancy observed between the 1st and 2nd time steps is very small which means, in the winter, the impact of the initialization is relatively weak.

2. Operational Setup:

The Operational Setup serves as a controlled environment for evaluating Surfex Offline's performance when the initialization from the operational configuration AROME 3km and forcing data comes from the AROME fullpos configuration at 500m. This setup allows for a direct comparison with Surfex Online, which is coupled with AROME at 3km of resolution. In this scenario, we examine how well Surfex Offline replicates land surface processes when it operates under conditions reflective of operational meteorological configurations. The primary focus is on assessing the impact of using data from different grid resolutions on the model's performance within this setup.

After running the three simulations online, offline and a continuous offline of the two month january and july 2023 in this Setup, the figures 4 and 5 show the calculated Bias and the Rmse against the observation data:

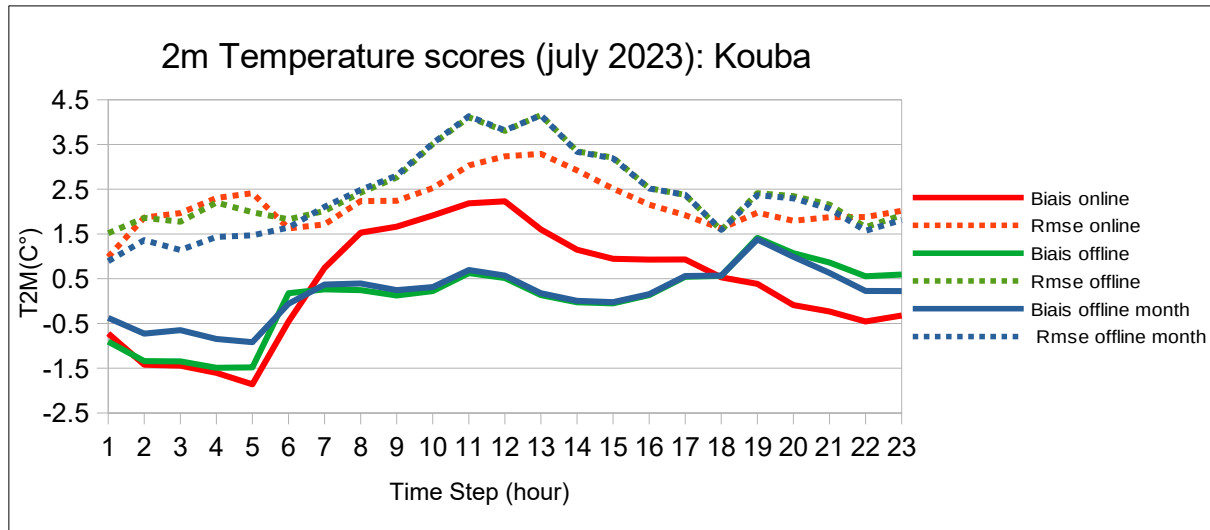


Figure 5: Statistical scores of 2-m temperature against observations at the Kouba station for July for Surfex online, Surfex offline and Surfex offline month simulations.

Figure 5 illustrates the scores obtained at the Kouba station for July, showcasing the evaluation of 2-meter temperature simulations. The assessment reveals that the model generally exhibits good conformity with observed values. Notably, a consistent negative Bias implies a tendency to underestimate temperatures, especially during nighttime hours. Despite this systematic tendency, the Root Mean Square Error (RMSE) values maintain a relatively low level, indicating an overall satisfactory fit. Diurnal patterns in model performance become apparent, with heightened discrepancies during nighttime. Furthermore, the comparison between offline and online simulations reveals consistent trends, demonstrating that offline simulations consistently outperform online simulations.

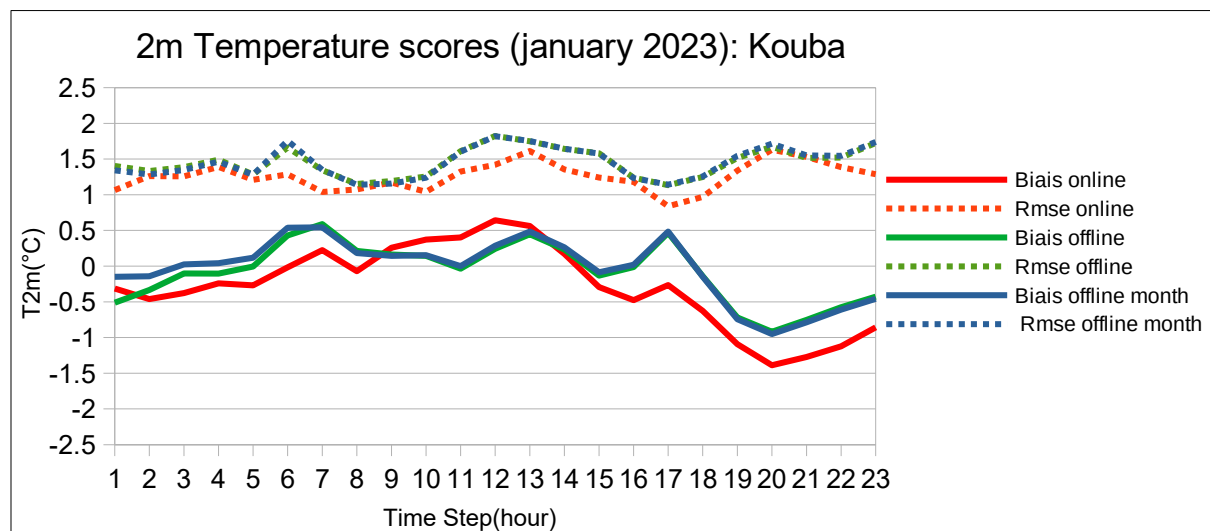


Figure 6: Statistical scores of 2-m temperature against observations at the Kouba station for January for Surfex online, Surfex offline and Surfex offline month simulations.

Figure 6 presents the scores obtained for the Kouba station for the month of January, the assessment of 2-meter temperature simulations at the Kouba station presents key findings. The model generally exhibits a reasonable agreement with observed values, as evidenced by consistently low Root Mean Square Error (RMSE) values. Noteworthy is the consistent negative Bias during various hours, indicating a tendency to underestimate temperatures, particularly during nighttime. The hourly analysis unveils diurnal patterns in model performance, with increased discrepancies observed during nighttime hours. In the comparison between offline and online simulations, it is evident that both represent better scores than the online simulation, with offline simulations consistently outperforming

online simulations. The minimal discrepancy observed between the 1st and 2nd time steps implies a relatively weak impact of initialization and low radiative fluxes during winter, further emphasizing the model's robustness in capturing temperature dynamics at Kouba station during January.

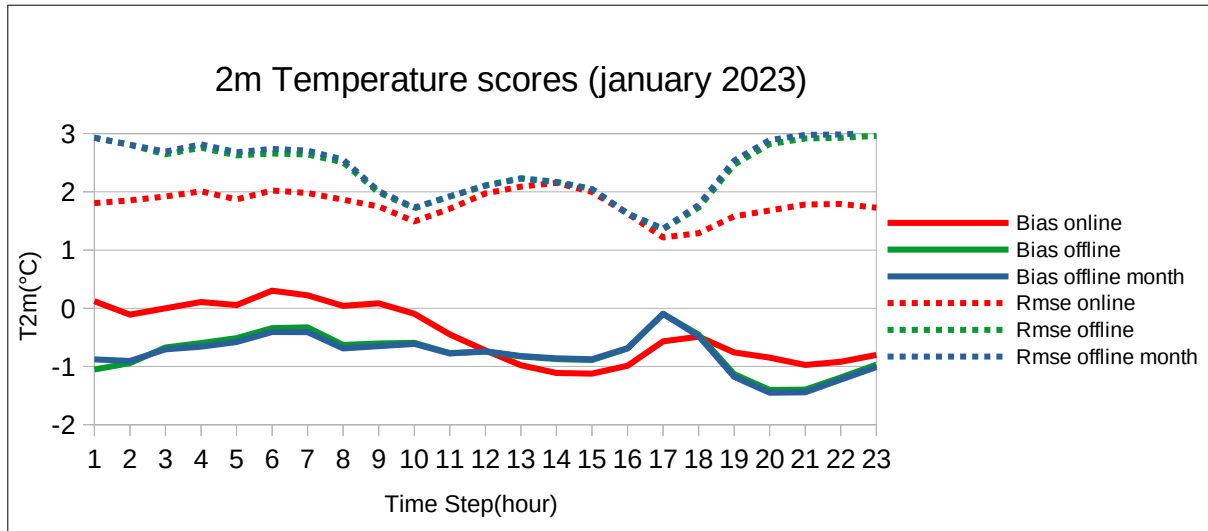


Figure 7: Statistical mean scores of 2-m temperature against observations for January for Surfex online, Surfex offline and Surfex offline month simulations across the five stations.

Figure 7 presents the mean scores across five stations (Ain Benian, Baraki, Mehalma, Kouba, and Reghaia) were calculated for the month of January, In terms of Bias, both online and offline simulations generally show a consistent pattern of underestimation, indicated by negative values. it is crucial to note that the underestimation pattern observed, particularly in the offline simulations, may be attributed to the fact that the analyzed stations (Ain Benian, Baraki, Mehalma, and Reghaia) are non-urban. Furthermore, Surfex offline treats these stations as rural, and during the winter season, rural areas tend to be colder than urban areas. Consequently, the more substantial negative Bias values in the offline simulations may stem from this distinction, where the model, considering these stations as rural, systematically underestimates temperatures. Similarly, the RMSE values, reflecting the overall fit of the model, vary across stations and hours. While both online and offline simulations exhibit relatively low RMSE values, offline simulations often result in slightly higher RMSE values than their online counterparts. This trend is consistent across the studied stations, highlighting the nuanced performance of the model.

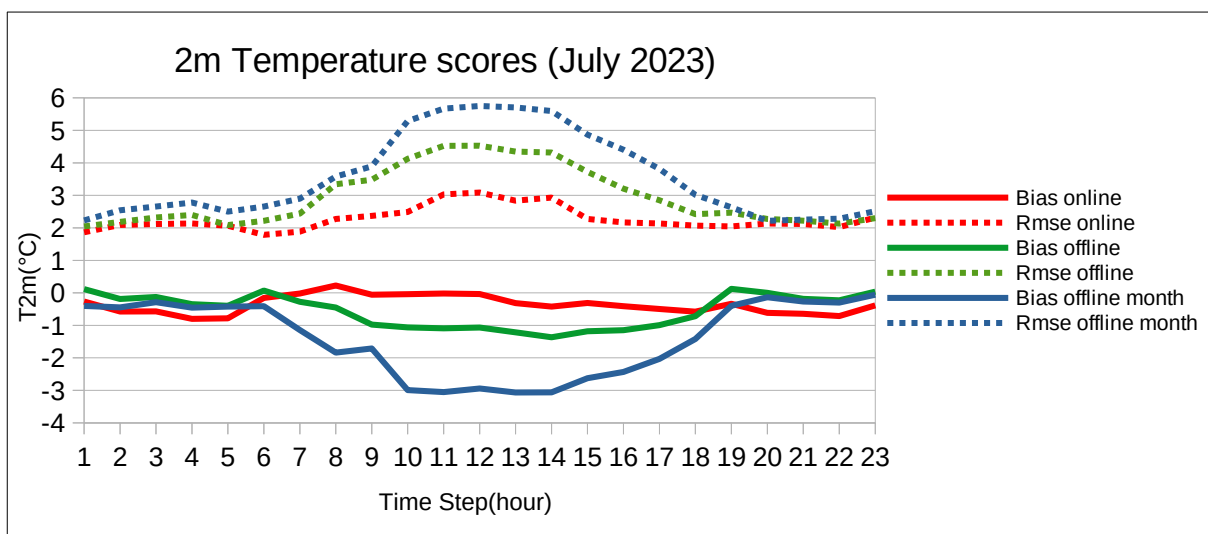


Figure 8: Statistical mean scores of 2-m temperature against observations of July for Surfex online, offline and offline month simulations across the five stations.

Figure 8 presents the mean scores across five stations (Ain Benian, Baraki, Mehalma, Kouba, and Reghaia) were calculated for the month of July, In terms of Bias, both online and offline simulations consistently exhibit negative values, indicating an overall tendency to underestimate temperatures across all stations. It is crucial to note that the underestimation pattern observed, particularly in the offline simulations, may be attributed to the fact that the analyzed stations (Ain Benian, Baraki, Mehalma, and Reghaia) are non-urban. Furthermore, Surfex offline treats these stations as rural, and during the summer season, rural areas tend to be colder than urban areas. Consequently, the more substantial negative Bias values in the offline simulations may stem from this distinction, where the model, considering these stations as rural, systematically underestimates temperatures. The RMSE values, reflecting the overall fit of the model, show variability across stations and hours. Generally, both online and offline simulations yield relatively high RMSE values, with offline simulations often resulting in slightly higher values than their online counterparts. This suggests that while the model captures temperature trends, there are significant discrepancies between simulated and observed values, particularly in the offline simulations.

3. Implementation of Ecoclimap SG:

After running the previous simulations using Ecoclimap v1.6 (1km of resolution), we generated a PGD file with the same domain using the latest version of ECOCLIMAP “Ecoclimap seconde generation” to see how represent the urban cover, it is produced at **300m-resolution**.

We downloaded the land Cover map, the map for the heights of trees, Albedo and Leaf Area Index from the external ftp site: <ftp.umr-cnrm.fr>

The figure 9 represent the sum of LCZ urban covers of ECO-SG and the COVER007 of Ecoclimap v1.6 over our study area. As we see that ECO-SG has more details then Ecoclimap v1.6 about urban cover.

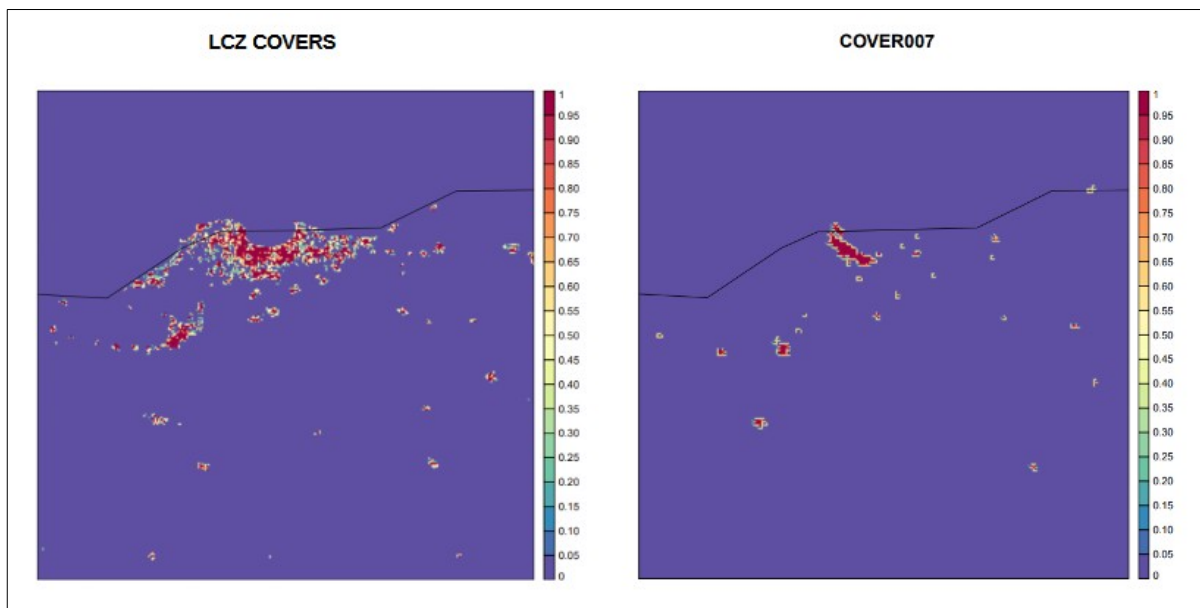


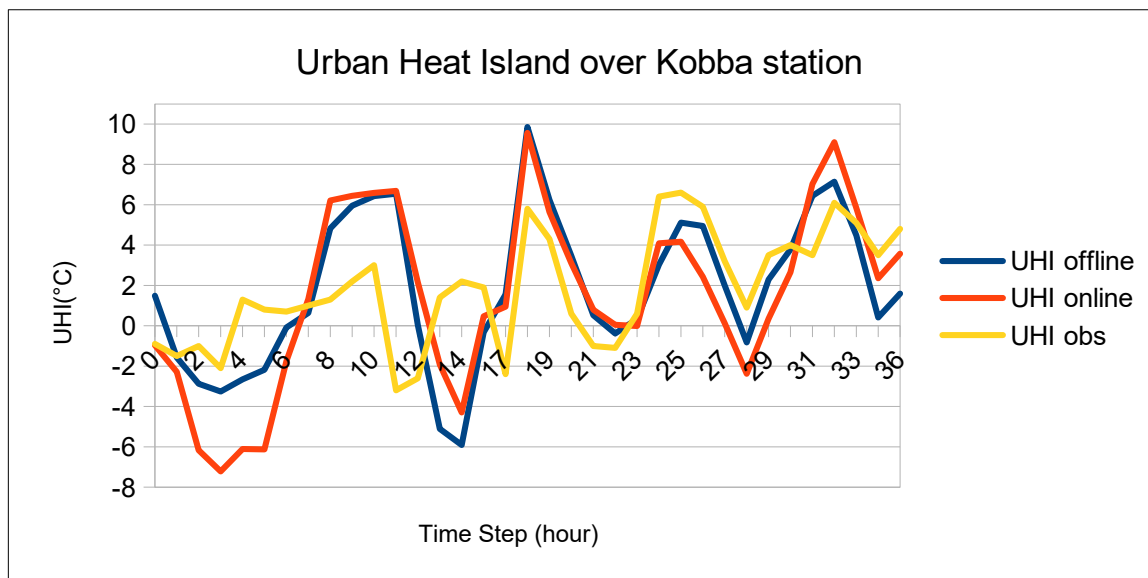
Figure 9: Urban Cover of ECO-SG (left) and Ecoclimap v1.6 (right).

4. Urban heat Island analysis in Algiers:

The strength of the UHI of Algiers is estimated using the 2m temperature simulated (offline and online) and the observed minus the 2m temperature of the rural station Mehalma situated 24km south-west of the urban station Kouba on 11 July 2023.

The figure 10 represents Urban Heat Island (UHI) measurements over Algiers, with Surfex offline and Surfex online. Surfex offline consistently shows positive UHI values, peaking in the afternoon (around hour 18), indicating significant urban warming. In contrast, Surfex online yields generally lower and occasionally negative UHI values, suggesting less pronounced urban warming and even instances of

urban cooling. It appears that Surfex offline illustrates a stronger UHI effect compared to Surfex online.



Figures 10: The time variation on 11 Jul 2023 of the UHI over Algiers defined as the difference between the 2-m temperature at the urban station Kouba and the rural station Mehalma.

4 Conclusion

During my research stay at the Royal Meteorological Institute of Belgium (RMI), significant strides were achieved in the evaluation of Surfex Offline version 8.1 with the Town Energy Balance (TEB) scheme. This study was motivated by the goal of assessing the performance of Surfex Offline v8.1 with TEB, integrated into the numerical weather prediction model AROME, with two configurations: one at a 500m resolution as an ideal setup, and the other at a 3km resolution as an operational setup. This study was focus on five automatic station (Kouba, Ain Benian, Baraki, Mehalma and Reghaia). The results obtained for the two setups for Kouba station, encompassing the months of January and July, showcase promising improvements in 2-meter temperature simulations when compared to observational data in urban areas, These findings lead to the conclusion that Surfex Offline performs a little better then Surfex Online.

Furthermore, the implementation of Ecoclimap Seconde Generation yielded notably superior results, especially in urban land cover, compared to the operational land use data provided by Ecoclimap v1.6. Results from a 36-h case study during a high-heat day (11 July 2023) indicate the urban heat island effect.

In sum, this research has contributed valuable insights into the capabilities and limitations of Surfex Offline in different configurations and scenarios, shedding light on its potential for accurate land surface simulations, particularly in urban environments.

5 References

[1] Hamdi R, Degrauwe D, Termonia P (2012) Coupling the Town Energy Balance (TEB) scheme to an operational limited area NWP model: evaluation for a highly urbanized area, Belgium. *Weather Forecast* 27(2):323–344

[2] Sara Chikhi, Mohamed Mokhtari, Abdenour Ambar, Islam Bousri, Mohamed Arab Benamara “Operational Numerical Weather Prediction Models Verification at Météo Algérie”, ACCORD NL1, pages 25-35, October 2021.

Evaluation of the ALARO temperature forecast for Romania

Mirela Pietriși, Alina Dumitru, Alexandra Crăciun, Simona Tașcu, Raluca Pomaga, Mihaela Neacșu

1 Introduction

This study focuses on the assessment of the temperature forecast of the model ALARO over Romania. The purpose of this evaluation comes in the context of the increase of temperatures observed during last years. In the summer of 2023, southern (July) and southwestern (August) Europe experienced extreme heatwaves and wildfires. In Romania, in summer, autumn and winter months, the average temperatures were significantly higher than the climatological norms (1961 - 2010), especially in southern regions. Figure 1 shows the monthly means of the recorded temperatures for all stations in Romania, as well for the city of Bucharest, which is located in the southern part of the country. In order to evaluate the temperature forecast accuracy from ALARO, a statistical validation was done for the summer months of last year for the operational model versions. Scores were compared to results from data assimilation experiments and the model output statistics (MOS) adaptation forecast.

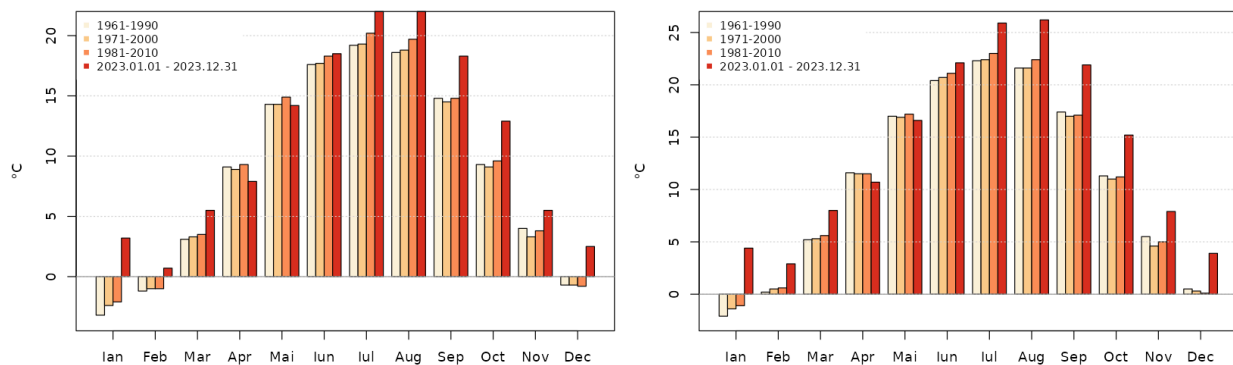


Figure 1: Mean temperatures for each month compared to the climatological norm for Romania (left) and for the city of Bucharest (right); source: MeteoRomania.

2 Statistical validation

2.1 Operational configurations

Currently, our operational applications are based on two configurations of the ALARO model version *cy43t2*. ALARO 6.5 and ALARO 4 differ in horizontal resolution (6.5 km and 4 km respectively), size of the integration domain (the size of the domain for the higher resolution version is larger and more extended to the eastern direction as to cover the whole Black Sea) and physical package, as it is described in Table 1. Figure 2 shows the size and position of the integration domains for each version. Both are

obtained using coupling files that come from the Météo-France global model ARPEGE, with a 3-hour frequency.

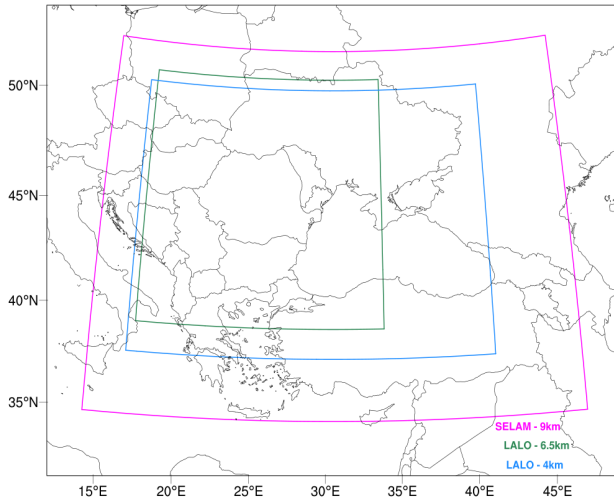


Table 1: Description of the operational configurations.

Name	ALARO 6.5	ALARO 4
Spatial resolution	6.5 km, L60	4 km, L60
Physics package	ALARO-0 baseline	ALARO 1vB
Tstep	240 s	180 s
Grid points	240 x 240	600 x 432

Figure 2: Integration domains for operational model configurations: ALARO 6.5 (in green) and ALARO 4 (in blue).

Concerning the 2 m temperature forecast obtained from ALARO, it was observed that both versions generally overestimate the temperature values, with larger biases over nighttime. Figure 3 shows the monthly bias and RMSE scores for 2 m temperature, for the months June, July and August for ALARO 6.5 and ALARO 4. The verification was done using observation data from 166 meteorological stations in Romania. Very similar pattern was found for all three months. While there is a larger variation of the scores within a day for ALARO 6.5, these differences are slightly smoothed in the ALARO 4 forecast. Since warmest temperatures were recorded in the Southern part of the country, we wanted to focus on how the model forecast behaves for these areas.

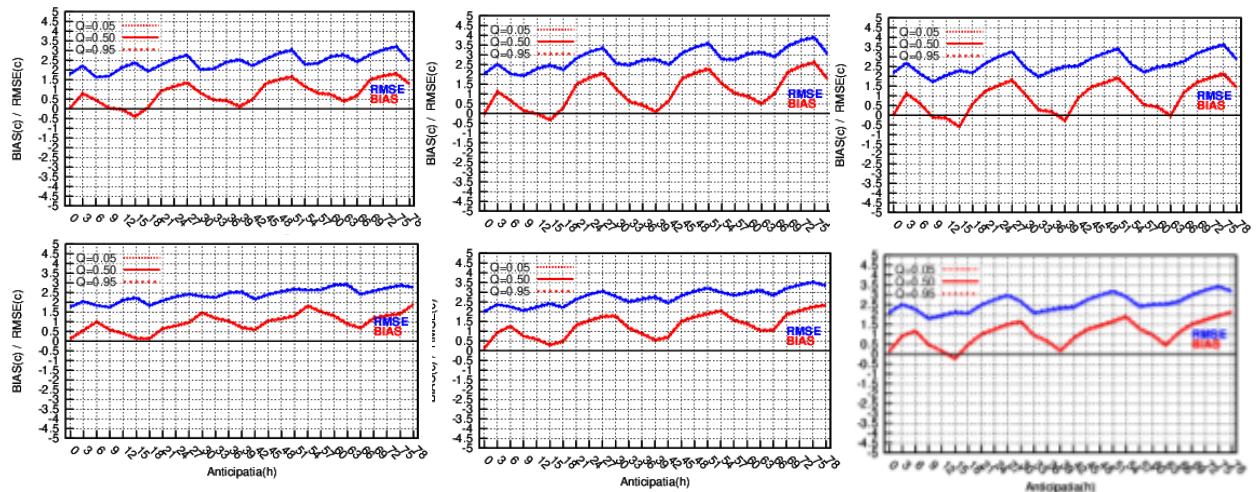


Figure 3: Monthly scores for the summer months (June - left, July - center, August - right) for Romania, for ALARO 6.5 (upper panel) and ALARO 4 (lower panel).

In figure 4 we can see the same scores for three regions that cover the Southern territory: Banat (14 stations), Oltenia (16 stations) and Muntenia (31 stations) for ALARO 4. It was found that the values of the scores (going up to 3.5°C in the bias 4.5°C in the RMSE) are larger in summer months for these regions compared to the whole country. Similar pattern was observed for ALARO 6.5. It seems that the forecast from both configurations follow the pattern found in the forecast from the global model ARPEGE (not shown).

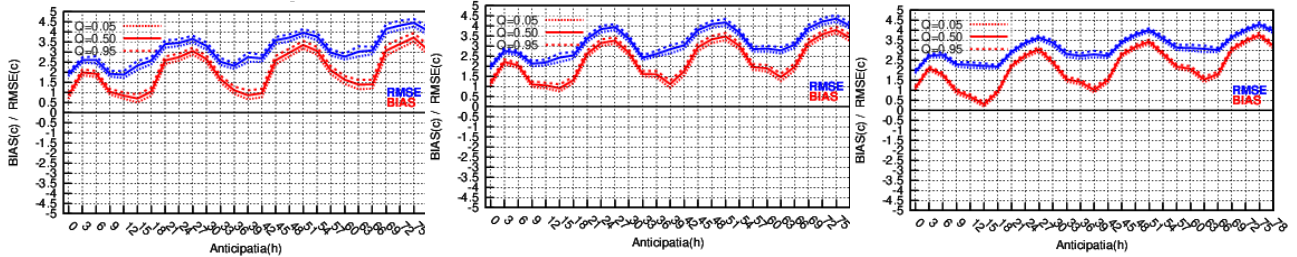


Figure 4: Monthly scores for the regions of: Banat (left), Oltenia (center) and Muntenia (right) for ALARO 4, July 2023.

For going into more detail, Figure 5 shows the boxplots for observed and estimated temperatures for the month of July, for the city of Bucharest which is situated in the center of the Muntenia region. Indeed, we can see the numerically simulated values are larger compared to the observations and that the difference between the two types of data increases with the forecast range.

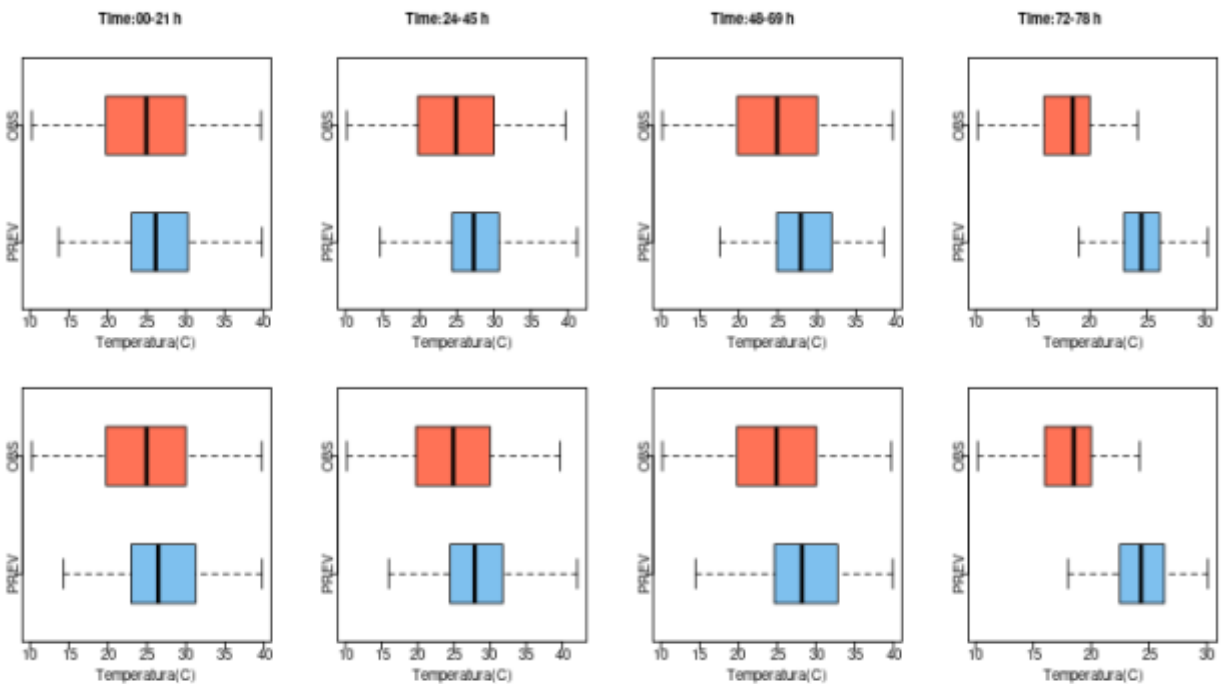


Figure 5: Boxplots for observed (red) and estimated temperatures (blue) for the city of Bucharest for ALARO 6.5 (upper panel) and ALARO 4 (lower panel), for July 2023.

Case study: heatwave 24 - 26 July 2023

The month of July 2023 was extremely warm in southern regions of the country and very warm in the rest of the areas. An important feature of this month was the large number of tropical days (with maximum temperature > 30° C) and nights (minimum temperature > 20° C). One episode of an intense heatwave in July 2023 is presented. The National Meteorological Administration issued a warning (a red vigilance level for the southern regions) for a persistent heatwave and a pronounced thermal discomfort, for the interval 24 - 26th July. The criteria for the heatwave warning was calculated using the daily temperature and the relative humidity. The result was the calculation of the thermal comfort index with the aim of determining the apparent temperature felt by the human body.

Using the Point-Stat tool (included in the MET package software) the verification scores were computed for these days, averaged for all stations. In Figure 6 the mean error (ME) and RMSE scores are shown. It can be seen that, on average, both ALARO versions overestimate the 2 m temperature. Yet, the values of ME score for the ALARO 4 version are slightly higher than the ALARO 6.5, especially for the 26th July when the maximum temperature reached 42° C in the southeastern region (the differences are up to 1.2° C during the day). The RMSE scores show that the accuracy of the ALARO 4 version is slightly higher than the ALARO 6.5 version.

In Figure 7 the same scores are shown, but the model integration has different start dates, valid for 26th July 2023. Therefore, DAY-0 represents the current date (forecast ranges: 00 - 24 h), DAY-1 is the forecast from the previous date (forecast ranges: 24 - 48 h) and DAY-2 represents the forecast from the date before the previous (forecast ranges: 48 - 72 h). The goal is to check the ability of the model to capture the evolution of the 2 m temperature values for the same valid interval that come from different integrations. As expected, it was observed that there is a lead-time dependence of the scores and that the forecast from the current day is usually most accurate. Although we can see that while the ME values are a little lower in the DAY-2 forecast, the RMSE values indicate higher spread of the error for the same forecast.

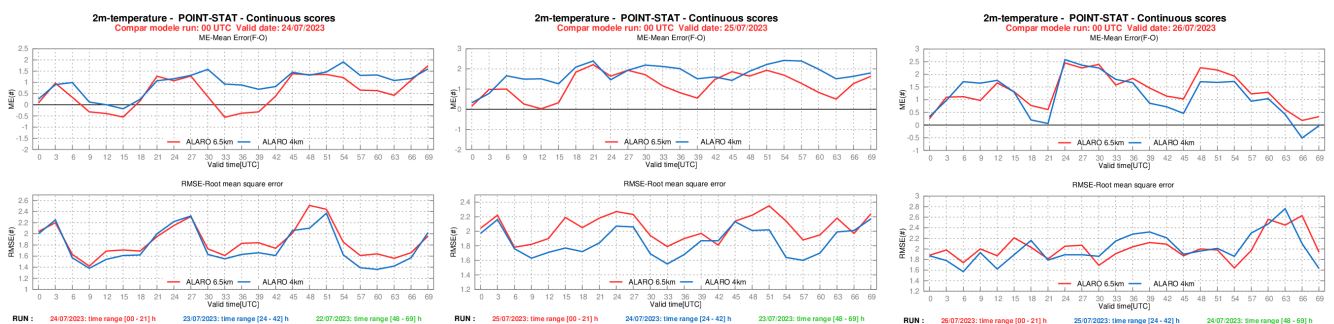


Figure 6: 2 m temperature scores: ME (upper row) and RMSE (lower row) for 24.07.2023 (left), 25.07.2023 (center) and 26.07.2023 (right) for ALARO 6.5 (red line) and ALARO 4 (blue line).

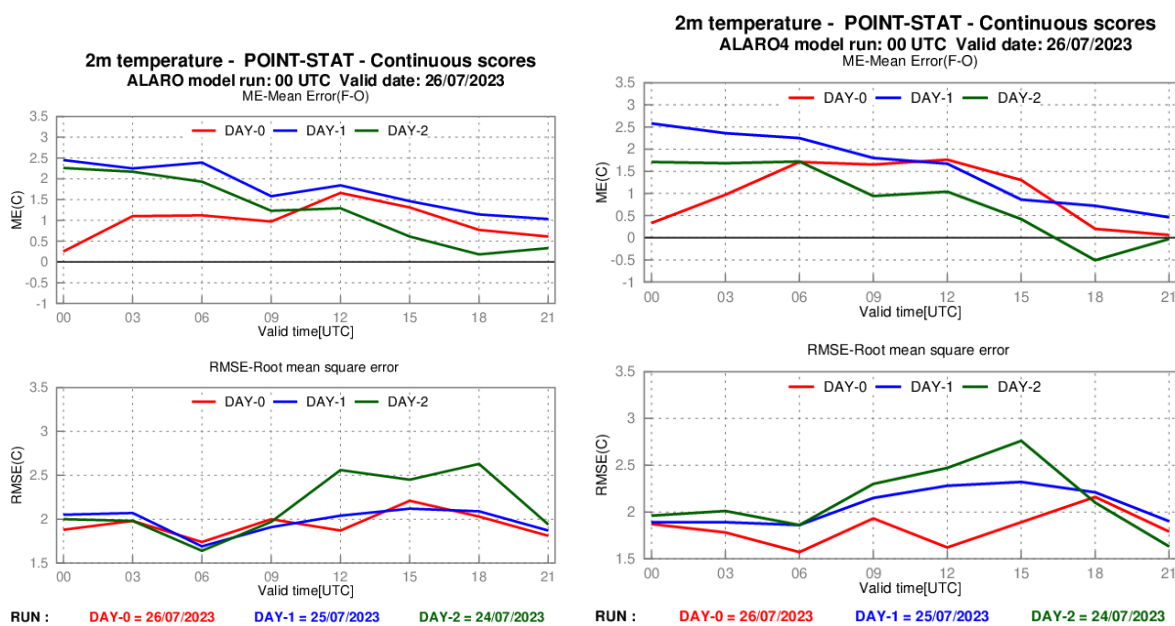


Figure 7: 2 m temperature scores: ME (upper row) and RMSE (lower row) for ALARO 6.5 (left) and ALARO 4 (right) for 26.07.2023.

2.2 Data assimilation

With recent developments regarding the implementation of a data assimilation system locally, a set of experiments was made. They were based on the 4 km horizontal resolution model version, 60 vertical levels with a 6h cycling. Four experiments which used different versions of ISBA polynomes in CANARI, as described in Table 2, were run for July 2023, for all runs and for 30 hours forecast range. In order to observe the impact on the temperature forecast the scores were computed for these experiments.

Table 2: Description of the data assimilation experiments.

Name of experiment	EXP 1	EXP 2	EXP 3	EXP 4
Version of <i>analyse.isba</i> file	Analyse.isba02	Analyse.isba03	Analyse.isba04	Analyse.isba05
Origin	Météo-France	Météo-France	Based on analyse.isba02 file, but the values from fourth column are multiply by 2	Based on analyse.isba03 file, but the values from fourth column are divided by 2

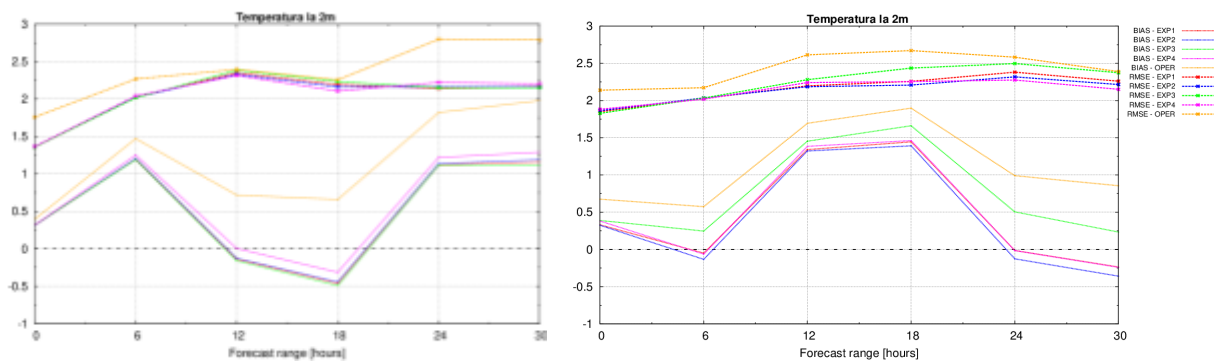


Figure 8: BIAS (continuous lines) and RMSE (dashed lines) for 2 m temperature, 00 UTC (left) and 12 UTC (right), for July 2023, where orange is the current operational configuration, EXP1 red, EXP2 blue, EXP3 green and EXP4 magenta.

Figure 8 shows the scores obtained for these experiments, for the 00 UTC and 12 UTC runs. It was found that there is an improvement that comes from the data assimilation experiments compared to the operational version, visible in both scores. Between the four experiments, there are only small differences, but we can conclude in this case that EXP 2 seems to lead to the most accurate results. The conclusion remains the same for both runs, though it is worth noticing the different pattern in the RMSE scores between 00 UTC and 12 UTC in the data assimilation experiments.

2.3 MOS forecast

A further step was to analyze how the statistical adaptation of the model forecast behaves for these situations and if it is able to reduce the error we encountered. For this purpose, the values estimated from the MOS approach, which is operationally available for the forecasters, were evaluated. The mean error and RMSE were computed for the summer months for 2 m temperature and extreme temperature for all stations in Romania. Two MOS estimations are considered, obtained from each of the operational versions of MOS from ALARO.

We can observe in Figure 9 that the mean error is almost completely reduced with MOS, while the RMSE scores are lower compared to the raw model forecast. The values of the scores are very similar between the two versions, slightly larger values in the mean error appears in the MOS for ALARO over daytime. Also, it seems that the maximum temperature is better estimated than the 2 m temperature.

Figure 10 shows the comparison between the MOS and ALARO forecasts for the 2 m temperature. We can see some lower values of the temperatures from some stations, in the southern-western part of the country, for example. In Figure 11 the maximum temperature estimated from ALARO 4 operational and with data assimilation (EXP 2) and the MOS forecast are represented, for the case of 26.07.2023, while the maximum temperatures registered for that day can be seen in Figure 12. It was observed that for the data assimilation experiment, estimated temperatures are slightly decreased compared to the operational version of the model. The MOS forecast seems to overestimate the temperatures compared to the registered maximum values over the south-eastern region for this case.

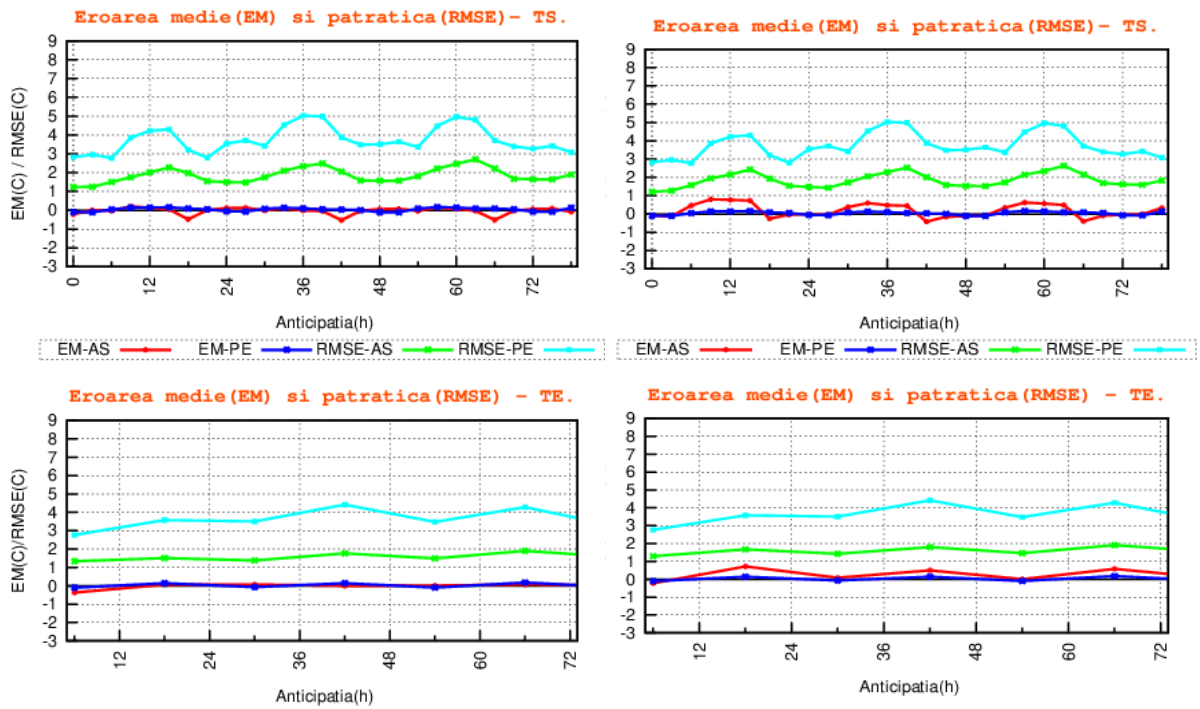


Figure 9: Monthly mean error (red) and RMSE (green) scores for the MOS forecast compared to the persistence method (blue and cyan) for 2 m temperature (upper panel) and extreme temperature (lower panel), July 2023, ALARO 6.5 (left) and ALARO (right).

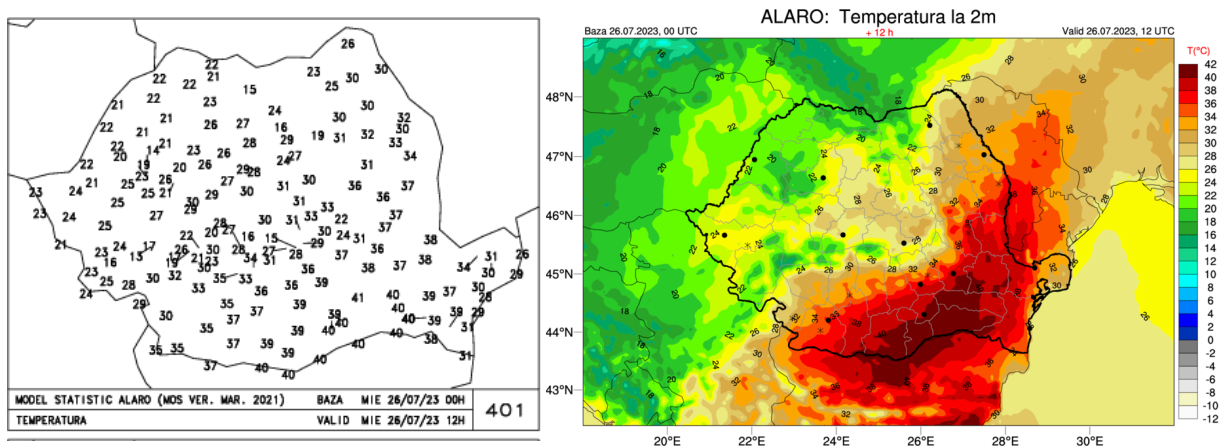


Figure 10: Station-point MOS forecast for temperature (left) and 2 m temperature from ALARO 6.5 (right), 26.07.2023, 12 UTC.

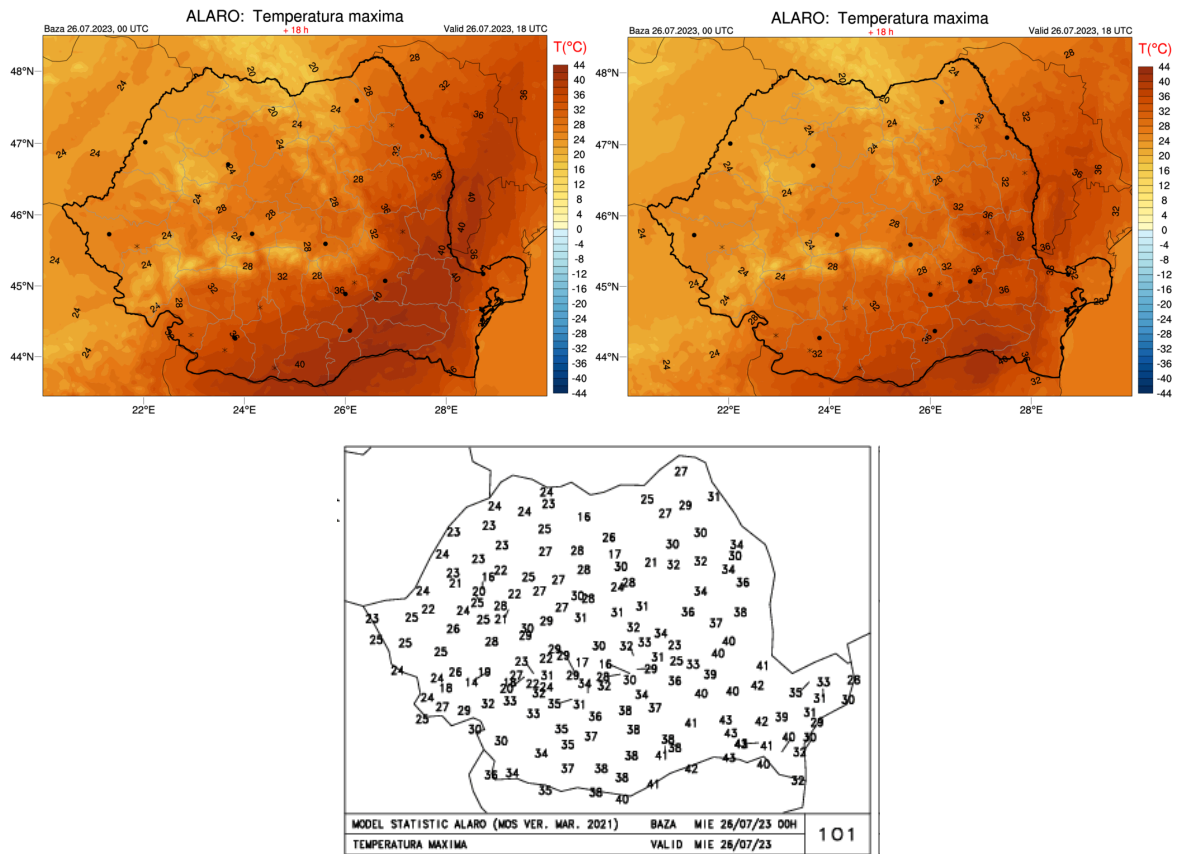


Figure 11: Maximum temperature from ALARO 4 operational (upper left), ALARO 4 with data assimilation EXP 2 (upper right) and station-point MOS forecast for maximum temperature (below), 26.07.2023.

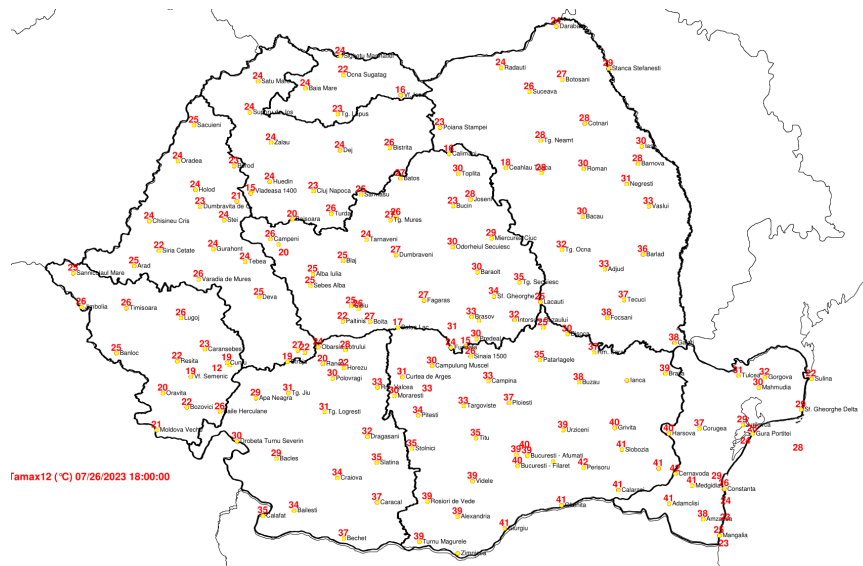


Figure 12: Maximum temperatures registered at meteorological stations in Romania, 26.07.2023; source MeteRomania.

3 Conclusion

The temperature forecast of ALARO was validated for the summer season of 2023 over Romania. An overestimation of these values was found for both configurations we currently run in operational mode, especially in Southern regions of the country. A solution to these shortcomings can be obtained through a data assimilation system that is able to better estimate the temperature in this situation. On the other hand, significant additional information can come from statistical adaptation practices such as MOS.

Evaluation of HARMONIE-AROME cycle 46h1 at AEMET

Gema Morales, Javier Calvo, Joan Campins, María Díez, Pau Escribà, Daniel Martín, Jana Sánchez-Arriola, Samuel Viana y Teresa García

1 Introduction

In June 2023, cy46h1rc1 was released for testing to potentially become the new reference version of the HARMONIE-AROME model. A common test configuration of the deterministic model was agreed upon by HIRLAM members to be run in the different operational domains. After a thorough benchmarking exercise, some conclusions were reached regarding the relevance of adopting cy46 as the operational version. This report presents a description of the main characteristics of the new version and comparison to the reference version cy43h2.2bf is done. An objective evaluation is then performed based on the results obtained from the AEMET's domain runs.

2 Experimental set up

The experimental setup was prescribed the same for all the domains based on HARMONIE-AROME CY46h1rc1 and conducted by MetCoOp, UWC-W and AEMET. The resolution is 2.5 km, with four cycles per day and hourly output up to 48 hours of forecast. All the experiments had an initial 15-day warm-up period with 3-hour cycling. It was agreed a whole month verification in each one of the four seasons.

Data assimilation was 3DVar analysis with 3hr cycle includes SAPP pre-processing for conventional observations, RADAR reflectivities, GNSS ZTD, AMSUA, MHS, IASI, ASCAT. IFS humidity enters in the blending process (LSMIX) with the ECMWF forecasts. SEVIRI DA was not included in the tests because when the integrations started the cycle 46 was not prepared to assimilate these data.

The experiments were run in local AEMET-ATOS computer system composed of two cluster each with 140 computed nodes mounted on Bull Sequana X440 A5 chasis. Each node with 2 AMD EPYC™7742 processors (64 cores). The peak performance of the system is 1350 TFlops.

SAPP preprocessing is used for conventional observations. Radar data comes from OPERA using BALRAD preprocessing and including Spanish, Portuguese and French radars. The control of the HARMONIE-AROME operational suite is based on ecfLOW.

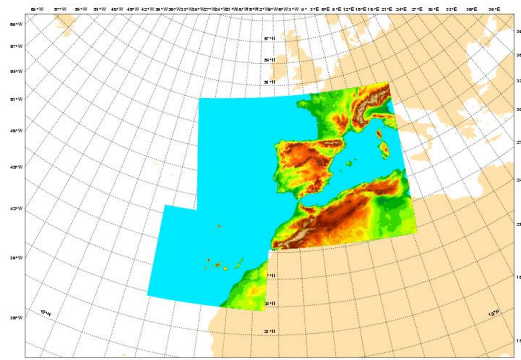


Figure 1: AEMET's operational domain

Cy43h2.2_bf is used as reference (although in AEMET the operational version is based on 43h2.1.1) to allow a cleaner comparison with Metcoop and UWC-W results.

3 Major changes in cycle 46h1

The major changes of cycle 46h1rc1 compared to cycle 43h2_bf are:

- Move back to ECUME instead of ECUME6
- Deactivate FAKETREES for Boreal grassland (not relevant for our domains)
- A more realistic melting of thin snow
- Better initialization of surface fields from IFS BCs taking into account the host model's fraction of land in addition to the land sea mask.
- Use of improved ECOCLIMAP-SG ALBEDO and LAI maps without gaps
- RFRMIN(24)=1 instead of RFRMIN(24)=2.5. A decrease in RFRMIN(24) implies a reduction of the variance term in the statistical cloud scheme producing a reduction of cloud cover (especially in low clouds).

It should be mentioned that HARMONIE-AROME cy46h1 includes the possibility of running the new surface and surface DA schemes: Diffusion Scheme (DIF), Multi Energy Balance (MEB), Multi-layer Snow Scheme (ES), Simplified Extended Kalman Filter (SEKF) and Python API to SURFEX (pysurfex) which are expected to substitute the current Force Restore (FR), Douville95 snow scheme and CANARI in the future. These new options are being intensively tested by members of the surface team and have not been the subject of the validation tests described in this article. Besides, there are a number of improvements in the use of observations in the DA which do not apply to observations included in our operational setup and therefore have not been tested.

4 Meteorological impact

This section discusses the impacts of cy46h1 for the winter season (1st January to 9th February 2021) and the autumn season (11th September to 15th October 2022). The Spring and Summer tests are not analysed here because they include some local deviations from the original release.

In general, the impact is rather neutral. In table 1 it can be seen a summary of the verification results for main surface variables.

Table 1: Summary of the verification results comparing cycle 46h1rc1 with cycle 43h22_bf. Filled triangles mean 90% confidence.

	Winter	Autumn
MSLP	⋯	△
T 2m	▼	⋯
10m wind	△	⋯
10m gust	△	⋯
Td 2m	▽	⋯
Precipitation	△	⋯

The impact on upper air variables is also neutral, improving in some periods/variables and degrading in others (Fig. 2 as an example). Probably, the most remarkable feature is the negative bias in wind speed in cy46h1.

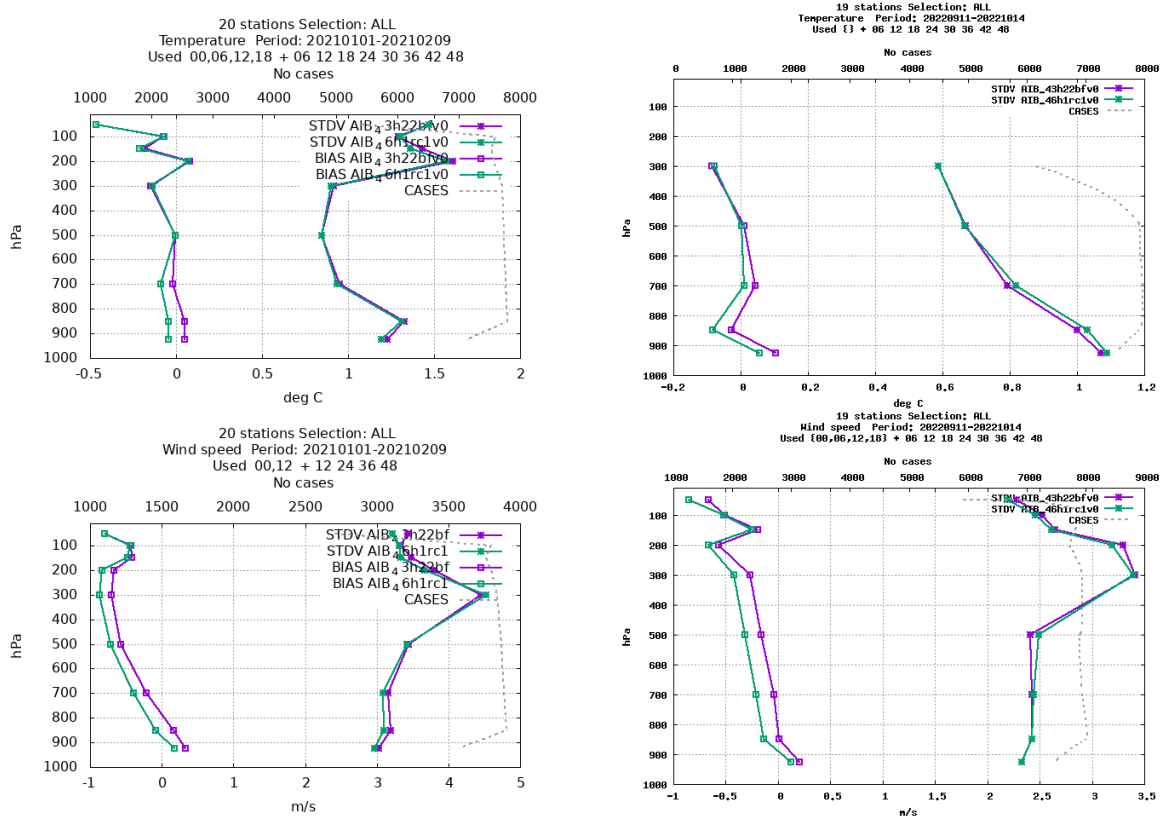


Figure 2. Upper verification at different pressure levels for temperature (upper) and wind speed (lower). Winter period (left) and autumn period (right). Cy43h2.2bf in purple and cy46h.1 in green.

Wind speed

In Fig. 3, the scores for 10m wind can be seen. The problems with wind bias traditionally seen in Aemet domains, remain in this version. The bias is significantly reduced by activating OROTUR (Rontu, 2006) orographic scheme (Fig. 4).

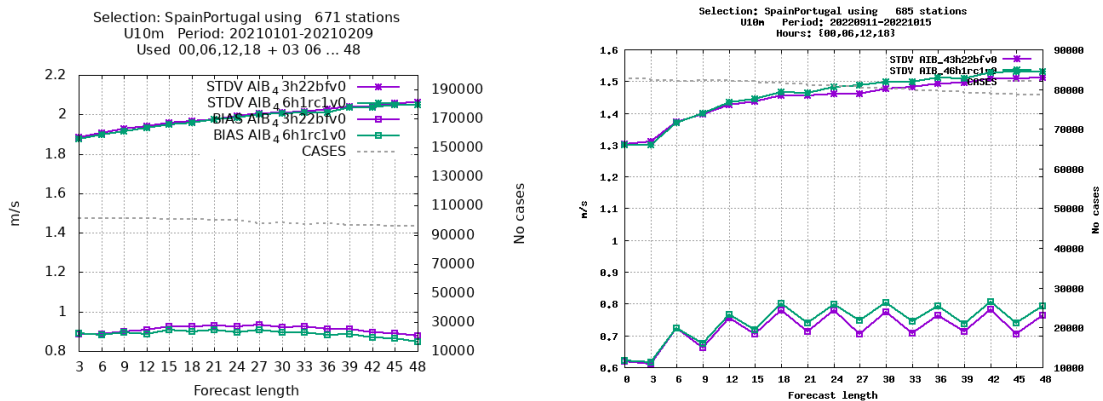


Figure 3. STDV and Bias of 10 m wind function of the forecast length for winter period (left) and autumn (right). Cy43h22 in purple and cy46h1 in green.

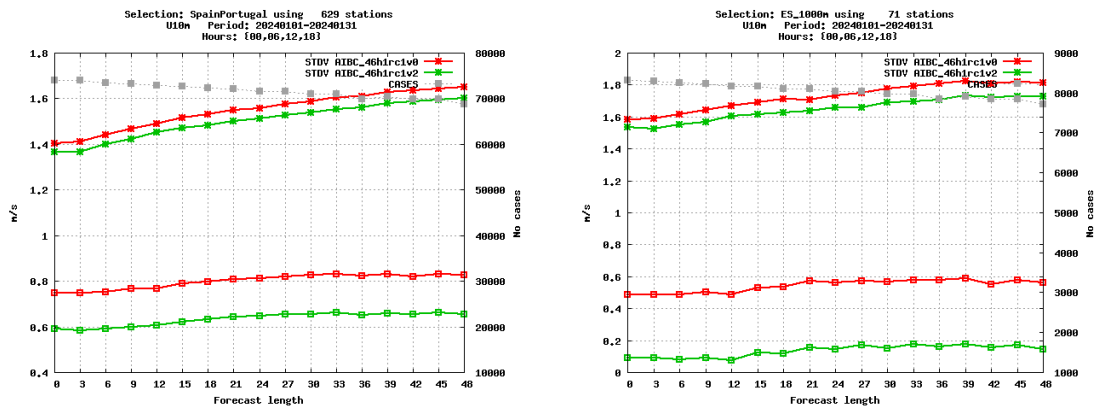


Figure 4. STDV and Bias of 10 m wind function of the forecast length for all Iberian stations (left) and only stations above 1000 m (right). Reference cy46h1 in red and activating OROTUR in green. Evaluation for January 2024 (different period).

Cloud cover and fog

The major impact of the version update is a decrease in cloud cover, especially in low clouds, as can be seen in the verification against SYNOPs (Fig. 5). This is due to a change in the variance term of the cloud scheme. The increase in the STDV can be explained by the impact of the variance term. On the other hand, the bias is much lower in cy46h1.

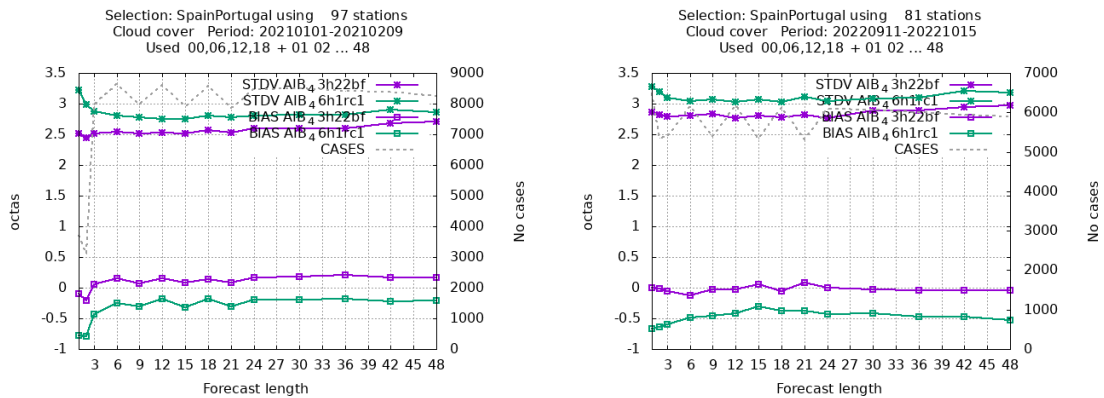


Figure 5. STDV and Bias of cloud cover as a function of the forecast length for winter (left) and autumn (right). cy43h22 in purple and cy46h1 in green.

Whether this decrease of the cloud cover is good or bad is a matter of debate. Besides, objective verification of cloud cover is a difficult task. SYNOP observations tend to overestimate cloud cover when compared with the model variables, which represent a mean value in each grid. We believe that radiation can provide a more accurate assessment of the quality of the model cloud cover. Fig. 6 shows the diurnal cycle of the Direct Normal radiation. Mean values of cy46h1 are closer to the observed values, which suggests a better cloud cover distribution in cy46h1.

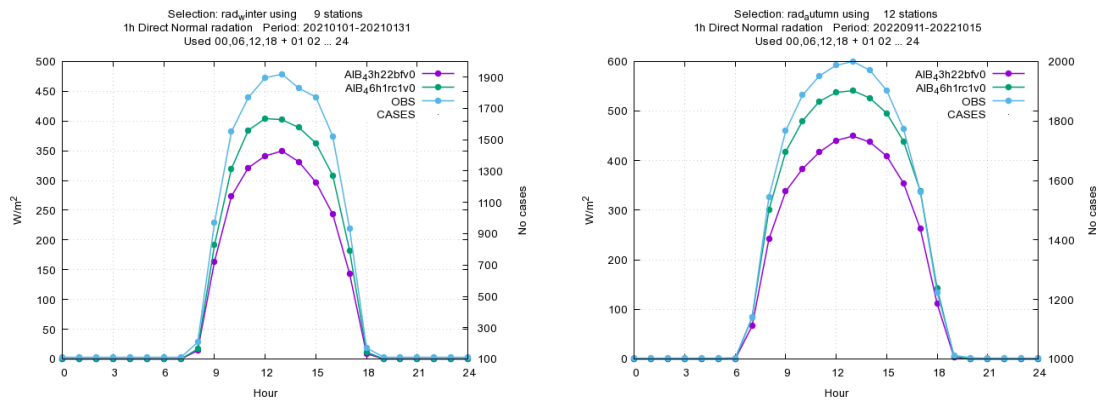


Figure 6. Daily cycle of the Direct Normal Radiation for winter (left) and autumn (right). Cy43h22 in purple and cy46h.1 in green.

A sensitivity test was conducted by changing RFRMIN(24) in cy46h1. The results confirm that the decrease in cloud cover seen in cy46h1 is almost exclusively due to the decrease in this parameter (refer to Figure 7).

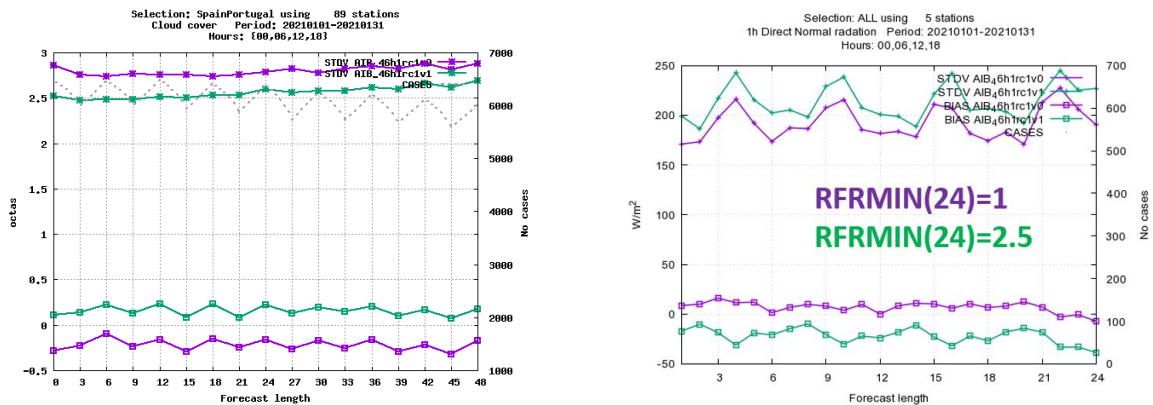


Figure 7. Only for cy64h1, STDV and Bias of Cloud Cover against synops (left) and Direct Normal Radiation as a function of the forecast length (right), for winter season. RFRMIN(24)=1 (pre-defined value) in purple RFRMIN(24)=2.5 in green.

From a subjective evaluation, operational forecasters think that there is an excess of cloud cover in cy43h22, so the decrease in cy46h1 may improve the performance of the model. Although this fact should be verified in the long term, there are evidences that confirm this behaviour from multiple examples analysed in these periods (Fig. 8).

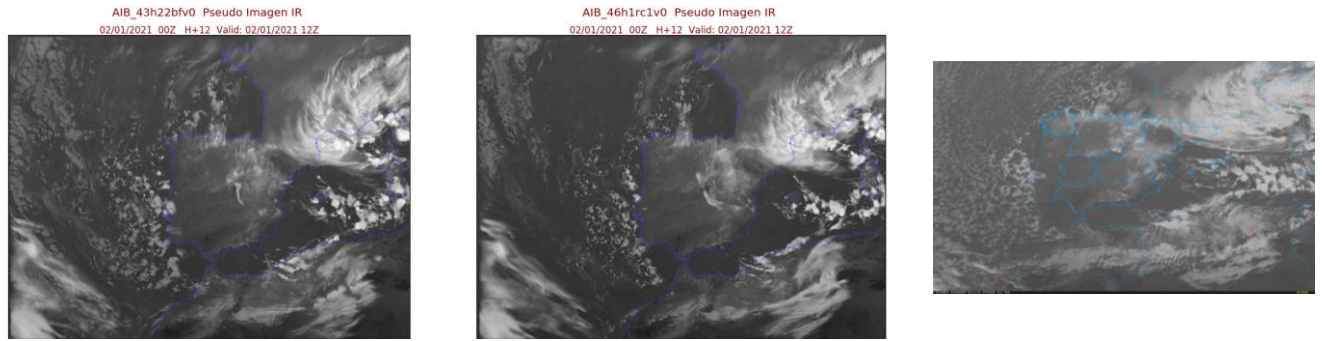


Figure 8. Simulated IR satellite image on the 2nd of January, 2021: cy43h22 (left), cy46h1(middle), Meteosat image (right).

What may be a side effect of reduced cloud cover is the unwanted reduction in fog developed by cy46h1. However, it is difficult to draw conclusions from such a small sample of fog situations that occurred during the periods analysed. As fog has a strong local character, we have found examples where cy46h1 improves the fog performance of the model compared to cy43h22 and vice versa. In Fig. 9, cy46h1 reduces the extent of fog in the Northern Plateau (black shape) compared to cy43h22 (which is not necessarily wrong). However, the new cycle is able to develop fog tracks along the Ebro basin (north-east of the peninsula), an area where fog typically occurs in winter and where cy43h22 has difficulty generating it and records a significant number of missing events.

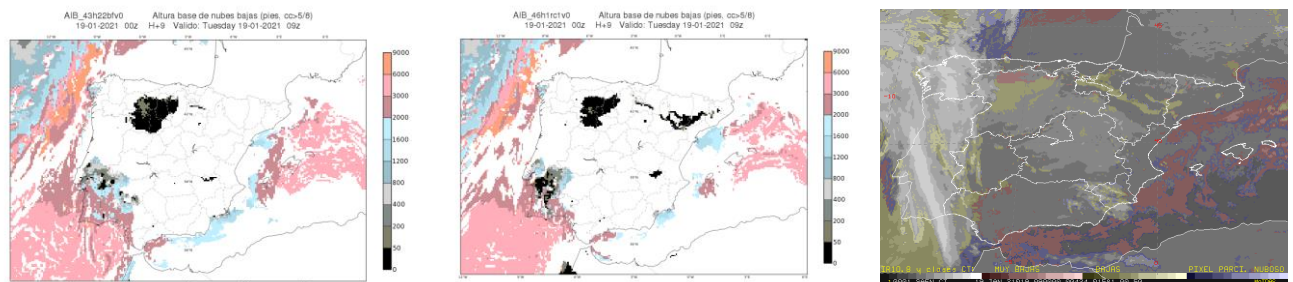


Figure 9. Left and middle, cloud height for cy43h22bf and cy46h1 respectively, where black color (height=0) corresponds to fog. Right, Nowcasting SAF product where orange and yellow patterns represent the fog extension.

Precipitation

Objective verification of precipitation shows a small decrease in cy46h1 what seems to be positive (Figure 10). Anyway the impact on ETS is very small.

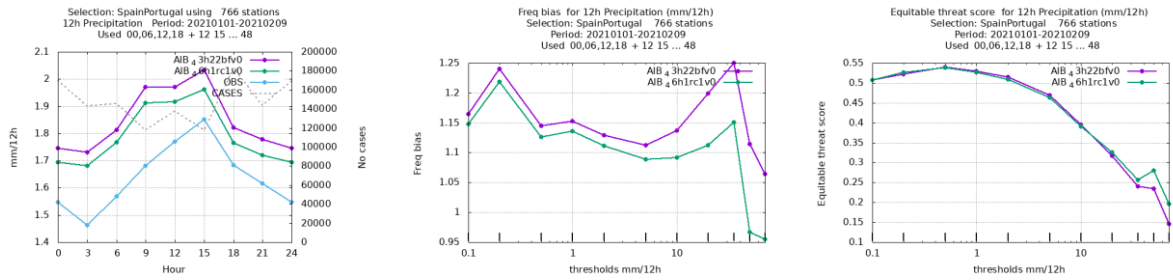


Figure 10. Precipitation acc. in 12hr: daily cycle (left), frequency bias (middle) and ETS (right) function of precipitation thresholds. Cy43h22 in purple, cy46h1 in green and observations in blue.

An example of one model output from the winter run is seen in Figure 12. The decrease of precipitation in cy46h1 is more evident over sea.

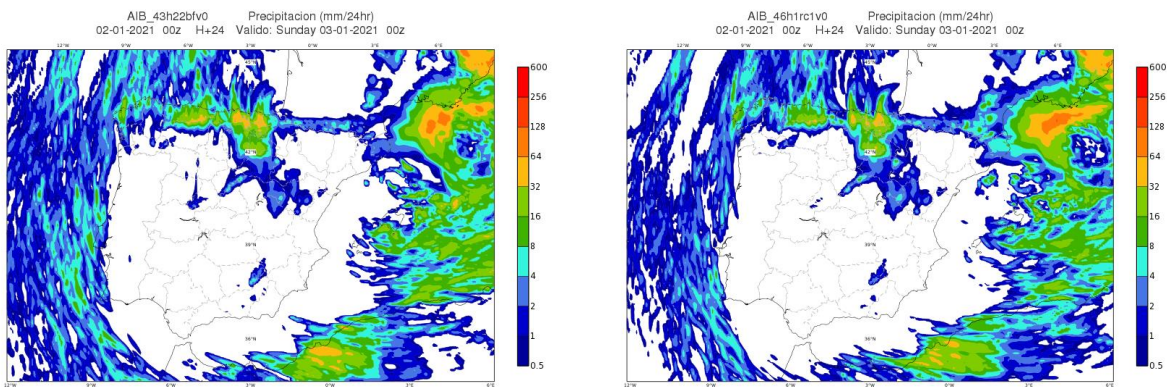


Figure 12. Precipitation in 24h on the 2nd of January, 2021. Cy43h22 (left) and cy46h1(right)

5 Single Precision

A one-month parallel run was performed in January 2024 to assess the impact of using Single Precision (SP) in the Forecast model, in a setup similar to the operational one but with a bigger domain. The scores obtained are almost identical to the Double Precision (DP) ones. See Figure 12 for the variables with bigger differences. The use of SP reduces the Forecast time by 25%.

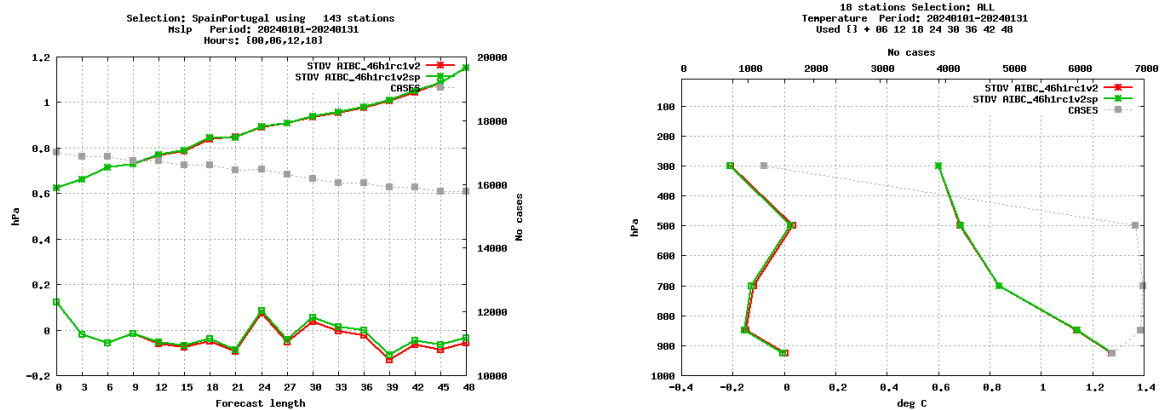


Figure 12. STDV and Bias of MSLP (left) and upper levels temperature (right) for January 2024. SP in green and DP in red.

6 Conclusions

The new version of HARMONIE-AROME cy46h1 shows no major changes in the model behaviour. However, there is a decrease in total cloud cover (mainly low clouds) compared to cycle 43h22bf, which in principle is positive, besides a slight decrease in precipitation.

The overestimation of 10 m wind speed in both cy46h1 and cy43h22bf can be alleviated activating the orographic parameterization OROTUR.

It is difficult to draw definitive conclusions about the performance of fog due to the limited number of cases analysed during the benchmark period. While this new version may not fully capture all fog episodes, it is expected to reduce the number of misses in some areas compared to cycle 43h22bf.

An important novelty in cy46h1 is that it allows for the use of more sophisticated surface schemes (DIF, MEB, Extended Snow) and surface DA (SEKF and pysurfex) to run the model. Currently, a big effort is on-going within the surface team to validate these schemes.

Single precision results are very close to the double precision ones, saving 25% of forecast time. Hence, it will be implemented in the operational suite in the near future.

7 References

- Rontu, L. (2006) A study on parametrization of orography-related momentum fluxes in a synoptic-scale NWP model. *Tellus A: Dynamic Meteorology and Oceanography*, 58:1, 69-81, doi: 10.1111/j.1600-0870.2006.00162.x

New version of harpSpatial

Alex Deckmyn, Ahto Mets, Daniel Yazgi

1. Introduction

During and after a recent visit of Daniel Yazgi and Ahto Mets at RMI (November 2023), significant progress was made with the implementation of several new scores and improved visualisation. In this Newsletter article, we describe this new version of harpSpatial.

harpSpatial is the spatial verification sub-package of **harp**, the R-based verification project developed within the ACCORD consortium. The code for all harp packages is available on github:

<https://github.com/harphub>

Currently, the most recent resource for harp information is the course that was given in 2022:

<https://harphub.github.io/harp-training-2022>

But there will be a new training course 4-8 March 2024, so soon there will be more up-to-date documentation available.

2. Main use

1. Main verification routine

The main function call for spatial verification is

```
verify_spatial()
```

There is a second, similar function

```
verify_hira()
```

for HiRA scores, which will be explained in detail in chapter 3.

These functions can take a *huge* number of command line options (specifying model and observation files and formats, verification domain, thresholds and scales etc.), which can make interactive use rather cumbersome. Therefore, harpSpatial offers the possibility to create **local configuration files** that define most command line options for a particular verification project. Such a local config file can be made by adapting the default configuration in `harpIO/conf/default_conf.R` and read with the command

```
read_spatial_config()
```

2. Input formats

harpSpatial reads model data and observations directly from the original data source files. Most standard data formats are supported:

- FA (including tar'ed FA files)
- GRIB 1 & 2
- NetCDF
- hdf5

However, for NetCDF and especially hdf5, there are many possible ways in which data can be internally organised and it is impossible to support all versions without the user having to provide at least some details on data organisation. For hdf5, ODIM (Opera format) is supported specifically.

3. Available scores

The spatial scores currently available in harpSpatial are:

- MSE, MAE, bias
- SAL
- Fractions Skill Score
- Neighbourhood Averaged Contingency Tables (ref. Stein & Stoop 2019)
- HiRA (see chapter 3)

4. Verification Output: SQLite

The scores calculated by harpSpatial are written to an SQLite file. This file contains the scores in separate data tables. While the exact format of these tables depends on the score (for instance, FSS depends on a choice of threshold and scale while SAL does not but has three separate values per case). All tables have columns for **model**, **prm** (parameter, e.g. Precip1h), **fcdate** (UNIX time, i.e. seconds since 1/1/1970), **leadtime** (in seconds).

Table 2.1: SAL score table

model	prm	fcdate	leadtime	S	A	L

Table 2.2: NACT score table

model	prm	fcdate	leadtime	threshold	scale	hit	fa	miss	cr

Note that the NACT score table has 4 columns for hits, misses, false alarms and correct rejections. These can be used to calculate various scores in the visualisation step (see chapter 5).

As the data is stored in SQLite format, the tables can be accessed and extended. In particular, this allows the user to calculate the score entries in a continuous way as the observations become available. The score tables need not be filled in one long run. The verification period can be fixed when visualising a score (chapters 5 & 6). However, the size of the SQLite file will then grow in time, and it can become quite large if there are many scales and thresholds in the score tables.

3. HiRA

Point-to-Point comparison of observations and forecasts does not show a consistent increase of skill by increasing model resolution to convective-permitting resolution and beyond. On the contrary, subjective analysis shows better model performance in higher resolutions (Mittermaier 2014). The purpose of High Resolution Assessment (HiRA) here is to compare conventional point observations against the model forecast in the neighbourhoods of the observational points which is referred to as *single observation - neighbourhood forecast* (SO-NF). In comparison to conventional approach, point-to-point verification requires interpolation of the forecast to the observation location, SO-NF assumes that the observational point is representative of its neighbourhood for some predetermined scale. As a neighbourhood method SO-NF approach also helps to reduce the double penalty effect. It is worth mentioning that the neighbourhood in this context is spatial, since the temporal dimension has not been included yet.

In contrast to spatial verification approaches that verified two-dimensional fields of both observation and forecast, the SO-NF approach considers a two-dimensional forecast against point observations

(zero-dimensional). Each observational point is surrounded by a forecast box that is centred by it as shown in Figure 3.1. The size of the surrounding box represents the scale of the considered neighbourhood. Next the SO-NF methods implemented in harp are explained briefly.

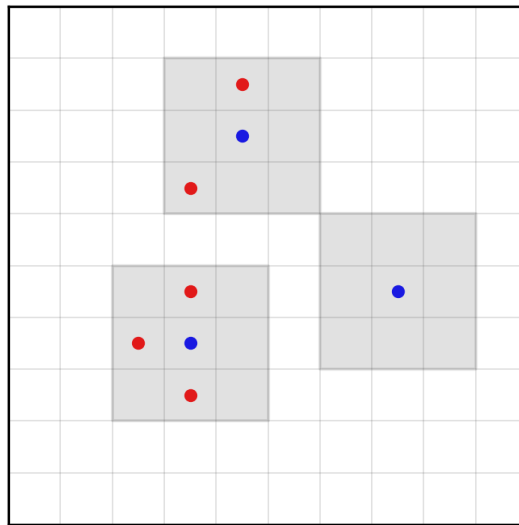


Figure 3.1: A Sketch showing observational points and neighbourhood around it in grey. Each observational point may have an event or not. The red points represent grid boxes that have an event in the neighbourhood of the observational point.

1. SO-NF methods in harp

Here we will present the methods currently implemented in harp. These methods were selected due to their low computational cost compared to other methods like Practically Perfect hindcast (Brooks et al., 1998). Table 3.1 gives a summary of the implemented SO-NF methods in harp.

As in spatial verification scores are saved data tables in a sqlite file and it flows the spatial verification conventions to organise the tables. Some methods like the contingency table do not have a direct score but values which are used to calculate different scores, these values (hit, fa, miss and cr) are saved in the same data table.

All methods can be calculated using one function called `verify_hira()` which takes parameters similar to `verify_spatial()` but with main differences as listed below:

- **stations**: defines the list of considered stations
- **padding_i, padding_j**: To eliminate stations close to the domain boundary less than `padding_i` and `padding_j` in the x and y directions, respectively.
- **scores**: To select what is computed (explained later).
 - **me**: multi-event contingency tables.
 - **pragm**: scores of the pragmatic approach BS and BSS
 - **csrr**: CSRR and RPS
- **obs_path**: path to the point observations

Table 3.1. A summary of methods implemented in harp. See the text or more details.

Fuzzy method	Description	At observation	Forecast neighbourhood
Multi-event contingency table (Atger, 2001)	Useful forecast predicts at least one event close to an observed event	0: Non-event 1: Event	0: Fraction of events is zero 1: Otherwise
Pragmatic (Theis <i>et al.</i> , 2005)	Useful forecast has a high probability of detecting events and none-events	0: Non-event 1: Event	Fraction of cells with events.
Conditional square root of RPS (German and Zawadzki, 2004)	Useful forecast has a high probability of matching the observed value	0: Non-event 1: Event	Fraction of cells with events.

2. Multi-event contingency table

In the context of forecast verification an observed event is when the parameter value exceeds a predefined threshold and a forecast event in this method is when at least one cell in the observation neighbourhood the parameter value exceeds the same threshold. Each unique pair of thresholds and scales is represented in a single row in the data table **hira_me**. Scores that currently can be computed and plotted from this table are mentioned in **chapter 5**. For more details on the implementation the reader can return to Atger (2001) and Ebert (2008).

3. The pragmatic approach

In this approach the fraction of forecast grid cells that represent an event is considered as the probability of event occurrence of the event at the observation point and the neighbourhood provides a pseudo-ensemble forecast in the observation point. The observed probability is set to 1 for the occurrence of an event, and 0 when a non-event is observed. From these pseudo-probabilities it is straightforward to calculate Brier score (BS) and Brier skill score (BSS). BSs and BSSs correspond to a unique pair of thresholds and spatial scales are stored in one single data row in the data table **hira_pragm**. For further information of this method and scores' formulae, the reader is referred to Theis *et al.* (2005).

4. Conditional square root of RPS (CSRR):

Using pseudo-probabilities as in the pragmatic approach, the Ranked Probability Score (RPS) is calculated from the cumulative probability distributions of both forecast and observation. Considering multiple observation points, the sum of RPSs is normalised by the number of observed events and then the square root is taken. This makes it possible to compare across different events and find out which event is the most predictable by the model. The RPS and CSRR are stored in a separate data row for each scale in a table called **hira_csrr**. The detailed formulation of this approach can be found in Germann and Zawadzki (2004).

4. Visualisation

Visualisations of spatial scores in harp are typically done from SQLite files produced by harpSpatial. New plotting functions are made available within the harpVis package that can be called, depending on the choice of score, through a calling function (*plot_spatial_verif*) from either the Shiny interface or the command line directly. Some scores, like FSS and SAL (Fig. 4.1), have plotting functions that are specific to them (but also scores that follow similar structure like from HiRA).

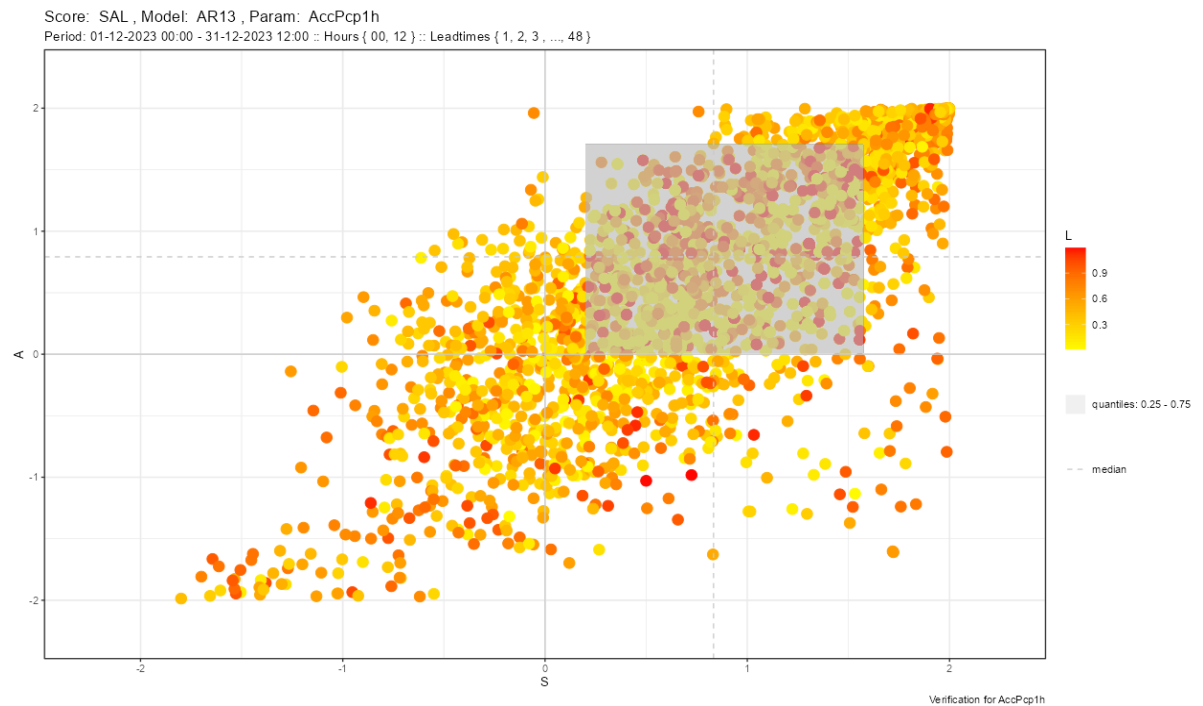


Figure 4.1: SAL plot produced by the plotting functions from harpVis over a December period 2023.

Other scores such as mean absolute error, mean squared error and bias are displayed in a simple line plot as a function of leadtime (Fig. 4.2). Additional scores (such as probability of detection, Heidke Skill score, etc.) can be calculated from neighbourhood based contingency tables (Stein and Stoop, 2019).

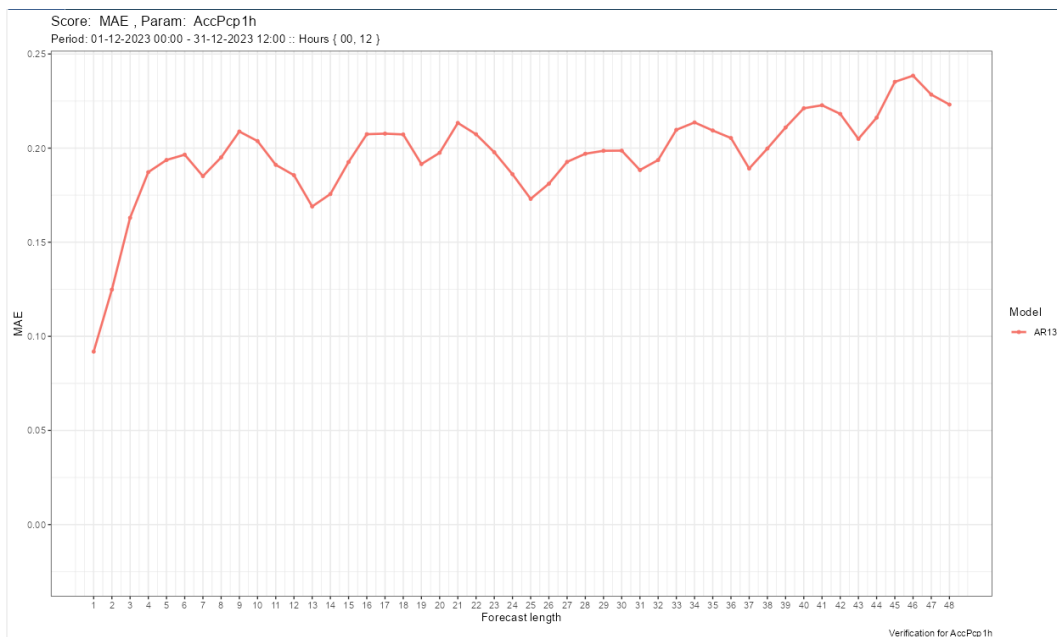


Figure 4.2: Mean absolute error plot produced by the plotting functions from harpVis over a December period 2023.

It is possible to pass arguments to the calling function such as plotting options (point sizes, line colors, etc.) or filters as a list of parameters. Several such examples would be (where 'verif_data' is a full path to the SQLite file.):

```
> plot_spatial_verif(verif_data, 'SAL')
> plot_spatial_verif(verif_data, 'FSS', filter_by = vars(threshold
%in% c(0.1,1.0), scale %in% c(15,20)))
> plot_spatial_verif(verif_data, 'NACT', plot_opts =
list(nact_scores = list("pod", "far"), colour_by = "scale"))
```

Much of this functionality is still being developed and is subject to change. More features will be added in the future.

5. The Shiny interface

The Shiny interface has been visually overhauled while keeping it easy to use. In its current state it is possible to use shiny’s built-in file browser to load an SQLite file (current maximum file size is 20 MB, which can be overwritten in server.R). Upon successful file reading many options will appear giving the user to filter the data before plotting (Fig. 5.1).

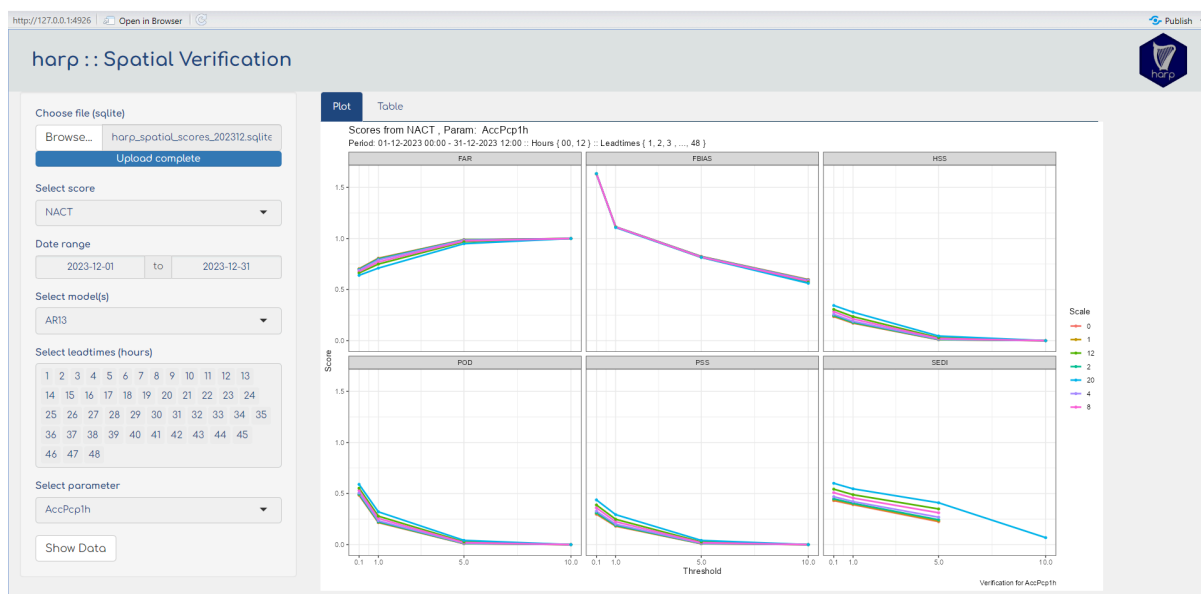


Figure 5.1: Shiny interface for harpSpatial after loading an SQLite file containing spatial scores. Plotted scores are from neighbourhood based contingency tables.

It is also possible to view the entire dataset from the file as a table at its original form before plotting (Fig. 5.2).

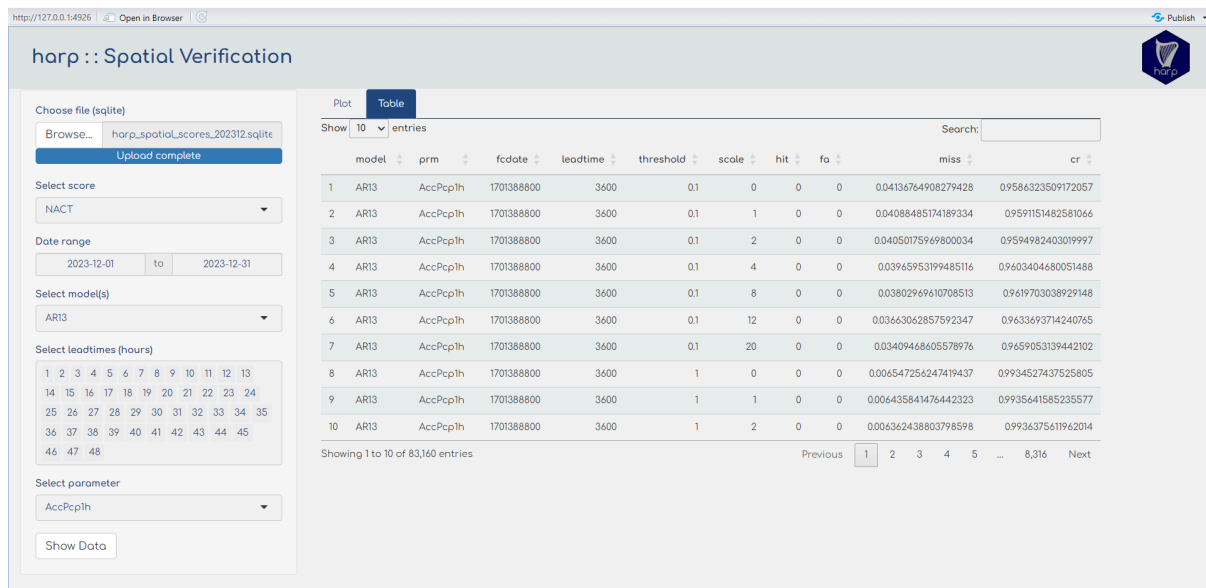


Figure 5.2: Shiny interface for harpSpatial. Table view of selected score table from loaded SQLite file.

As with the visualisations, the shiny interface also continues to be developed. Plotting options, among new possible features, will be added to the interface in the future.

6. References

- Atger, F, 2001.: Verification of intense precipitation forecasts from single models and ensemble prediction systems, *Nonlin. Processes Geophys.*, **8**, 401–417, <https://doi.org/10.5194/npg-8-401-2001>.
- Brooks, H. E., Kay M. , and Hart J. A. , 1998: Objective limits on forecasting skill of rare events. Preprints, *19th Conf. on Severe Local Storms*, Minneapolis, MN, Amer. Meteor. Soc., 552–555, [https://doi.org/10.1175/1520-0450\(2004\)043%3C0074:SDOTPO%3E2.0.CO;2](https://doi.org/10.1175/1520-0450(2004)043%3C0074:SDOTPO%3E2.0.CO;2).
- Ebert, E. E., 2009: Neighborhood Verification: A Strategy for Rewarding Close Forecasts. *Wea. Forecasting*, **24**, 1498–1510, <https://doi.org/10.1175/2009WAF2222251.1>.
- Germann, U., and Zawadzki I. , 2004: Scale dependence of the predictability of precipitation from continental radar images. Part II: Probability forecasts. *J. Appl. Meteor.*, **43** , 74–89.
- Mittermaier, M. P., 2014: A Strategy for Verifying Near-Convection-Resolving Model Forecasts at Observing Sites. *Wea. Forecasting*, **29**, 185–204, <https://doi.org/10.1175/WAF-D-12-00075.1>.
- Stein, J., and F. Stoop, 2019: Neighborhood-Based Contingency Tables Including Errors Compensation. *Mon. Wea. Rev.*, **147**, 329–344, <https://doi.org/10.1175/MWR-D-17-0288.1>.
- Theis, S. E., Hense A. , and Damrath U. , 2005: Probabilistic precipitation forecasts from a deterministic model: A pragmatic approach. *Meteor. Appl.*, **12** , 257–268, <https://doi.org/10.1017/S1350482705001763>.

Optimisation of Regional Weather Forecasts for Northern Algeria Using a Convolutional Neural Network and AROME Model Analysis

Islam Bousri

Directorate of Climatology, National Office of Meteorology, Algiers, Algeria.

1 Introduction

The use of statistical post-processing techniques can enhance the quality of weather forecasts [1]. These probabilistic approaches generally outperform conventional procedures based on simply correcting the bias of forecasts from a single model [2]. However, a comprehensive study highlights the application of artificial neural networks in weather forecasting [3], thus indicating a promising new avenue for improving forecast accuracy. We introduce a methodology that combines the power of convolutional neural networks (CNN) with the analysis provided by the AROME model. Our aim is to refine the accuracy of surface parameters, such as temperature, humidity, wind speed, and mean sea-level atmospheric pressure (MSLP), while preserving the model's resolution through integration of the AROME analysis.

2 Experiment Design

Table 1: Experience details

Training period	Jan 2020-oct 2023
Validation period	November 2023
Hourly frequency	6 hours
NWP model	AROME Cycle 43.2.5km
Features	Forecast t2m,MSLP,RH2m, wind speed, lead time
Target	Analysis t2m,MSLP,RH2m, wind speed

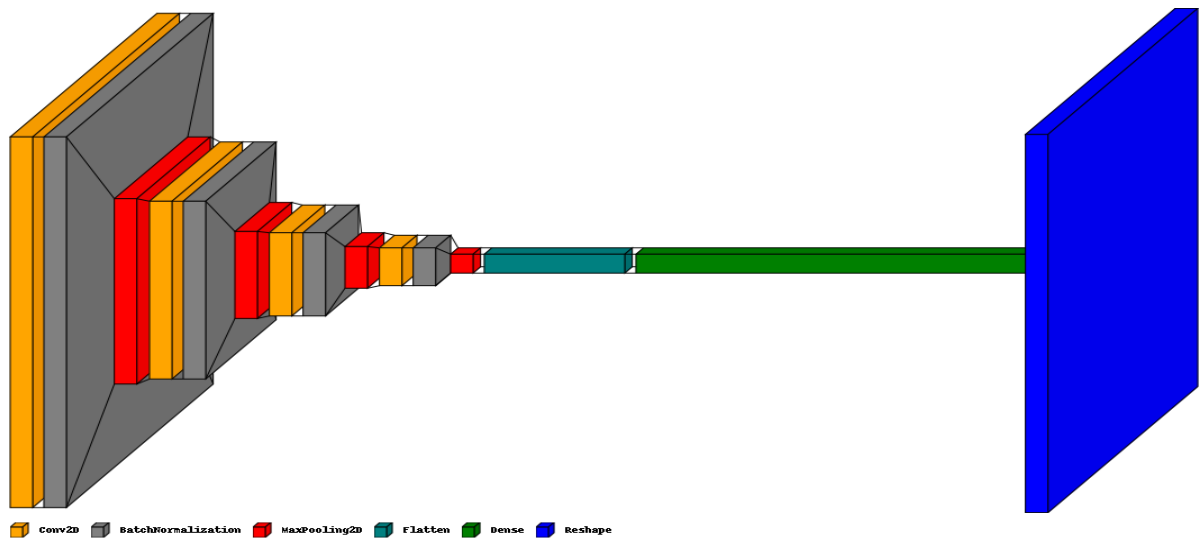
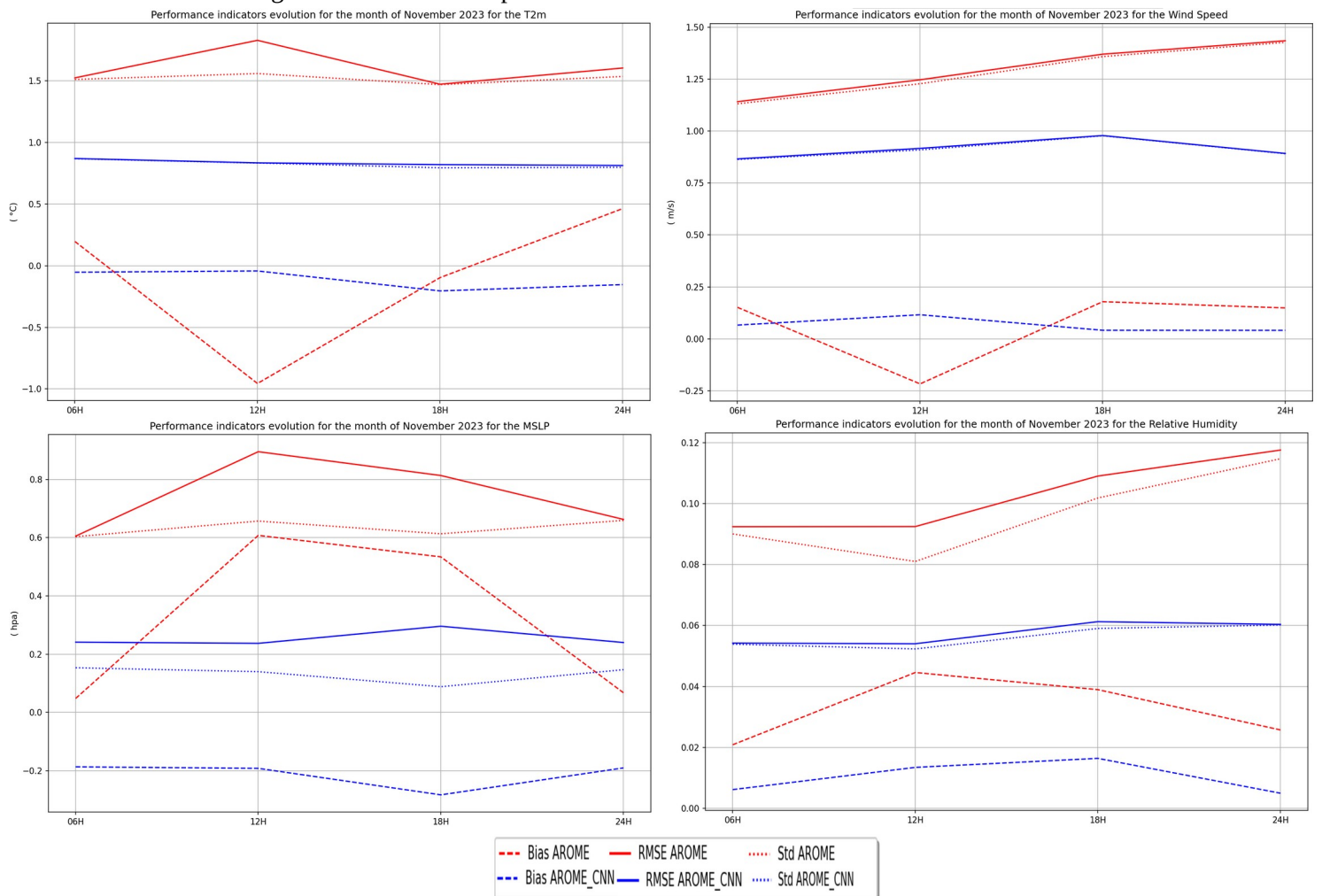


Figure 1: Architecture of the CNN model.

3 Results

1. Performance indicators

Figure 2: Evolution of performance indicators for the month of November 2023



2. Temperature results

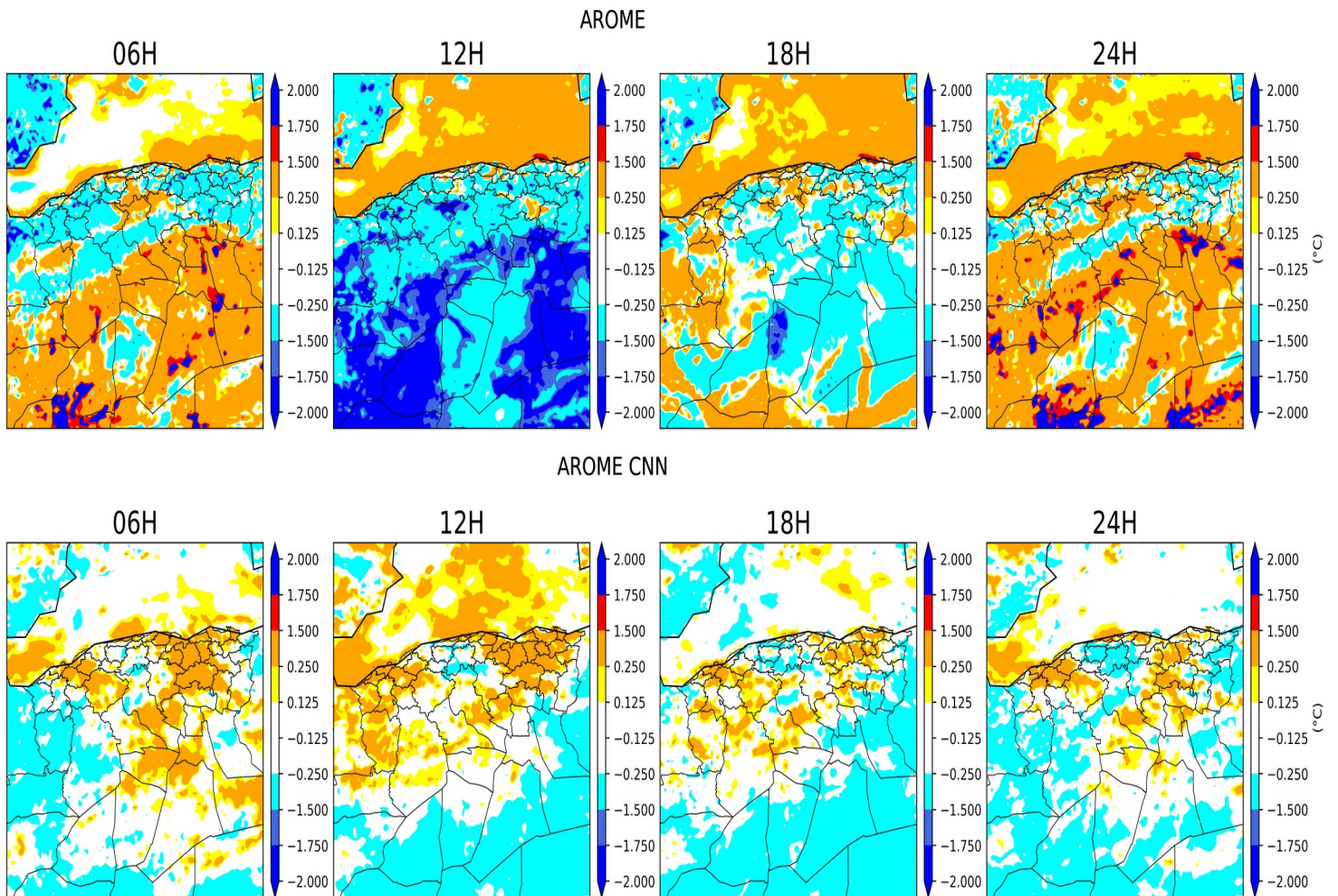


Figure 3: Temperature (T2m) anomaly (Forecast – Analysis) for November 2023.

3. RMSE gain

$$rRMSE = \frac{cnnRMSE - aromeRMSE}{aromeRMSE} \times 100 \%$$

Table 2: Rate of change of the RMSE expressed as a percentage

Parameters	t2m	MSLP	WindS	RH2m
06H	-42.9	-60.1	-24.1	-41.3
12H	-54.4	-73.5	-26.5	-41.6
18H	-44.3	-63.6	-28.6	-43.8
24H	-49.3	-63.7	-37.8	-48.6

4 Conclusion and Outlook

The integration of convolutional neural networks presents a promising frontier for improving the accuracy of weather forecasts. By leveraging the strengths of this approach, we have demonstrated the potential to refine surface parameter predictions while retaining model resolution. In the future, incorporating additional parameters such as altitude-related variables and extending forecast lead times to 48 hours holds great promise for further improving forecast accuracy and reliability. This innovative methodology not only enhances our understanding of atmospheric processes but also provides significant benefits to various sectors that rely on accurate weather information. As we continue to refine and develop these techniques, the future of weather forecasting looks increasingly bright, with broader applications and more accurate forecasts on the horizon.

5 References

- [1] Gneiting, T. (2014). 719 Calibration of Medium-Range Weather Forecasts.
- [2] Medina, H., and Tian, D. (2020). Comparison of probabilistic post-processing approaches for improving numerical weather prediction-based daily and weekly reference evapotranspiration forecasts. *Hydrology And Earth System Sciences*, 24(2), 1011-1030.
- [3] Shrivastava, G., Karmakar, S., Kowar, M. K., and Guhathakurta, P. (2012). Application of Artificial Neural Networks in Weather Forecasting : A Comprehensive Literature Review. *International Journal Of Computer Applications*, 51(18), 17-29.

ALARO and AROME analysis of derecho case in Poland.

Bogdan Bochenek, Małgorzata Szczęch-Gajewska, Piotr Sekuła, Gabriel Stachura, Natalia Szopa, Marcin Kolonko

1 Introduction

On average, a derecho occurs once a year in Poland while bow echoes happen several times per year. On 11 August 2017, severe meteorological phenomena were observed in Poland, including extremely strong wind gusts. We focused especially on the convective windstorm of a derecho type which occurred on that date in northern and north-western Poland. A rapidly moving mesoscale convective system (MCS) resulted in a bow echo, a mesoscale convective vortex (MCV), and finally fulfilled the criteria for a derecho. To establish whether our operational models in the Institute of Meteorology and Water Management, National Research Institute (IMGW-PIB) could reproduce a derecho of such intensity as that of 11 August 2017, the results from two mesoscale numerical weather prediction models were analyzed. The Application of Research to Operation at Mesoscale (AROME) and the ALADIN & AROME (ALARO) models were applied in the non-hydrostatic regime. We also examine how models differ with respect to mesoscale convective system drivers (such as vertical wind shear and convective available potential energy) and representation of deep convection (e.g., vertical velocities, cold pool generation). Forecasts are compared with observations of wind gusts and radar data. Severe weather phenomena, such as rear inflow jet and cold pool, were predicted by both models, visible on the maps of the wind velocity at 850 and 925 hPa pressure levels and on the map of air temperature at 2 m above the ground level, respectively. Relative vorticity maps of the middle and lower troposphere were analyzed for understanding the evolution of MCV.

Severe thunderstorms accompanied by strong wind gusts, intense precipitation, hail, and even tornadoes occur every summer in central Europe. In Poland, such phenomena are most frequent in July, between 14 and 16 UTC and over the southeastern parts of the country (Poręba et al. 2022). Well-organized storm complexes, which create their own internal circulation and require stronger environmental wind shear, are called mesoscale convective systems (MCS). The squall bow (radar signature of bow echo) happens a few times a year in Poland, whereas its more dangerous version, derecho, happens once per year on average (Celiński-Mysław, Matuszko 2014; Celiński-Mysław et al. 2019).

The evolving convective system observed on 11 August 2017 fulfilled criteria for a derecho, with observed maximal wind gusts exceeding $42 \text{ m}\cdot\text{s}^{-1}$ ($150 \text{ km}\cdot\text{h}^{-1}$; Taszarek et al. 2019) and was accompanied by a Mesoscale Convective Vortex (MCV). In northwestern Poland huge material damages were reported, including almost 80,000 ha of devastated forest and 6 fatalities (Chmielewski et al. 2020).

Detailed analysis of radar data from 11 August 2017 (using composite maximum reflectivity and radial velocities) confirmed the presence of MCV within the mature stage of MCS (Taszarek et al. 2019; Figurski et al. 2021; Łuszczewski, Tuszyńska 2022).

The research reported here was undertaken to assess quantitatively different configurations of ALARO and AROME models for the derecho of 11 August 2017. We have verified how different initial and boundary conditions affect the quality of simulations by using two non-hydrostatic models, ALARO and AROME. Studies were also designed to estimate which meteorological fields (e.g., wind gusts, CAPE, 0-3 km wind shear) would be appropriate for prediction of such phenomena. All the analyses of the forecasts of severe weather phenomena (related to wind gusts) by ALARO and AROME refer to the forecasts for 11 August 2017. Both models were computed for 3 sets of different initial conditions: 00 UTC (from now on, r00 run), 06 UTC (r06 run) and 12 UTC (r12). In Section 2, the synoptic context of the 11 August 2017 derecho is described; as well as our data and methods. The results

(mainly forecast maps and their description) can be found in Section 3. Section 4 is their discussion, and general conclusions and outlook.

2 Synoptic situation, data and methods

Synoptic situation

Developing storms in a warm air mass before a waving front (Fig. 1) transformed from single cells and disorganized multi-cell systems into supercells and coalesced into the large MCS (Taszarek et al. 2019; Łuszczewski, Tuszyńska 2022). Then a quasi-linear-convective-system (QLCS) developed and finally turned into a strong bow echo and MCV. The radar signature of the bow echo indicates the possibility of strong wind gusts in that area. We checked that it corresponds with the maps of CMAX simulated by NWP models. Additionally, on the basis of vertical wind profiles from Prag, Prostějov, and Wrocław we reasoned the existence of a strong jet stream. The velocities of wind gusts that exceeded $10 \text{ m}\cdot\text{s}^{-1}$ on 11 of August 2017, as well as station names, are plotted on Figure 2. Stations marked with stars are later used for quantitative evaluation of forecasted wind gusts.

Data and methods

We used ALARO and AROME in their cy43t2 version. They were not available in 2017. The ALARO version uses a $4 \text{ km} \times 4 \text{ km}$ horizontal grid, 60 hybrid vertical sigma-levels (following the orography) and has a forecast range of 72 h. Horizontally, the computing grid had 789×789 points and the domain was $3156 \text{ km} \times 3156 \text{ km}$. The initial and boundary conditions come from the global model ARPEGE in its cy42 version. The AROME model was implemented with a horizontal grid size of $2 \text{ km} \times 2 \text{ km}$ and 60 hybrid vertical levels (following the orography); it is non-hydrostatic and assumed to represent convection explicitly. It employs 799×799 grid points and the domain size is $1630 \text{ km} \times 1630 \text{ km}$. The forecast range equals 30 hours and one time step of integration is less than 1 minute. Coupling of AROME version cy43t2 with ALARO occurs once every hour. The shallow convection scheme is described by Pergaud et al. (2009). Microphysics is parameterized by the three-phase ICE3 scheme, and the surface by the SURFEX module (Masson et al. 2013). The parameterization of clouds is done statistically, and there is no parameterization of deep convection (Seity et al. 2013).

For quantitative evaluation of forecast wind gusts, data from three automatic weather stations were used: Gniezno, Grudziądz, and Starogard Gdański. These stations were situated on the track of the MCS. Since model data were available hourly and data from stations were recorded every 10 minutes, for comparison we use maximum wind gust values from every hour. We also computed root mean square errors (RMSE) and bias for ALARO and AROME models for all synoptic stations in Poland (Table 1).

3 Results

ALARO forecast.

Analysis of vertical velocity maps from ALARO (not shown) prove that the convective phenomena were far more extended for r06 and r12 runs. Vertical velocities of convective upward motions cover a wider area, and the maps show that strong, dominating upward motions neighbor on downward motions in many places (not shown). These dynamics reflect a highly unstable atmosphere, with convective potential energy strengthened by a warm tropical air mass which occupied eastern Poland. Strong upward motions were visible up to the 300 hPa pressure level and persisted through the whole duration of MCS over Poland.

The ALARO r00 forecast underestimates the strength of wind gusts but reflects well the position of the moving MCS (Fig. 3). The ALARO r06 and r12 forecasts are late in comparison with observations, but still the MCS track is well-predicted. As the MCS moved northwards, the intensity of wind and convection increased, with culmination after 18UTC and persistence until the

late evening hours on 11 August 2017. In each of the forecasts (Fig. 6) wind gusts velocity exceed 63 knots ($32.4 \text{ m}\cdot\text{s}^{-1}$), with maximum local values of $55.49 \text{ m}\cdot\text{s}^{-1}$ (21 UTC), $69.3 \text{ m}\cdot\text{s}^{-1}$ (22 UTC) and $43.78 \text{ m}\cdot\text{s}^{-1}$ (23 UTC) for run r12. The shift in time of forecasted track position in comparison with observations may be explained by the fact that for r06 and r12 there was too little time to develop a derecho fully from the forecast initiation.

During the analyzed period the MCV was accompanying the MCS. The most developed MCV (Fig. 6b) was forecasted by ALARO r12. According to ALARO r12, the vorticity of the MCV appears at 925 hPa level and then propagates upwards, reaching 700 hPa level at 20 UTC (not shown). In its culmination (21 UTC) it stretches from 500hPa downwards, reaching top values from $3.7\cdot 10^{-3}\text{s}^{-1}$ (500 hPa) to $6.6\cdot 10^{-3}\text{s}^{-1}$ (for 925 hPa). At that time, in the high troposphere (at the 300 hPa level), directly above the MCV, there is an increase of the geopotential, and rise of air pressure. After 21 UTC the vortex in the middle troposphere weakens, lasting longest at 850 and 925 hPa levels.

Other phenomena accompanying MCS are RIJ and cold pool. R06 and r12 runs forecasted the consistent structure, at the back of which we found strong current in the direction of MCS motion (Fig. 3b for r12). As it is a gradually descending current, its length was greater at higher levels, and the shortest was near the surface. This structure is well represented in the forecasts for 22 UTC.

For ALARO, the cold pool forecast is most distinct for the r00 run. We noticed it between 19 and 20 UTC on the map of temperature at 2 m AGL, and we saw it at 21 UTC in the form of closed isotherms of colder air (Fig. 3a). Despite the modest temperature contrast ($2\text{-}4^\circ\text{C}$), the cold pool is clearly imposed over the area of higher pressure near the ground (not shown) closely behind the squall line, in the northwestern direction from the low-pressure region, which overlaps the area of relatively high surface temperatures. The area of lower temperature was also visible on the maps of temperature at altitudes of 850 and 925 hPa (not presented).

AROME forecast.

The AROME was created as non-hydrostatic, high-resolution (convective scale) model for prediction of storms and torrential rain. It appeared to precisely describe a wider family of severe weather phenomena including bow echoes, derechos, and tornadoes, as well as strong wind gusts connected to these events (Seity et al. 2011). The simulated maximum reflectivity CMAX predicted by AROME (not shown) is higher than measured by radars (Fig. 5), suggesting a larger quantity of hydrometeors than in actuality. The bow echo (visible on radar maps) is well reconstructed in the AROME forecasts. Also, the area of lower reflectivity (appearing usually behind a squall bow) is visible, as well as the eddy on the northern west end of the squall bow. For the r12 run, the maps of simulated radar maximum reflectivity were in best agreement with observed maximal reflectivity in terms of position and signal intensity in dBZ.

The AROME r12 forecast underestimated wind gusts but reflected well the position of the moving MCS (Fig. 6). The predicted wind gust velocity exceeded 63 knots ($32.4 \text{ m}\cdot\text{s}^{-1}$), with maximum local values of $49 \text{ m}\cdot\text{s}^{-1}$ (20 UTC), $43 \text{ m}\cdot\text{s}^{-1}$ (21 UTC), and $47 \text{ m}\cdot\text{s}^{-1}$ (22 UTC) for r12.

Another severe weather phenomenon forecasted by AROME was a cold pool. Despite a small temperature contrast, it is clearly visible on the maps of 2 m temperature for the 21 UTC r12 run (Fig. 4a) and overlaps the area of increased pressure (not shown) right behind the squall line. At the levels of 925 and 850 hPa (not shown), one can notice a decrease of air temperature in that area. In the middle and lower troposphere, at the back of the system, a strong influx of air towards the squall line can be found. For r12, RIJ was most visible on the 21 UTC map (Fig. 4b) in the area stretching close to the ground from the squall line up to about 100 km southwest from it, parallel to MCS movement. At the levels of 850 and 925 hPa, the zone of high wind speeds (exceeding $63.5 \text{ m}\cdot\text{s}^{-1}$) is more extended than for ALARO (Fig. 3b). Considering MCV, from 19 UTC at 850 hPa one can see a cyclonic curl of wind, faintly visible also at 700 hPa (Fig. 6b for r12). It is accompanied by a local minimum of relative vorticity. For 20 UTC, the mesocyclone is visible also at 925 hPa (Fig. 4b). About 21 UTC the relative vorticity reaches its peak of $1.6\cdot 10^{-3}\text{s}^{-1}$ (850 hPa) and an expansion of the high vorticity region follows (Fig. 6b).

Forecast evaluation.

In order to better visualize the capability for forecasting wind gusts by ALARO and AROME models, a quantitative verification is presented in Figure 9. Three stations that recorded high values of wind gusts were selected (stations are ordered from southernmost to northernmost): Gniezno, Grudziądz and Starogard Gdański. For both models and 12 UTC run, wind gust forecasts are presented along with recorded values. All runs and both models are characterized precisely by the timing of the greatest wind gusts. For Gniezno station (Fig. 9, left), the AROME model (green line) performs better both in terms of timing and magnitude, but the maximum wind gusts are underestimated by almost $10 \text{ m}\cdot\text{s}^{-1}$. The best forecasts for Grudziądz (Fig. 9, middle) are obtained from 12 UTC runs (Fig. 9, right) with almost perfect timing and values for observed peak wind gusts (blue line), especially for AROME forecasts, whereas the ALARO model (red line) predicted the maximum value better, but one hour later than observations. For the Starogard Gdański station (Fig. 9, right) the forecasts from 12 UTC turned out to be the worst for both models, with overestimation of wind gusts and forecasting them one (AROME) or two hours (ALARO) late.

ALARO and AROME wind gust forecasts starting from 00, 06, and 12 UTC were also compared with measurements from all synoptic stations in Poland. Table 1 presents RMSE and bias scores for both models. The AROME model starting at 00 UTC outperforms other forecasts both in terms of RMSE and bias. The biggest errors were noted for both models for 12 UTC runs.

The AROME forecast values of CAPE and 3-0 km wind shear (Fig. 8) were higher compared to those predicted by ALARO (Fig. 7). At 15 UTC the maximum value for MU CAPE from the AROME forecast reached $5956 \text{ J}\cdot\text{kg}^{-1}$, while for ALARO it was $4669 \text{ J}\cdot\text{kg}^{-1}$. Until 21 UTC for both models maximum CAPE values were decreasing, but still were over $4000 \text{ J}\cdot\text{kg}^{-1}$. Wind shear in the 0-3 km layer from 15 to 21 UTC has constantly high values ($>35 \text{ m}\cdot\text{s}^{-1}$ for ALARO and $>45 \text{ m}\cdot\text{s}^{-1}$ for AROME). The models predicted the greatest wind shear at 20 UTC: ALARO $40.8 \text{ m}\cdot\text{s}^{-1}$ and AROME $48.3 \text{ m}\cdot\text{s}^{-1}$. The values of vertical velocity at 500 hPa (not shown) were significantly higher for the model using full deep convection equations, reaching $20 \text{ m}\cdot\text{s}^{-1}$ (18 and 20UTC) and $26 \text{ m}\cdot\text{s}^{-1}$ (19 UTC). For AROME, the strongest convection regions at 925 hPa were very narrow and overlapped the convergence lines of wind (not shown).

It is not straightforward to evaluate models based on observational data in the case of such an intensive phenomenon, and using forecasts up to 24 hours instead of reanalysis. Models can predict the behavior of an event accurately, but with a small number of synoptic stations or coarse resolution of gridded data, standard scores can be misleading. Therefore we decided to evaluate the possibility of predicting the intensity of the derecho by analyzing the distribution of wind gusts in Poland (grid points from ALARO and AROME models within the Polish border and over the Baltic Sea up to 55.5 N) from various models and runs. Figure 10 presents the distribution of forecasts of wind gusts from 12 UTC to 24 UTC on 11 August 2017, with the AROME model on the top row and ALARO on the bottom row. Runs for 00 UTC are displayed on the left column, 06 UTC runs on the middle column, and 12 UTC runs on the right column. All runs for both models predict very strong wind gusts, but the ALARO model for 12 UTC predicts values exceeding $60 \text{ m}\cdot\text{s}^{-1}$ at 22 UTC; ALARO from 06 UTC predicts values slightly less than $60 \text{ m}\cdot\text{s}^{-1}$ at 24 UTC, while AROME runs from 00 and 12 UTC predicted maximum wind gusts close to $50 \text{ m}\cdot\text{s}^{-1}$.

4 Conclusions, summary and outlook

Conclusions

Both ALARO and AROME models forecasted a mesoscale convective system (MCS), a bow echo structure as well as MCV – a mesoscale convective vortex. The fields, such as: pressure and wind, geopotential and wind, temperature, as well as vertical velocity maps, CAPE and wind shear were valuable for the analysis of the atmospheric state. The maps of simulated reflectivity (C_{MAX} from ALARO, not shown) visualize the path of the phenomenon for evening hours on 11 August 2017, thus both the evolution of a structure and a position of MCS. AROME model forecast from 12 UTC predicted properly MCV, however the prediction of position of convective phenomena like MCV

(for AROME r00 and r06) was more misleading than for ALARO. One should be aware of necessity for forecasters to use better resolution maps which can be obtained by downscaling the most complex areas. That seems to be the future but would be crucial in the process of immediate diagnosis of the meteorological situation by the team of forecasters.

Summary and outlook

The post-factum weather forecast by the means of the presently available model, a non-hydrostatic one with $4\text{ km} \times 4\text{ km}$ horizontal resolution (unavailable in 2017), predicted wind gusts of velocity exceeding $150\text{ km}\cdot\text{h}^{-1}$. It would be valuable to explore the weather system by AROME model with different initial and boundary conditions or run models with higher horizontal and vertical resolution. Such models could be a test version of AROME with horizontal resolution $1\text{ km} \times 1\text{ km}$ and over 100 vertical levels, or ALARO with horizontal resolution of $2\text{ km} \times 2\text{ km}$. Operational run of higher resolution models may help forecasters to predict future severe convective events more efficiently.

Table 1: Evaluation of wind gust forecasts for all synoptic stations in Poland.

	ALARO			AROME		
	00	06	12	00	06	12
RMSE [m·s ⁻¹]	5.56	5.37	7.41	5.19	6.21	7.88
BIAS [m·s ⁻¹]	1.81	2.9	3.71	0.42	2.26	4.03

Figures

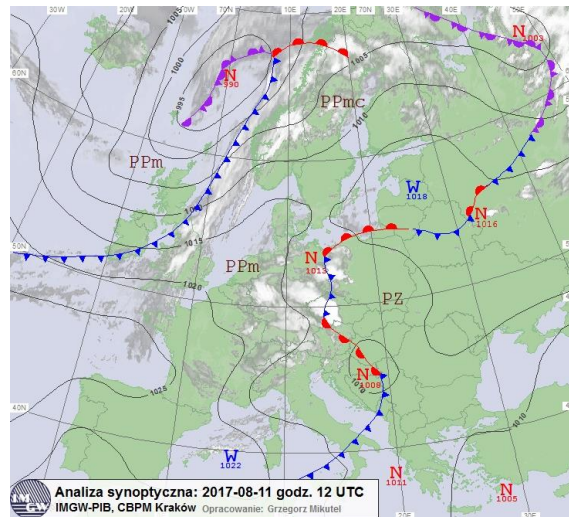


Figure 1: The synoptic situation on 11 August 2017, 12 UTC. Credit: IMWM-NRI, Central Office for Meteorological Forecasts, Krakow.

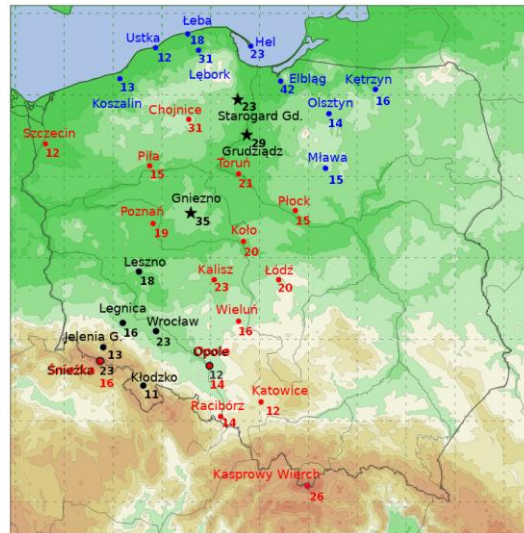


Figure 2: Synoptic stations on which wind gusts exceeded $10 \text{ m}\cdot\text{s}^{-1}$ on 11 of August 2017. Colors refer to the following time spans: 15:00-18:00 UTC (black), 18:00-21:00 UTC (red) and 21:00-24:00 UTC (blue). Stations marked with stars are later used for quantitative evaluation of forecasted wind gusts.

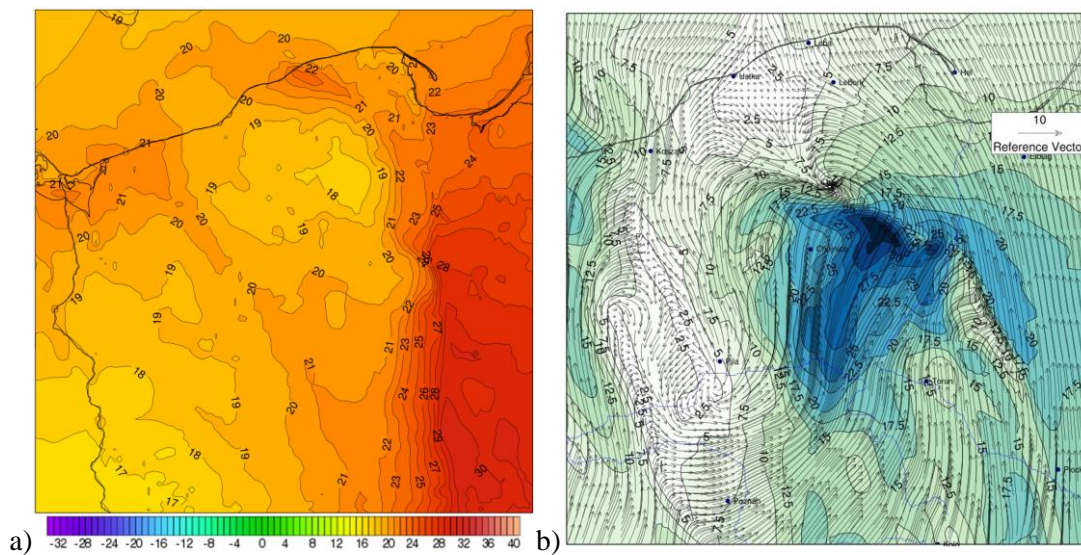


Figure 3: a) Cold pool from ALARO: temperature at 2 m AGL. The forecast for 21 UTC, 11 August 2017, r00; b) Wind and the module of velocity (color) at 850 hPa pressure level. ALARO r12 forecast for 22 UTC 11 August, 2017.

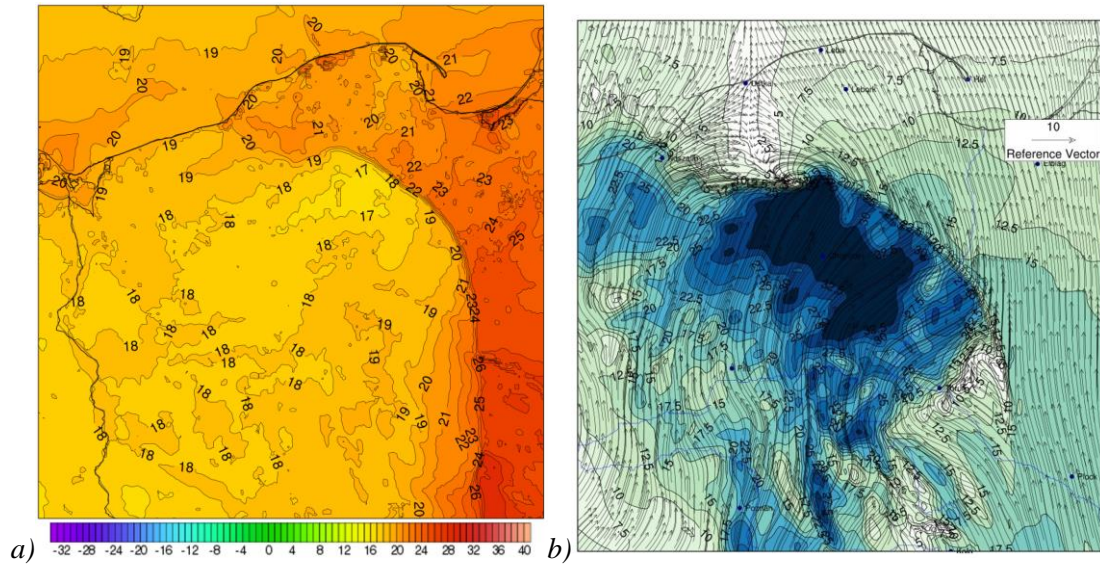


Figure 4: a) Cold pool from AROME: temperature at 2 m AGL. The forecast for 21 UTC, 11 August 2017, r12; b) Wind and the module of velocity (color) at 850 hPa pressure level. AROME r12 forecast for 21 UTC 11 August, 2017.

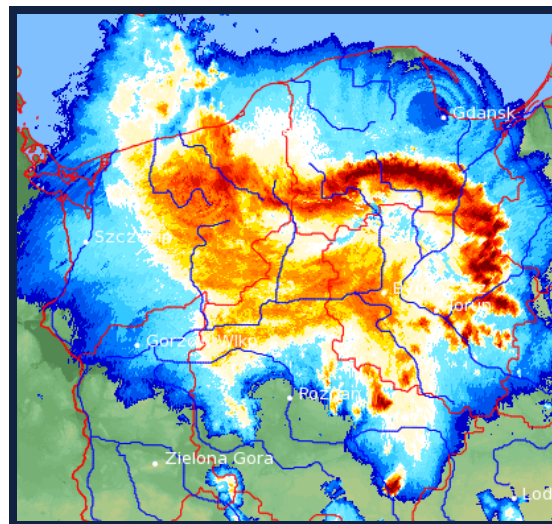
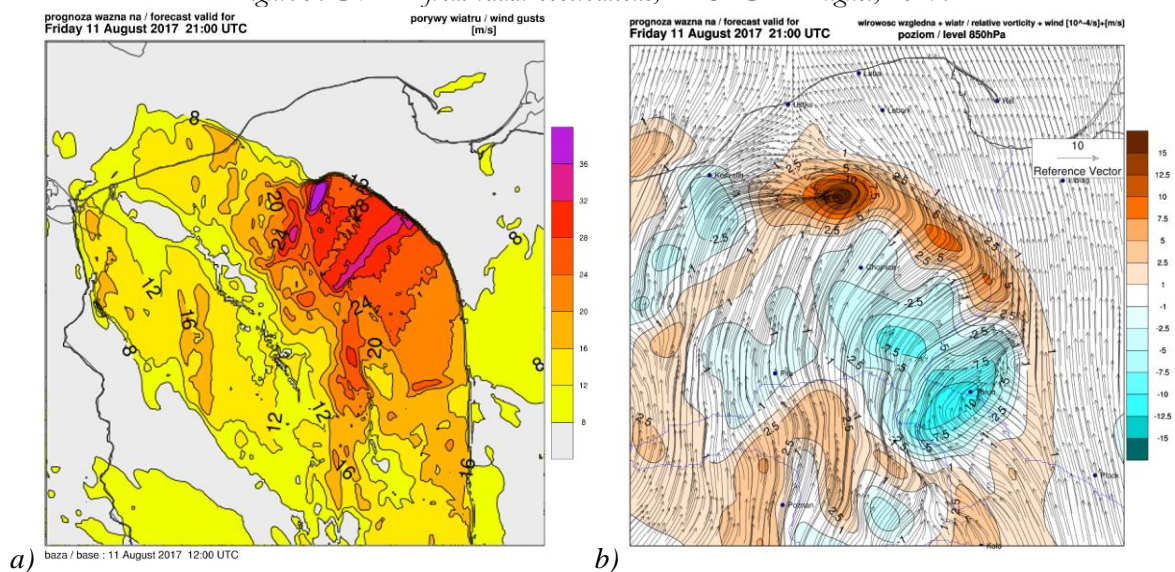


Figure 5: CMAX from radar observations, 21 UTC 11 August, 2017.



a) baza / base : 11 August 2017 12:00 UTC

Figure 6: a) Wind gusts from AROME r12 forecast; b) Mesoscale Convective Vortex as seen at relative velocity and wind (colors) map at 850 hPa pressure level. Both AROME r12 forecast for 21 UTC, 11 August, 2017.

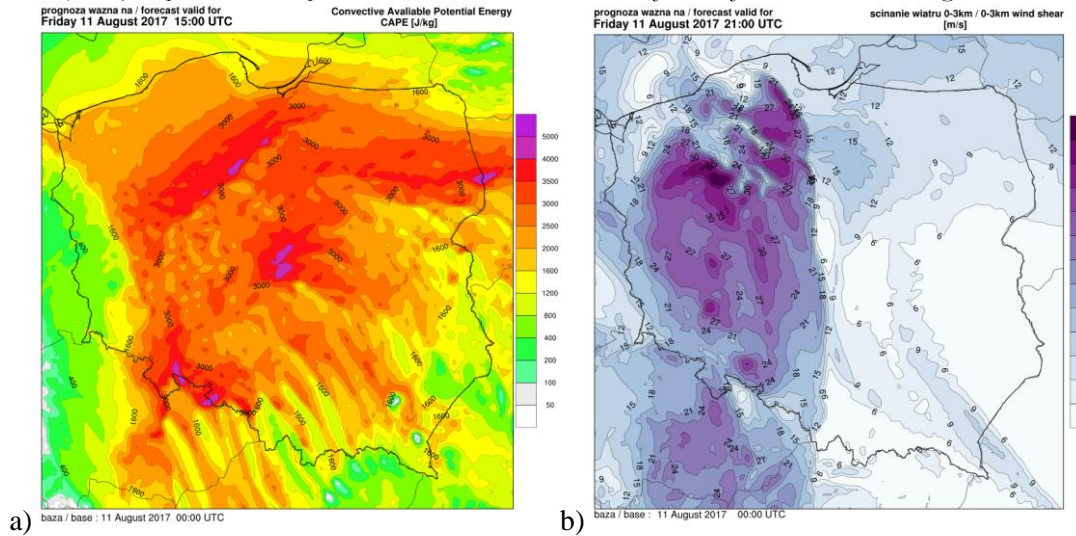


Figure 7: a) MU CAPE [$J \cdot kg^{-1}$] at 15UTC and b) 0-3km wind shear [$m \cdot s^{-1}$] at 21UTC for ALARO cy43t2 r00 forecast on 11 August 2017.

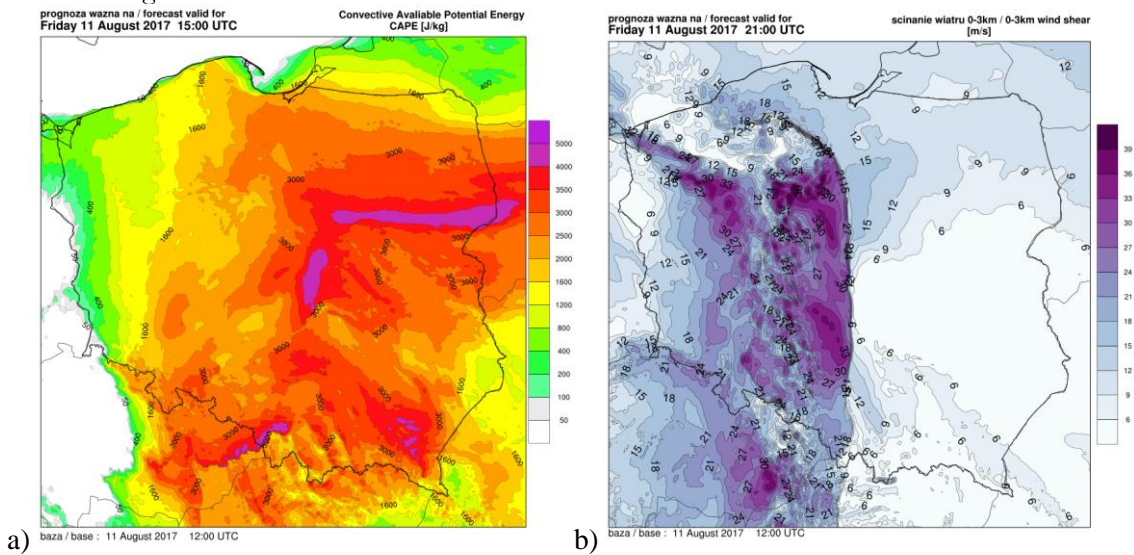


Figure 8: a) MU CAPE [$J \cdot kg^{-1}$] at 15UTC and b) 0-3km wind shear [$m \cdot s^{-1}$] at 21UTC for AROME cy43t2 r12 forecast on 11 August 2017.

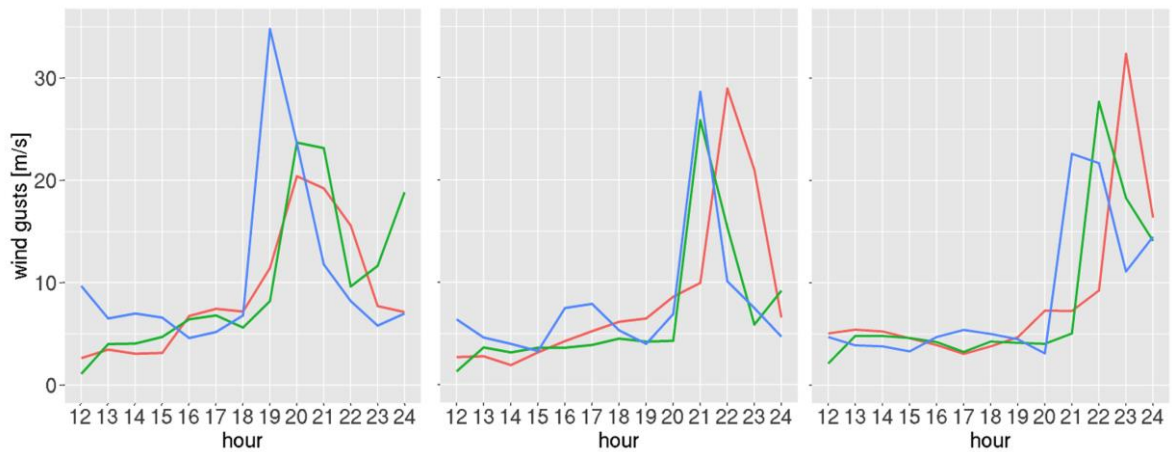


Figure 9. Wind gust measurements (blue lines) and forecasts from ALARO (red lines) and AROME (green lines) models starting from 12 UTC for stations Gniezno (left), Grudziadz (middle) and Starogard Gdanski (right) for 11 August 2017 from 12 UTC to 24 UTC.

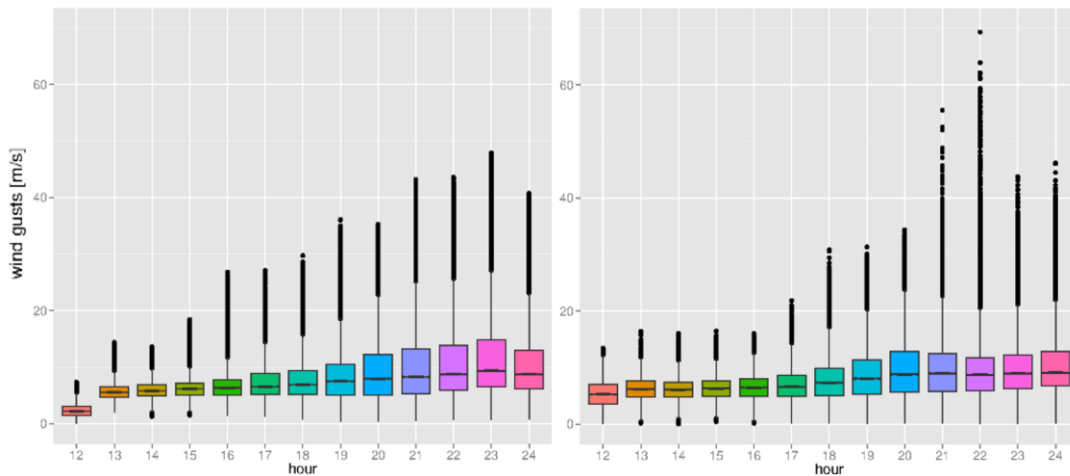


Figure 10. Distribution of wind gust values in Poland for 11 August 2017 from 12 UTC to 24 UTC. AROME left, ALARO right, both 12 UTC run.

Full article available:

Kolonko, M., M. Szczęch-Gajewska, B. Bochenek, G. Stachura, and P. Sekuła, 2023: Using ALARO and AROME numerical weather prediction models for the derecho case on 11 August 2017. Meteorol. Hydrol. Water Manage., 10, 88–105, <https://doi.org/10.26491/mhwm/156260>.

5 References

- Celiński-Mysław, D., Matuszko, D., 2014. An analysis of selected cases of derecho in Poland. Atmospheric Research 149, 263–281. <https://doi.org/10.1016/j.atmosres.2014.06.016>
- Celiński-Mysław, D., Palarz, A., Łoboda, Ł., 2019. Kinematic and thermodynamic conditions related to convective systems with a bow echo in Poland. Theoretical and Applied Climatology. <https://doi.org/10.1007/s00704-018-2728-6>
- Chmielewski, T., Szer, J., Bobra, P., 2020. Derecho wind storm in Poland on 11–12 August 2017: results of the post-disaster investigation. Environmental Hazards 19, 508–528. <https://doi.org/10.1080/17477891.2020.1730154>
- Figuerski, M., Nykiel, G., Jaczewski, A., Baldysz, Z., Wdowikowski, M., 2021. The impact of initial and boundary conditions on severe weather event simulations using a high-resolution WRF model. Case study of the derecho event in Poland on 11 August 2017. Meteorol. Hydrol. Water Manage. <https://doi.org/10.26491/mhwm/143877>
- Łuszczewski, H., Tuszyńska, I., 2022. Derecho analysis of August, 11. Meteorol. Hydrol. Water Manage. <https://doi.org/10.26491/mhwm/152504>
- Masson, V., Le Moigne, P., Martin, E., Faroux, S., Alias, A., Alkama, R., Belamari, S., Barbu, A., Boone, A., Bouyssel, F., Brousseau, P., Brun, E., Calvet, J.-C., Carrer, D., Decharme, B., Delire, C., Donier, S., Essauouini, K., Gibelin, A.-L., Giordani, H., Habets, F., Jidane, M., Kerdraon, G., Kourzeneva, E., Lafaysse, M., Lafont, S., Lebeaupin Brossier, C., Lemonsu, A., Mahfouf, J.-F., Marguinaud, P., Mokhtari, M., Morin, S., Pigeon, G., Salgado, R., Seity, Y., Taillefer, F., Tanguy, G., Tulet, P., Vincendon, B., Vionnet, V., Voldoire, A., 2013. The SURFEXv7.2 land and ocean surface platform for coupled or offline simulation of earth surface variables and fluxes. Geoscientific Model Development 6, 929–960. <https://doi.org/10.5194/gmd-6-929-2013>
- Pergaud, J., Masson, V., Malardel, S., Couvreur, F., 2009. A Parameterization of Dry Thermals and Shallow Cumuli for Mesoscale Numerical Weather Prediction. Boundary-Layer Meteorol 132, 83. <https://doi.org/10.1007/s10546-009-9388-0>

- Poręba, S., Taszarek, M., Ustrnul, Z., 2022. Diurnal and Seasonal Variability of ERA5 Convective Parameters in Relation to Lightning Flash Rates in Poland. *Weather and Forecasting* 37, 1447–1470. <https://doi.org/10.1175/WAF-D-21-0099.1>
- Seity, Y., Lac, C., Bouysse, F., Bouteloup, Y., Riette, S., Masson, V., Thouron, O., Beucher, F., Barthe, C., n.d. Cloud and microphysical schemes in ARPEGE and AROME models 35. <https://www.ecmwf.int/node/12167>
- Taszarek, M., Pilguy, N., Orlikowski, J., Surowiecki, A., Walczakiewicz, S., Pilorz, W., Piasecki, K., Pajurek, Ł., Półrolniczak, M., 2019. Derecho Evolving from a Mesocyclone—A Study of 11 August 2017 Severe Weather Outbreak in Poland: Event Analysis and High-Resolution Simulation. *Monthly Weather Review* 147, 2283–2306. <https://doi.org/10.1175/MWR-D-18-0330.1>

ALADIN activities in Poland

Marcin Kolonko, Jadwiga Róg, Piotr Sekuła, Gabriel Stachura, Małgorzata Szczęch-Gajewska, Natalia Szopa, Bogdan Bochenek

1 Introduction

In 2023, we held the same operational configuration for ALARO and AROME. Piotr Sekuła did the CY46 tests, Małgorzata Szczęch-Gajewska succeeded at running the data assimilation scripts as Gabriel Stachura dealt with CROCUS and ESS models intercomparison. We employed new mathematically specialised colleague, Natalia Szopa. At the beginning of 2024 Jadwiga Rog supported the ACCORD Poland group. The examples of our activities are described below.

2 Operational suite

Specification

There was no substantial change in both our (mesoscale and high resolution) model specification. We use the same HPC for 9 years and for stability reasons we don't introduce radical improvements in the model parameters. Main parameters of ALARO and AROME are listed in the tables below.

Table 1: Configuration of mesoscale model.

Model version	<u>ALARO-v1B NH (CY43T2)</u>
Resolution	4.0 km
Levels	70
Domain	E040 (789x789 points)
Projection	Lambert Conformal
Coupling zone	16 points
Number of runs per day	4 (00, 06, 12 and 18 UTC)
Coupling frequency	3 h
LBC	ARPEGE 9.4 km
Time step	150 s

Table 2: Configuration of high resolution model.

Model version	AROME (CY43T2)
Resolution	2.040 km
Levels	70
Domain	P020 (799x799 points)
Forecast range	30 h
Projection	Lambert Conformal
Number of runs per day	4 (00, 06, 12 and 18 UTC)
Coupling frequency	1 h
LBC	ALARO-1 4.0 km
Time step	50 s

3 Tests of CY46 and verification

New suite

The tests of CY46 were conducted according to Jan Masek report. Modification covers namelist analogous to ALARO 2.3 km for Czech Republic. Our model (ALARO) is 4 km in resolution, non-hydrostatic with preserved number of vertical levels (70). The new tests are conducted from December, 2023.

After change to old (CY43) climatological files verification was satisfactory (see examples in Fig. 1 and 2). We will continue with the tests by analysis of the skill scores for specific weather cases.

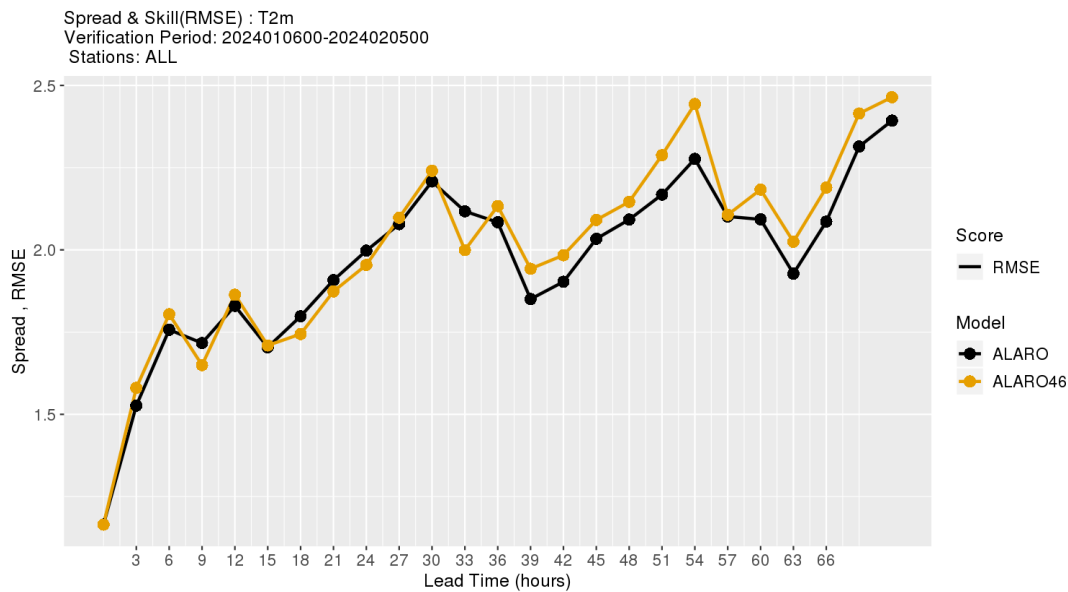


Figure 1: Verification of CY46 vs CY43 results – 2m temperature.

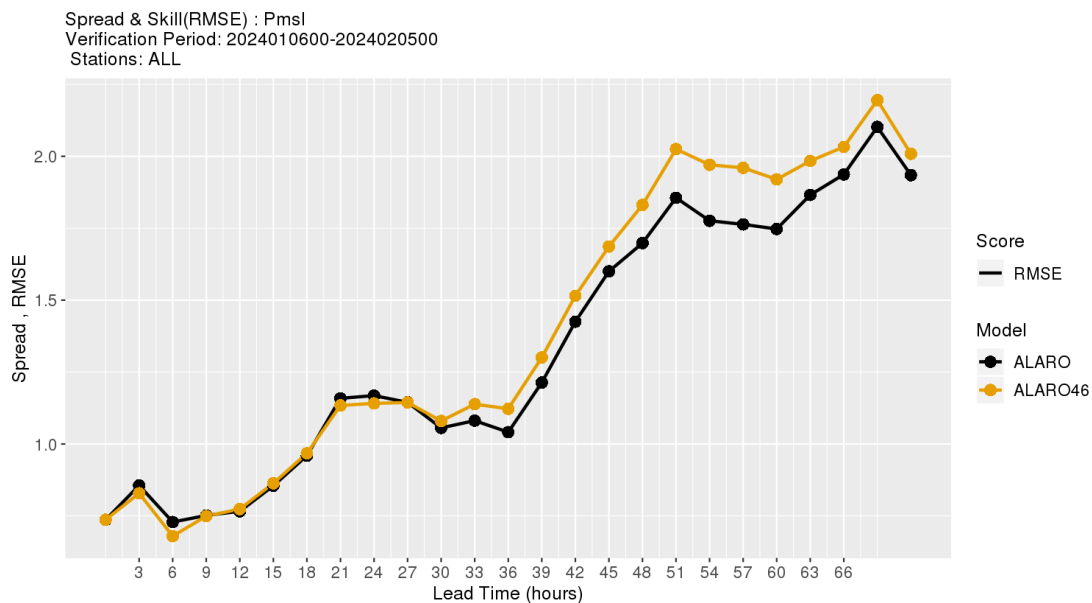


Figure 2: Verification of CY46 vs CY43 results – mean sea level pressure.

4 Data assimilation

Description

After long time we finally started to obtain the improvement of our assimilation results. Our verification scores substantially improved and gave us sense of assimilation of the data in our ALARO cycle. The training period was several months. We have made such diagrams for T2m and 12h accumulated precipitation, and some more variables (Hu2m, Pmsl, wind) available in HARP.

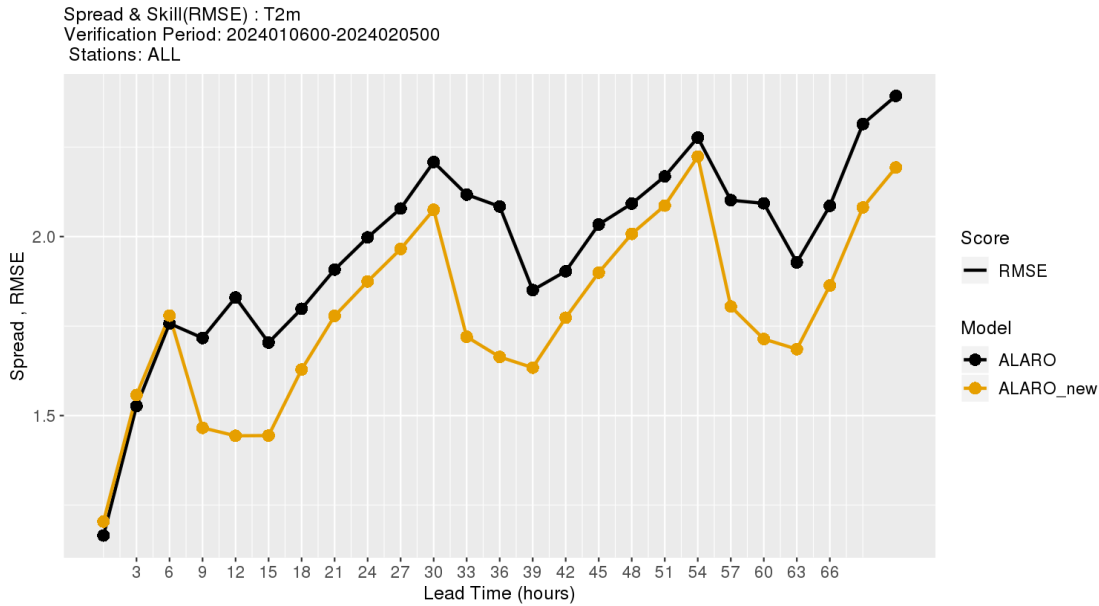


Figure 3: Verification of CY43 results with (ALARO_new) and without (black ALARO curve) assimilation– 2m temperature.

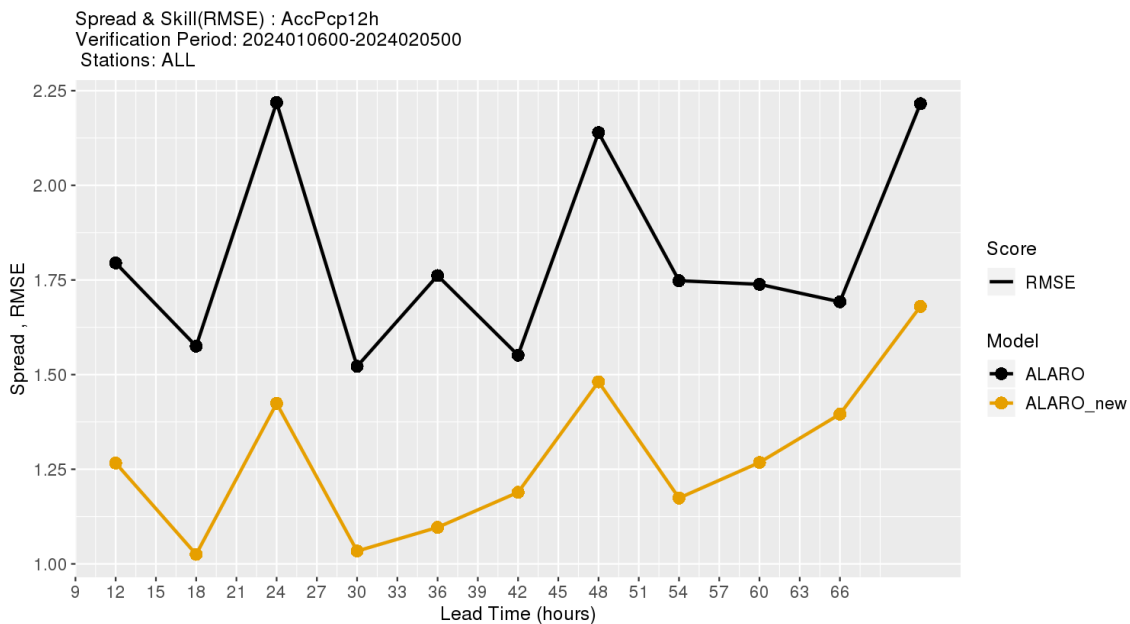


Figure 4: Verification of the assimilated (ALARO-new) and non-assimilated results (black ALARO curve) – 12h accumulated precipitation.

5 CROCUS snow model and its tests

Methodology

Besides CROCUS we tested D95 and ESS (Explicit Snow Scheme) models. We compared them at the basis of 3-month observations of the SD (snow depth) and SWE (snow water equivalent) in 6 mountain stations and 2 highlands stations. CROCUS is similar (as for the physics) to ESS, whereas D95 is the simplest. The number of possible snow layers is highest in CROCUS (up to 50). They also have slightly differing set of prognostic variables.

Results

We present one of the most snowy station, „Dolina Pięciu Stawów Polskich” (5 Polish Lakes valley) Tatra station at the altitude around 1600 m a.s.l.

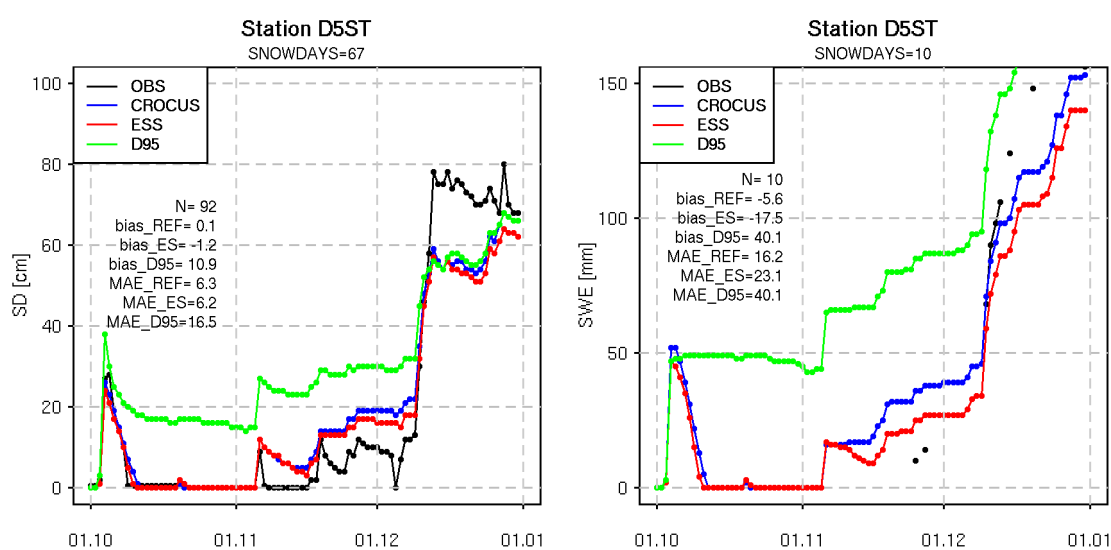


Figure 5: SD (snow depth) and SWE (snow water equivalent) at 5 Lakes Valley in 3 latest months of 2022. Observed values in black, snow models in blue, red and green.

Conclusions

The simplest snow scheme, D95, clearly produces the worst results, mainly due to too slow melting of snow in October. ESS and Crocus also tends to slightly overestimate snow depth and SWE but to a much lesser extent than in case of D95. Crocus and ESS are very much alike, but we can notice that ESS melts the snowpack a little bit faster. After heavy snowfall, all the snowschemes underestimate the amount of snow accumulated. In case of this station, it compensates the overestimation of snow which occurred before the event, however, one need to take into account that systematic errors in snow cover can accumulate throughout the season, while this experiment captures only the beginning of the winter. More effort is needed to identify sources of the biases, e.g. by inspecting atmospheric forcing or running SURFEX with at least 2 patches.

Table 3: Comparison of verification scores for snow depth for all stations (ESS is the best of snow models for both types of errors).

SD	CROCUS	ESS	D95
bias [cm]	2.94	1.9	2.16
MAE [cm]	4.85	4.35	6.19

Table 4: Comparison of verification scores for snow water equivalent for all stations (ESS is of best bias, CROCUS – MAE, mean absolute error).

SWE	CROCUS	ESS	D95
bias [cm]	4.21	-0.6	11.57
MAE [cm]	25.59	26.21	28.56

6 Vine copula application to ensemble postprocessing

Mathematical background

A d -dimensional copula is a multivariate distribution function on $[0,1]^d$ with uniformly distributed marginal distribution functions. Fundamental Sklar’s theorem states that for a d -dimensional cumulative distribution function, there exists a *copula* function denoted by C , such that $F(x_1(t), \dots, x_d(t)) = C(F_1(x_1(t)), \dots, F_d(x_d(t)))$, where F is a joint cumulative distribution function and F_1, \dots, F_d are marginals. This theorem allows to separate univariate margins from the dependence structure.

Method

The goal of the copula based method is the error mitigation of the temperature forecast given by the ALARO model. We construct a copula that contains both the information about the correlations between variables affecting the forecast error and their individual probability distributions. From a copula-given conditional probability distribution we are able to obtain a sample of pseudo-observations. We aim to check whether the choice of different conditioning variables has a significant effect on the correct fit of the model to pre-existing real data. We then calculate the average of these generated forecast errors, which we then add to the ALARO model's temperature forecast and check how much the corrected forecast is better than the original forecast using RMSE.

Data

Considered data will include forecasts of air temperature values at 2m above ground level of NWP models at 12UTC (forecast start at 00UTC) for 35 Polish synoptic stations. The dataset was divided into a training set (forecasts from January 1, 2019 to December 31, 2019) and a test set (forecasts from January 1, 2020 to December 31, 2020).

Indicator	Description of the conditioning variables
a	AROME model forecast for the current day
b	COSMO model forecast for the current day
c	Forecast error of the ALARO model on the previous day
d	Value of observed temperature at 00UTC
e	Forecast error of the AROME model on the previous day
f	Forecast error of the COSMO model on the previous day
g	Forecast error of the AROME model on the current day
h	Forecast error of the COSMO model on the current day
i	Difference between the forecast on the previous day and the current day of the ALARO model
j	Difference between the previous day's relative humidity forecast and the current day's ALARO model forecast

Results

We see that the chosen method introduces a slight correction in the temperature prediction of the ALARO model. We verify the results by observing the percentage change in the root mean squared error (RMSE) of the ALARO model's temperature prediction. RMSE is an indicator that measures the average difference between the model's forecast values and actual values.

The largest improvement due to using that method was for stations with high systematic errors – mountain and seashore ones. Significant reductions in RMSE are observed at the station located at Śnieżka, where the error was reduced by an average of 45%, and in Hel, by 28% per year. In Zakopane and on Kasprowy Wierch, by 18% and 17% respectively. The average largest improvement for all 35 stations was observed with the conditioning variables of temperature forecasts of different models (AROME and COSMO) and the value of observed temperature at 00UTC.

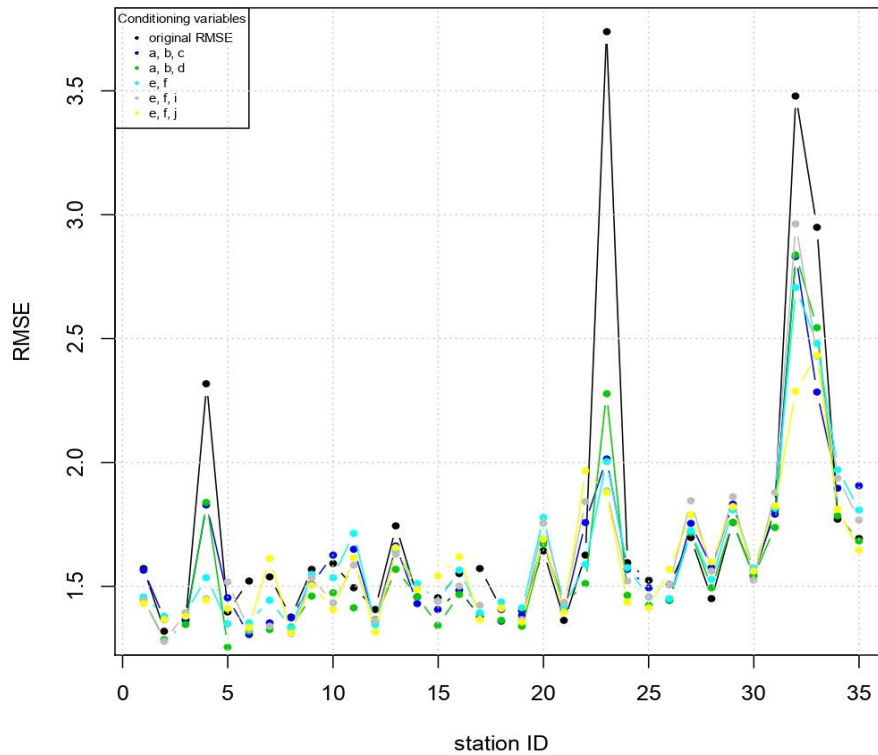


Figure 6: On the X axis – meteorological stations by ID, on Y-axis – Root Mean Squared Error for various sets of conditioning variables.

Conclusions

The vine copula method allows reduction of systematic errors and generation of synthetic multi-dimensional data obtained by models in the hindcast. We can generate a sample from copula probability distribution and thus save CPU which is critical to the ensemble forecasting.

Adaptation of C-LAEF for Türkiye

Mustafa BAŞARAN

1 Introduction

This scientific stay was aimed to adapt the C-LAEF Project (Wastl et al., 2021) of Geosphere for Turkish domain. In this sense, the necessary technical and scientific studies were realized during the stay in Vienna 8-13 May 2023 under the supervision of Clemens Wastl.

2 Model Configuration

For the adaptation, we chose the same characteristics (except for model version) as AROME model (model domain is represented in the Figure 1) which is running operationally at TSMS. And the table below shows the configuration details of C-LAEF for Turkish domain. During the stay the first option for C-LAEF was initiated. The process was finalized after the stay and semi-operational technical steps were completed at TSMS.

The first option for C-LAEF is called pure dynamical adaptation. We utilized the first 16 members of ECMWF-ENS. For the control member, we preferred to use ECWMF-ENS since the difference between ECMWF HRES and ECMWF ENS is very minor.

After receiving the initial and boundary conditions, 927, 927_surf and 001 configurations were run for each and control member. The details are shown in the ecfow Figure 2 below.

The model now runs every six hours starting from 00 UTC and produces forecast up to 24 hours. And the model is running in the semi-operational mode on ATOS.

Table 1:C-LAEF Türkiye Configuration

Model version	cy46 (with some scheme specific tuning)
Resolution	1.7 km
Levels	72
Initial conditions	ECMWF-ENS
Boundaries	ECMWF-ENS
Starting times	00 UTC,06 UTC,12 UTC and 18 UTC
Cycle interval	6 hours
Forecast lead times	+24 hours.

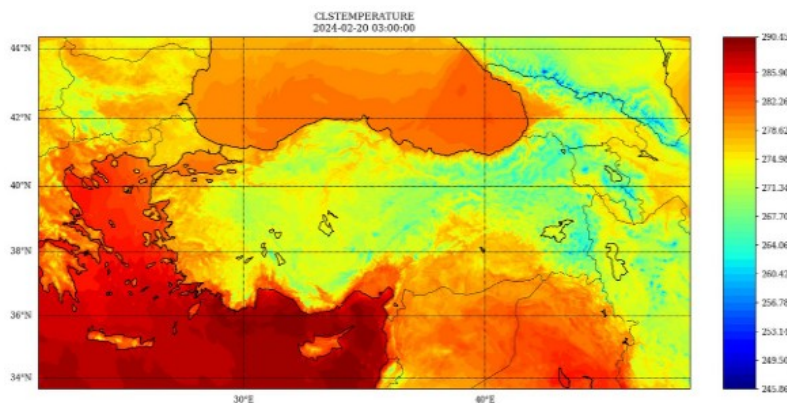


Figure 1:2 meter temperature forecast map of C-LAEF for Türkiye

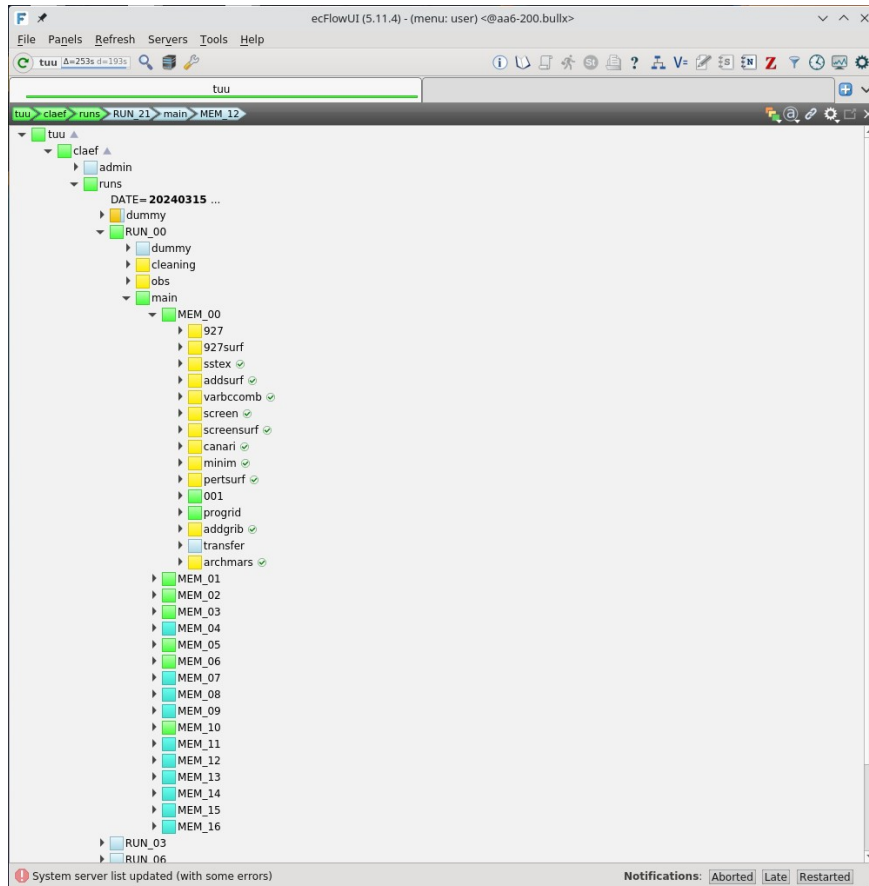


Figure 2: Screenshot of ecflow of C-LAEF for Türkiye running on ATOS.

3 Conclusion

We plan to make the C-LAEF for Türkiye operational on ATOS system and further improve by using the next option for the model. The author also would like to thank Clemens Wastl, Christoph Wittmann and Yelis Cengiz from TSMS for their kind support.

4 References

Wastl, C., Wang, Y., Atencia, A., Weidle, F., Wittmann, C., Zingerle, C. and Keresturi, E. (2021) C-LAEF: Convection-permitting Limited-Area Ensemble Forecasting system. *Quarterly Journal of the Royal Meteorological Society*, 147(735), 1431–1451. <https://doi.org/10.1002/qj.3986>.

Patricia around ACCORD 26 beautiful countries

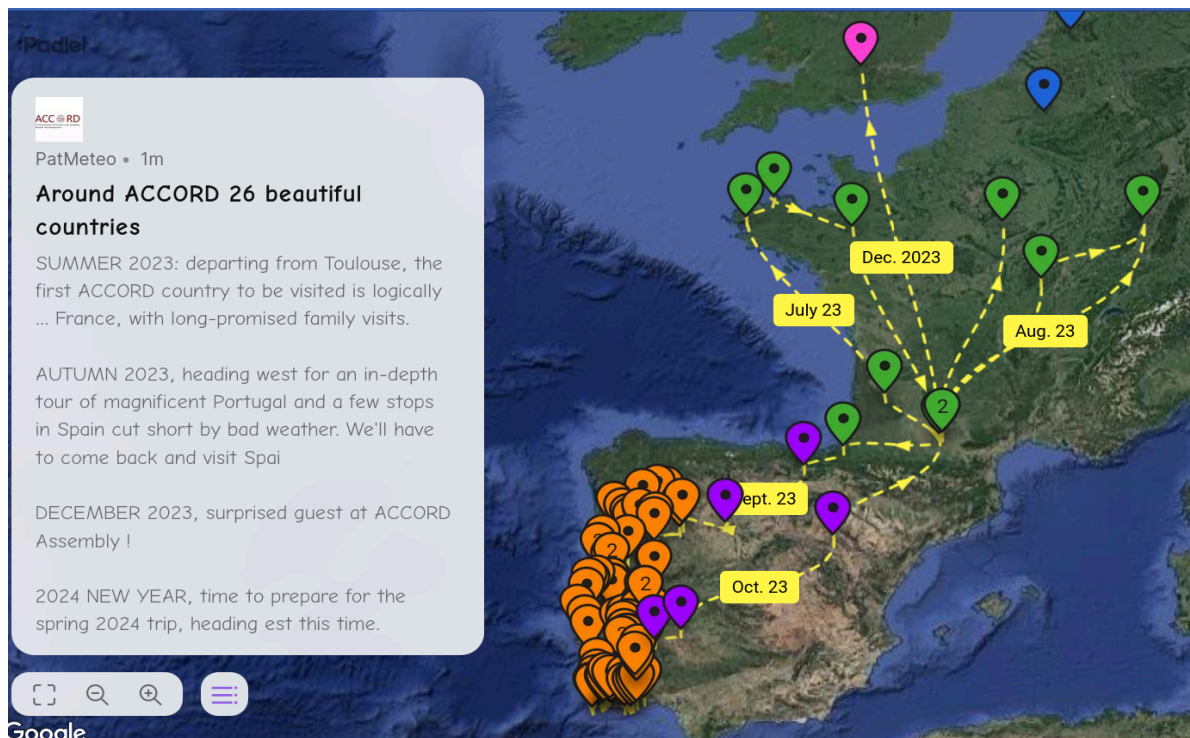
Patricia Pottier

1 Since leaving ACCORD CSS position

After saying goodbye to my dear ACCORD colleagues (with great emotion), I've followed ACCORD's adventures on the ACCORD web, started travelling to our 26 beautiful countries and prepared a webpage to share these visits with you and keep in touch: <http://pottier.pat.meteo.free.fr/>

2 Travel blog

The [travel blog](#) offers for real-time or slightly delayed tracking

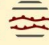



You can zoom in by using CTRL + scroll wheel; click on a pin (green in France, purple in Spain, orange in Portugal) to open the slide for that location and double-click on the slide to enlarge it. Once the slide is open, you can move from one slide to another using the arrows (please note that the slides appear in reverse chronological order, with the most recent first). Comments are very welcome.


3 Slide shows of the travel blog

The travel blog is updated during trips and pages piled up in anti-chronological order. Once back home after a trip, I made a slideshow of it as some kind of photobook.

The [Volume 1](#) was published in November 2023 with Summer and Autumn 2023 in France, Portugal and Spain.

Patricia around ACC  RD 26 beautiful countries
[Vol.1 Nov. 2023]



 **SUMMER 2023:** departing from Toulouse, the first ACCORD country to be visited is logically ... France, with long-promised family visits to Brittany, to Alsace and finally to the Paris region.

AUTUMN 2023, heading west for an in-depth tour of magnificent Portugal and a few stops in Spain cut short by bad weather. We'll have to come back and visit Spain.

END of 2023: it's time to prepare for the spring 2024 trip, heading east this time.

Travel blog for real-time or slightly delayed tracking:
[https://padlet.com/pottierpatmeteo/Around accord 26 beautiful countries](https://padlet.com/pottierpatmeteo/Around%20accord%2026%20beautiful%20countries)

4 What's next ?

After changing our tiny house-on-wheels, the spring trip will be heading east. A 3-month itinerary is ready, but will probably be shortened or postponed for family constraints.

Anyhow, let's hope the next journey crosses paths with ACCORD colleagues, somewhere, sometime.

Previous editions of the ACCORD Newsletter

Anne-Lise Dhomps, ACCORD Consortium Scientific Secretary



[1st ACCORD Newsletter](#),
published on 5 October 2021



[2nd ACCORD Newsletter](#),
published on 28 February 2022



[3rd ACCORD Newsletter](#),
published on 24 October 2022



[4th ACCORD Newsletter](#),
published on 19 June 2023

The joint ALADIN-HIRLAM Newsletter (2013-2021, 16 editions) can be found on the [ALADIN dedicated webpage](#).

Elaboration of the ACCORD Newsletters

For the concrete writing of an article, please refer to the editorial guidelines, accessible at: <http://www.accord-nwp.org/?Recommendations-templates>

The newsletter content is based on voluntary contributions by the scientists and the teams in the consortium. We want it to be a useful tool for sharing both “practical” information and experience (code engineering, quality assurance, system aspects) and “more fundamental” results (advances in research work, outcome of specific meetings or working days etc.).

NL6 is expected for late 2024, however contributors can upload their material at any time during the year [on this shared folder](#). Do also not hesitate to encourage scientific contributions by young scientists (PhDs, post-docs etc.) or technical contributions (codes, porting, optimization etc.).